

QUASISTATIC AND DYNAMIC FORCE MICROSCOPY OF SINGLE ANTIGEN-ANTIBODY COMPLEXES AND FIBRIN-FIBRINOGEN SYSTEMS

THÈSE N° 2946 (2004)

PRÉSENTÉE À LA FACULTÉ SCIENCES DE BASE

Institut de physique de la matière complexe

SECTION DE PHYSIQUE

ÉCOLE POLYTECHNIQUE FÉDÉRALE DE LAUSANNE

POUR L'OBTENTION DU GRADE DE DOCTEUR ÈS SCIENCES

PAR

Lilia CHTCHEGLOVA

DEA en physico-chimie des matériaux moléculaires et macromoléculaires, Université Strasbourg I, France
et de nationalité russe

acceptée sur proposition du jury:

Prof. G. Dietler, directeur de thèse
Prof. D. Anselmetti, rapporteur
Prof. A. Haeberli, rapporteur
Prof. J.-J. Meister, rapporteur

Lausanne, EPFL
2004

À ma fille, Dasha

Посвящается моей дочке, Даше

Remerciements

Bien qu'une thèse de doctorat soit un travail de recherche essentiellement personnelle, de nombreuses personnes de notre entourage portent une influence importante sur ce travail par leur idées, conseils, encouragements et aide.

Je tiens à remercier le Fonds Nationale Suisse de la Recherche Scientifique (FNRS), l'Université de Lausanne (UNIL) et Ecole Polytechnique Fédérale de Lausanne (EPFL) pour avoir financé cette thèse. Je remercie également la fondation ERNA HAMBURGER pour avoir accordé la bourse pour la fin de ce travail.

Je remercie tout d'abord Monsieur le Professeur Giovanni Dietler, directeur du Laboratoire de Physique de la Matière Vivante de l'EPFL, de m'y avoir chaleureusement accueilli et de proposé un sujet de thèse tout à fait dans mes goûts. Il a suivi cette thèse en suggérant sans imposer et en guidant sans brider. J'ai beaucoup apprécié la très grande liberté d'action qu'il m'a laissé. Gracie mille.

J'ai eu la chance de travailler avec Serguei Sekatski, mon compatriote. Ses conseils judicieux, son regard critique sur le travail, son enthousiasme ainsi que son amitié et ce de sa femme, Elena, m'ont été très précieux. Спасибо большое.

Je suis très sensible à l'honneur que me font Messieurs les Professeurs André Haerberli, Dario Anselmetti et Jean-Jacques Meister de juger ce travail.

Mes remerciements vont aussi à Dmitri Lapshine, un autre compatriote, pour la trop courte mais fructueuse collaboration que nous avons entretenue pour la partie de travail concernant des mesures d'élasticité des molécules. Je remercie également « ammick » Georges Shubeita, ex-membre du groupe G. Dietler, pour son aide précieuse pour le travail concernant des mesures d'élasticité ainsi que pour son amitié et ses blagues inoubliables.

Je suis très reconnaissant à Laurent Libioulle, qui a accepté de lire ma thèse très attentivement. Ses conseils apportaient beaucoup pour la rédaction de mémoire de cette thèse.

Merci à Michel Kessous, informaticien, d'avoir toujours aider très rapidement et efficace avec les problèmes informatiques.

Mes remerciements vont à Madame Franca Pretzsch pour son grand travail d'une secrétaire, pour son amitié, son aide et de sa bonne humeur.

Un grand merci à tous les membres et ex-membres du groupe de G. Dietler que j'ai rencontré au cours de ces quatre années : Francesco, Aleksandra, Eva, Alexandre, Anna, Sandor, Jim, Gerit. Nos discussions drôles et animées lors de dîners, de pose café, dans un couloir ou un bureau, participent grandement au délicieux souvenir que je conserve de cette période. Je salue aussi chaleureusement mes autres collègues du BSP qui ont su créer une excellente ambiance de travail.

Merci beaucoup à mon amie Emile Rey, « Micky », pour son amitié, son aide et sa présence pour les moments difficiles.

Enfin, un énorme merci à mes parents, grands-parents et mon frère, Alexandre, ainsi que à ma fille, Dacha, pour tout. Спасибо, мои дорогие, за всё !

Abstract

The molecular processes based on the specific receptor-ligand interactions (e.g. immune response to a foreign antigen, communication between nerve cells, etc.) are essential for a good and stable performance of living organisms. The aim of the present work is to study such molecular processes with the Atomic Force Microscope (AFM) operated in Force Spectroscopy (FS) mode.

Information such as the force and length of the ligand-receptor bond rupture could be obtained from the standard quasistatic FS studies, whereas no external dithering applied to the AFM tips. Firstly, the antigen-antibody interactions were examined with the Bovine Serum Albumin (BSA) protein and its poly- and two different monoclonal antibodies. It was shown that the peak unbinding force depends on the type of antibody and the antibody concentration. The single potential barrier is dominant for the interaction between BSA and monoclonal antibodies and was revealed from the loading rate-dependent measurements. Secondly, we are interested in the process of fibrin gel formation, in particular in the forces involved in this process. It was demonstrated that the fibrin-fibrinogen interaction is the specific one. The unbinding force rupture for single fibrin-fibrin(ogen) complex was determined to be of about 320 pN at a loading rate of 3.5 nN/s. The single potential barrier is also dominant for this interaction.

Moreover, a new method of direct and continuous measurement of the spring constant of single molecules or molecular complexes has been elaborated in our laboratory. To this end, the standard FS technique with functionalized tips and samples is combined with a small dithering of the AFM tip. The change of the dithering amplitude as a function of the pulling force is measured in order to extract the spring constant of the complex. The potentialities of this technique were demonstrated for the experiments with single BSA – polyclonal antibody to BSA (Ab-BSA) and fibrinogen – fibrinogen complexes.

Résumé

Les processus moléculaires basés sur les interactions spécifiques récepteur – ligand (réponse immune vers l'antigène étranger, communication entre les cellules nerveuses, etc.) sont essentielles pour bonne et stable performance d'organismes vivants. Le but de cette thèse est l'étude de ces processus moléculaires avec l'aide de la Microscopie de Force Atomique (AFM) opérée dans le mode de Spectroscopie de Force (FS).

L'information comme la force et longueur de liaison ligand - récepteur peut être obtenue par des études FS standard où il n'y a pas d'excitation externe appliquée sur les leviers. Dans un premier temps, les interactions antigène – anticorps entre BSA (Bovine Sérum Albumine) et ses anticorps polyclonaux et monoclonaux ont été examinées. Par l'expérience de « loading rate », nous avons démontré qu'une seule barrière de potentiel est dominante dans l'interaction entre BSA et ses anticorps monoclonaux. Nous nous sommes ensuite intéressés aux premières étapes de polymérisation de la fibrine, en particulier, aux forces responsables dans ce processus. On a montré que l'interaction fibrine – fibrinogène est spécifique. La force de rupture du complexe fibrine – fibrinogène a été déterminée comme 320 pN à « loading rate » de 3.5 nN/s. Une seule barrière de potentiel est également dominante pour cette interaction.

Une nouvelle méthode pour la mesure directe et continue de la constante de ressort de molécules et de complexes moléculaires a été élaborée dans notre laboratoire. Pour cela, la technique standard de FS a été combinée avec la petite modulation de leviers d'AFM. Le changement d'amplitude de vibration modulée est mesuré en fonction de force appliquée pour extraire la constante de ressort de système étudié. Les potentiels de cette technique ont été démontrés dans les expériences avec les complexes de BSA – anticorps polyclonaux et fibrinogène – fibrinogène.

Table of abbreviations

Ab – antibody;
ADC - Analog-to-Digital Converter;
AFM – atomic force microscope (microscopy);
Ag – antigen;
APTES - 3-aminopropyltriethoxy silane;
BSA - Bovine Serum Albumin;
Da – Dalton;
DAC - Digital-to-Analog Converter;
DIPEA - N-ethyl-diisopropylethylamine;
EDAC - 1-ethyl-3 (3-dimethylaminopropyl) carbodiimide;
FS – force spectroscopy;
HOPG - highly oriented pyrolytic graphite;
HSA - Human Serum Albumin;
mAb – monoclonal antibody;
MES - 2-[N-Morpholino] ethanesulfonic acid;
PBS – phosphate buffered saline buffer;
SAM - self-assembled monolayer;
UHQ - ultra high quality;
UV – ultraviolet;
WLC - Worm-Like Chain (model).

Table of Contents

Introduction	1
---------------------------	----------

CHAPTER I

Atomic Force Microscopy and Standard Force Spectroscopy

1.1 Atomic Force Microscopy	3
1.1.1 Introduction.....	3
1.1.2 Basic principles of AFM.....	3
1.1.3 Different AFM operating modes.....	5
1.1.3a Contact mode imaging or constant-force mode.....	5
1.1.3b Dynamic (or tapping) imaging modes.....	7
References.....	10
1.2 Quasistatic Force Spectroscopy	13
1.2.1 Introduction.....	13
1.2.2 Force curves.....	14
1.2.2a Force resolution of the AFM.....	15
1.2.3 Application of force curves.....	17
1.2.4 Energies and rates of a molecular reaction.....	17
1.2.4a Equilibrium reactions.....	18
1.2.4b Far from equilibrium reactions.....	18
1.2.4b/1 Force spectroscopy of simple bonds.....	19
References.....	25

CHAPTER II

Sample and Tip Preparation Methods for Force Spectroscopy Study

2.1 Sample preparation.....	29
2.1.1 Mica.....	29
2.1.2 Silanization method (APTES-mica).....	30
2.1.2a Characterization of APTES-mica samples by AFM.....	32
2.1.3 Functionalization of APTES-mica with proteins.....	33
2.2 Tip preparation.....	33
2.2.1 Tip cleaning.....	34
2.2.2 Functionalization of the AFM tips with proteins	35
2.2.2a Functionalization of the tips with antibodies	36
2.2.2b Functionalization of the tips with fibrinogen molecules....	36
References.....	37

CHAPTER III

Complexes of Bovine Serum Albumin with its different antibodies

3.1 Introduction	39
3.2 Bovine serum albumin, structure and properties.....	41
3.2.1 BSA structure.....	41
3.2.2 BSA conformational transitions.....	43
3.3 Antibodies, their function and general structure.....	44
3.3.1 Affinity and specificity of antigen-antibody bond.....	47
3.3.1a Affinity or tightness of binding.....	47
3.3.1b Specificity, the relationship between affinity and specificity	49
3.4 Quasistatic force spectroscopy study of polyclonal and monoclonal	
anti-Bovine Serum Albumin antibodies – BSA complexes.....	50
3.4.1 AFM instrumentation.....	50
3.4.2 Tip and sample functionalization.....	51
3.4.3 Data analysis and control experiments.....	53
3.4.4 Experimental results and discussion.....	55
3.4.4a Constant loading rate measurements.....	56
3.4.4b Loading rate-dependent measurements	
and dissociation rates estimation.....	63
3.5 Conclusion.....	64
References.....	66

CHAPTER IV

Fibrinogen and Fibrin

4.1 Fibrinogen and fibrin.....	70
4.2 Introduction.....	70
4.2.1 Molecular structure of fibrinogen.....	71
4.2.2 Fibrin polymer formation.....	73
4.2.3 About the symmetry of the fibrinogen molecule.....	76
4.3 Fibrinogen to fibrin formation visualized with the AFM.....	77
4.4 Quasistatic force spectroscopy study of fibrin gel formation.....	84
4.4.1 AFM instrumentation, tip and sample preparation, data analysis.....	84
4.4.2 Fibrinogen – fibrinogen interaction.....	85
4.4.2a Control experiments.....	85
4.4.2a/1 Bare tip – fibrinogen system.....	85
4.4.2a/2 Fibrinogen-functionalized tip – mica system	88
4.4.2b Fibrinogen – fibrinogen complex.....	90
4.4.3 Fibrin – fibrinogen complex.....	93
4.4.3a Constant loading rate measurements.....	94
4.4.3a/1 Fibrin (thrombin) – fibrinogen system.....	94
4.4.3a/2 Fibrin (Reptilase) – fibrinogen system.....	99
4.4.3a/3 <i>Gly-Pro-Arg-(His)₄</i> fibrin(ogen) interaction.....	103
4.4.3b Loading rate dependence of the unbinding force and	
dissociation rate estimation for the fibrin – fibrin(ogen) complex...	105
4.5 Conclusion.....	106
References.....	108

CHAPTER V

Force Spectroscopy with modulation of the AFM tips

5.1 Introduction.....	111
5.1.1 AFM instrumentation	112
5.1.2 Tip and sample preparation, control experiments.....	114
5.2 Experimental results and discussion.....	114
5.2.2 Calculation of the spring constant for tip-sample complex.....	115
5.2.3 BSA – Ab-BSA complex.....	116
5.2.3a Interpretation of data.....	119
5.2.3b Estimation of the elasticity of linkers.....	123
5.2.4 Fibrinogen – fibrinogen complex	124
5.3 Perspectives.....	126
5.4 Conclusion.....	129
References.....	130
General conclusions.....	133

*О, сколько нам открытий чудных
Готовят просвещенья дух
И опыт, сын ошибок трудных,
И гений, парадоксов друг,
И случай, бог изобретатель.*

А.С. Пушкин

*"При пути ведут к знанию: путь размышления -
это путь самый благородный, путь подражания -
это путь самый легкий и путь опыта - это путь
самый горький".*

Конфуций

Introduction

The subject of this thesis is situated on the boundary between biology, medicine, chemistry and physics. How do molecules interact with each other? In order to answer to this question we should provide detailed information about the structure, the function and the properties of molecules studied as well as about the energy and the force landscapes of interaction.

Molecular recognition processes (e.g. recognition of antigens by their antibodies, enzymatic catalysis, cell adhesion, communication between nerve cells, etc.) play a pivotal role in nature. The basic working principle of a molecular recognition event is the specific binding of a ligand molecule (“key”) to a receptor molecule (“lock”). Many diseases are related to a malfunction in such molecular recognition processes. A detailed understanding of the molecular binding process, together with information about binding forces, could assist in development of highly specific drugs.

Of course, the most natural and simple method of understanding how well molecules are attached to each other is to measure the binding forces. For many years, experimentalists have been able to measure the binding or folding energies/forces of the interactions involved. For example, ensemble-averaged information about binding enthalpies can be obtained from calorimetry experiments. However, such experiments, where many molecules are simultaneously examined in parallel at the same time, do not yield information as to the actual behavior of an *individual molecule*. Since the recent introduction of *force spectroscopy techniques* (atomic force microscopy, optical tweezers, the biomembrane force probe and flexible microneedles) this situation has radically changed. Our work is based on the use of the Atomic Force Microscope (AFM), first developed by Binnig, Quate and Gerber in 1986 as an imaging technique.

The aim of this thesis work is to study different molecular complexes with the AFM. Two biosystems are investigated. Firstly, we are interested in the antigen-antibody

interactions studied with the Bovine Serum Albumin (BSA) protein model and its poly and two different monoclonal antibodies. Secondly, we focus on the process of fibrin gel formation, largely responsible for the process of blood coagulation.

In Chapter I, the instrumentation and basic principles of atomic force microscopy are briefly described. This is followed by a detailed presentation of a standard quasistatic force spectroscopy technique, where no external modulation is applied to the AFM tip. Because the chemistry of tip and sample surfaces, with functionalization procedures, is essential for our study, a complete explanation of sample and tip preparation methods is given in Chapter II. Chapters III and IV first, describe the structure and functional properties of the proteins studied; and second, present the experimental results obtained with quasistatic force spectroscopy for antigen-antibody complexes and molecular interactions involved in fibrin gel formation. In addition, some AFM images revealing the first steps of molecular organization in fibrin strands are shown in Chapter IV.

Up to now, the specific bond force rupture (or unbinding force) easily measured with quasistatic force spectroscopy has served as the unique characteristic parameter for the molecular recognition process. We introduce in equal position a new physical parameter, the spring constant of the molecular complex, which gives us complementary information about the elasticity of molecules, molecular structure, and the mechanism of the tip-sample interaction. To this purpose, a new method, based on the combination of standard force spectroscopy with a small dithering of the AFM tip, has been developed in our laboratory and is proposed in Chapter V. Some experimental results, such as the spring constant of the single antigen-antibody and the fibrinogen-fibrinogen complexes, are described with the perspective of measuring molecular bond lifetimes.

Chapter I

Atomic Force Microscopy and Standard Force Spectroscopy

1.1 Atomic Force Microscopy

1.1.1 Introduction

The atomic force microscope (AFM), invented in 1986 by Binnig, Quate, and Gerber [1], has opened new perspectives in investigating surfaces with high lateral and vertical resolution. In our days, AFM has become a very powerful technique for achieving high resolution imaging of biological samples and for surface property characterization with measurement of biophysical and mechanical properties of molecular complexes at work.

The basic principles of AFM are outlined in the first part of this chapter, followed by the description of different AFM operating modes. The second part describes standard quasistatic force spectroscopy (FS) mode of the AFM.

1.1.2 Basic principles of AFM

A schematic diagram of the basic instrument setup of an AFM is shown in fig. 1.

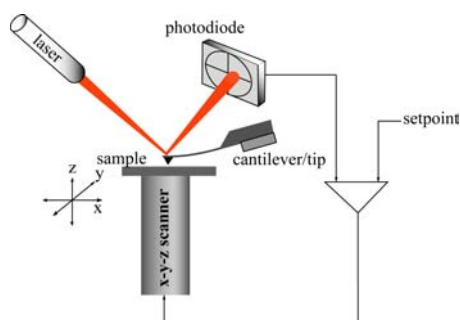


Figure 1. Schematic diagram showing the main components of a typical AFM: piezoelectric scanner, cantilever/tip assembly, laser and multisegmented photodiode detector system, and the feedback loop between the detector and piezo.

The main components of an AFM are the scanning probe, the scanning sample stage and the detector. The sample is scanned with a probe whose deflections are recorded by a computer. To raster scan over a desired area a sensitive x - y scanning system is required and normally provided by computer-controlled piezo scanner. The third dimension z correlates with height movement in the piezo, which is usually linked to an optical lever detection system (e.g. laser beam and a split-photodiode). The scanning probe component is the key element of an AFM; typically it consists of a mounted triangular or rectangular cantilever, 100-200 μm in length, with an integrated pyramidal Si_3N_4 (silicon nitride) or Si (silicon) probe tip (fig 2.) A standard probe tip is about 3-5 μm tall with a radius of curvature at the tip apex of about 35-60 nm.

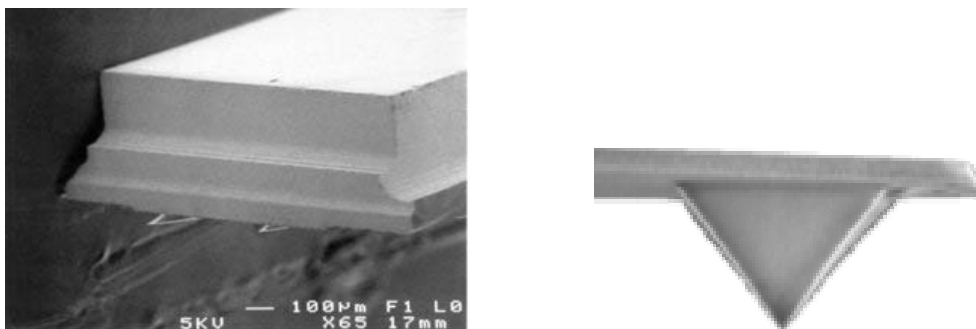


Figure 2. Scanning electron micrograph of a typical commercial cantilever/tip (Veeco Instruments, USA) assembly (left) and image of pyramidal probe tip (right).

The size and shape of the tip, along with the pixel density/unit area scanned, directly affect the resolution obtained for the imaged object. While the instrument setup is relatively simple, the interactions between probe tip and sample are not so simple.

1.1.3 Different AFM operating modes

A wide range of AFM imaging modes has been proposed using close contact tip-sample interactions, combined with the ability to control and/or monitor the cantilever drive signal input or output. This flexibility allows nanoscale examination of different structure-property relationships of a sample under vacuum, at low temperatures, ambient air, or aqueous conditions. Some common modes of AFM operation, which are used in the study of biological samples, are briefly illustrated in this paragraph.

1.1.3a Contact mode imaging or constant-force mode

In this mode, the tip is placed into “physical” contact with the sample, and the raster-scanned through the x-y plane (fig. 2a). “Physical” contact means that the tip is pressed against the sample until a repulsive force is sensed by the lever. At each x, y position, the change in surface topography induces a deflection of the cantilever, which is measured by the detection system. Several methods for measuring the cantilever deflection have been explored: optical lever technique, optical interferometry, capacitance measurements, scanning tunneling microscopy [2] and piezoelectric bimorphs [3]. The optical lever technique using photodiode detector is the most common method. Briefly, a laser light is reflected off the back of the gold-coated cantilever to a multi-segmented photodiode. The long optical path greatly amplifies the small movements of the cantilever (in the range of Å) into measurable voltage signals at the detector. The amount of light striking the upper and lower photodiode segments is compared with an unperturbed null value and used to generate a difference signal (error signal). This difference signal is used as the input to a digital feedback loop to the z component of the piezo. The feedback loop maintains tip-sample contact, through the voltage signal output applied to the z -component of the piezo. Under

constant force conditions, this provides quantitative height information into the AFM image. If the feedback loop detects a deviation in error signal, it will force the z-piezo to change the height of the sample stage relative to the tip, bringing the deflection signal back to the reference value, canceling the error signal. The resulting vertical position of the sample corresponding to the lateral x - y position is recorded as a topographical map of the sample, named the “height” image. Since the photodiode must detect a tip deflection before activating the piezo scanner, there can be significant deflection at sharp edges of the sample if the scan speed is too fast.

In contact mode, the tip is always in *constant contact* with the sample and it can be problematic for imaging “soft” biological samples (proteins, cells, DNA, polymers and etc.). While imaging, a significant lateral shear force is produced and applied to the sample. This force (on the order of few nN) can be sufficient to deform, disrupt and/or destroy a delicate sample, or to sweep adsorbed molecules to the periphery of the imaging area [4-6]. Thus, contact mode is often unsuitable for truthful imaging of non-fixed biological samples under aqueous conditions.

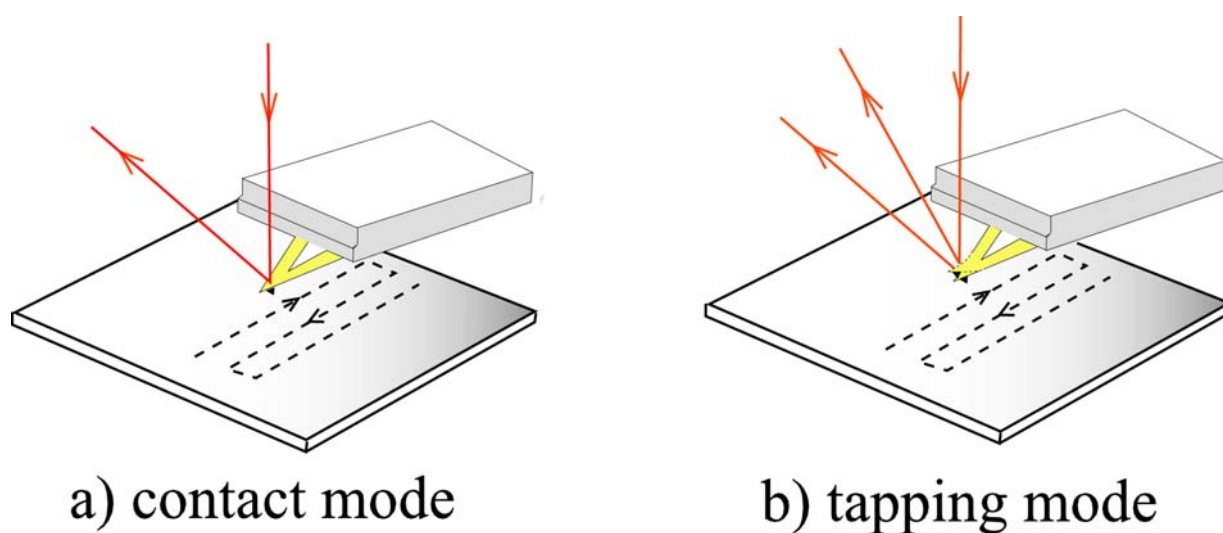


Figure 2. Contact and tapping modes with part of x - y raster scanning pattern.

1.1.3b Dynamic (or tapping) imaging modes

In order to prevent large lateral forces applied during contact mode, various dynamical operational modes were successfully introduced [7]. When working in these dynamical modes the cantilever is oscillated in the z -direction at its resonance frequency or near its resonance frequency (fig. 2b). Because the oscillating tip touches the sample when it reaches the lowest point, this imaging mode is now called the “tapping mode” [7, 8]. Therefore, the tip is only in *intermittent contact* with the sample [7-12] and applied shear forces are often negligible. Under optimum conditions, the resolution has been demonstrated to be as low as 0.5 nm in the x - y plane, and approximately 1 Å in the z direction [9]. A recent development also allows the tracking of biomolecules at a relatively high speed [10].

During scanning the tip-sample interaction causes attenuation of the root mean square (RMS) oscillation amplitude. The RMS amplitude is compared to a reference value in order to compute the error signal and is used, in the feedback loop, to measure topographic variations of the sample (analogous to the difference signal used in contact mode). A three dimensional image of the sample is obtained by recording the position of the sample required to keep the attenuation of the RMS amplitude at a constant value. Several studies have been performed in order to understand better the tip-sample interactions in terms of force and energy dissipation [13-16].

A second type of dynamic force microscopy is based on the same principles as tapping mode and consists of amplitude, phase, and force modulation modes (fig. 3). An oscillating signal is imposed on the tip, resulting in only intermittent contact between the tip and sample [17-20]. Phase and amplitude imaging modes measure phase shift and amplitude feedback error in the frequency of the response signal, respectively, while force modulation monitors amplitude attenuation under a constant cantilever deflection.

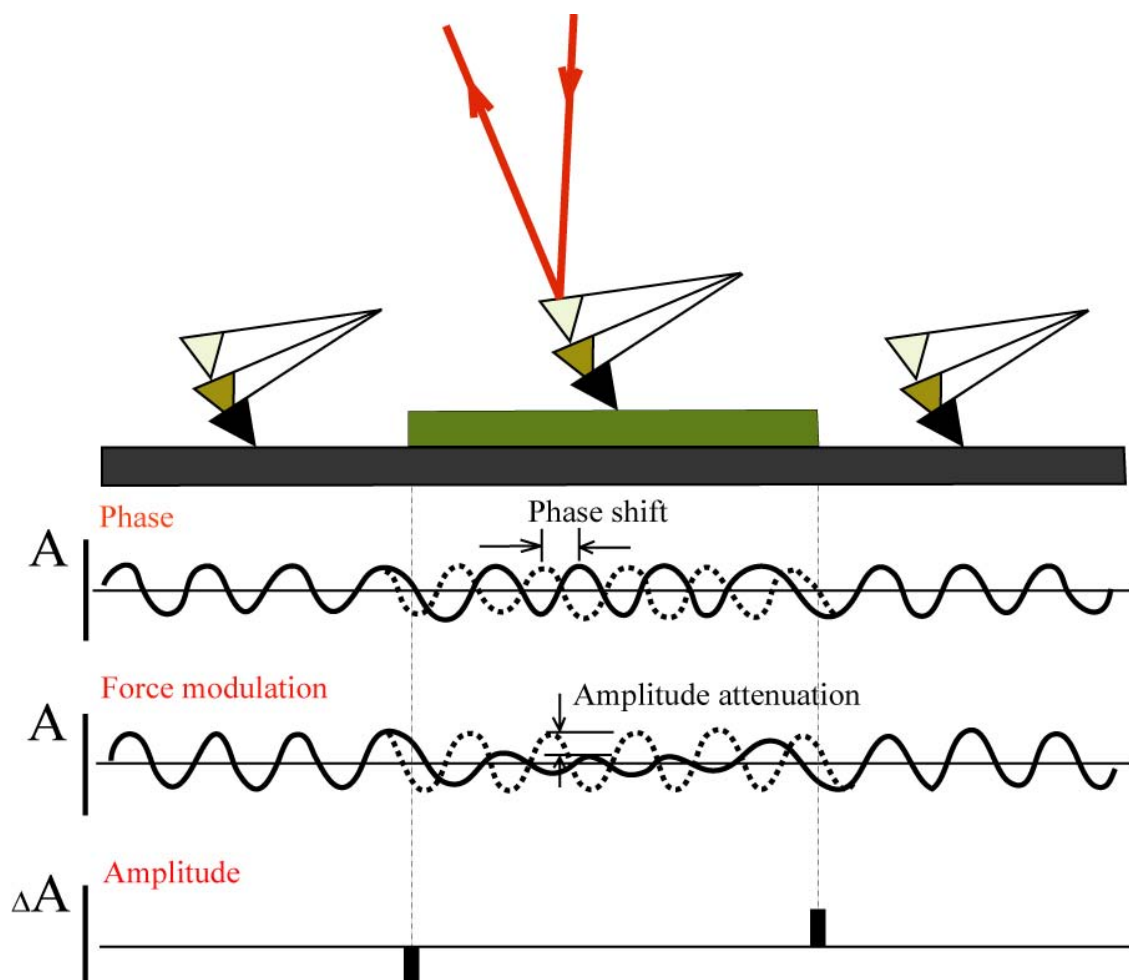


Figure 3. Phase, force modulation and amplitude modes of an AFM (A as amplitude).

When the tip is in contact with the sample, the force causes a small indentation, characterized by the mechanical properties of the sample [21-23]. When the signal responses are compared with the driving signal, the differences are a measure of the viscoelastic properties of the sample. The amplitude response to the driving signal is related to the elastic properties, and the phase shift is a response to the viscous properties of the sample [21]. In force modulation, the amplitude attenuation of the oscillating tip is observed on regions with different viscoelastic

properties. The attenuation is larger on a soft region relative to harder regions. A corresponding change also is observed in phase imaging. An out-of-phase signal is detected when the tip interacts with a soft region. Dynamic AFM modes have been widely explored to examine the mechanical properties of cell membranes, DNA, and for imaging protein molecules on rough materials [24-28]. In amplitude modulation and phase imaging, the frequency and amplitude of the tip oscillation can be optimized to give improved contrast of a sample compared with topographic height imaging [22, 25, 27].

Further improvements in the ability to manipulate objects reproducibly on molecular and even atomic scales have applications in the growing field of nanoengineering.

References

1. Binning, G., Quate, C., Gerber, C. H. Atomic force microscope. *Phys. Rev. Lett.* **56** (1986) 930-933.
2. Sarid, D. Scanning Force Microscopy: With applications to electric, magnetic and atomic forces. 1991. Oxford Publishing, New York.
3. Itoh, T, and Suga, T. Scanning force microscope using a piezoelectric microcantilever. *J. Vac. Sci. Technol. B.* **12** (1994) 1581-1585.
4. Marchant, R. E., Lea, S., Andrade, J. D., and Bockenstedt, P. J. 1992. Interactions of von Willebrand-factor on mica studied by atomic force microscopy. *Colloid Interface Sci.* **148** (1992) 261-272.
5. Grafström, S., Ackermann, J., Hagen, T., Neumann, R., and Probst, O. Analysis of lateral force effects on the topography in scanning force microscopy. *J. Vac. Sci. Technol. B.* **12** (1994)1559-1564.
6. Siedlecki, C. A., Lestini, B., Kottke-Marchant, K., Eppell, S. J., Wilson, D. L., and Marchant, R. E. Shear-dependent changes in the three-dimensional structure of human von Willebrand factor. *Blood.* **88** (1996) 2939-2950.
7. Hansma, H. G., Sinsheimer, R. L., Groppe, J., Bruice, T. C., Elings, V., Gurley, G., Bezanilla, M., Mastrangelo, I. A., Hough, P. V. C., and Hansma, P. K. Recent advances in atomic-force microscopy of DNA. *Scanning.* **15** (1993) 296-299.
8. Hansma, P. K., Cleveland, J. P., Radmacher, M., Walters, D. A., Hillner, P. E., Bezanilla, M., Fritz, M., Vie, D., Hansma, H. G., Prater, C.B., Massie, J., Fukunaga, L., Gurley, J., and Elings, V. Tapping mode atomic force microscopy in liquids. *Appl. Phys. Lett.* **64** (1994) 1738-1740.
9. Möller, C., Allen, M., Elings, V., Engel, A., and Müller, D. J. Tapping-mode atomic force microscopy produces faithful high-resolution images of protein surfaces. *Biophysical J.* **77** (1999) 1150-1158.
10. van Noort, S. J. T., van der Werf, K. O., de Grooth, B. G., and Greve, J. High speed atomic force microscopy of biomolecules by image tracking. *Biophysical J.* **77** (1999) 2295-2303.
11. Putman, C. A., van der Werf, K. O., de Grooth, B. G., van Hulst, N. F., and Greve, J. Viscoelasticity of living cells allows high resolution imaging by tapping mode atomic force microscopy. *Biophysical J.* **67** (1994) 1749-1753.

12. Putman, C. A. J., van der Werf, K. O., de Grooth, B. G., Van Hulst, N. F., and Greve, J. Tapping mode atomic force microscopy in liquid. *Appl. Phys. Lett.* **64** (1995) 2454-2456.
13. Cleveland, J. P., Anczykowski, B., Schmid, A. E., and Elings, V. B. Energy dissipation in tapping-mode atomic force microscopy. *Appl. Phys. Lett.* **72** (1998) 2613-2615.
14. Gotsmann, B., Anczykowski, B., Seidel, C., and Fuchs, H. Determination of tip-sample interaction forces from measured dynamic force spectroscopy curves. *Appl. Surf. Sci.* **140** (1999) 314-319.
15. Gotsmann, B., Seidel, C., Anczykowski, B., and Fuchs, H. Conservative and dissipative tip-sample interaction forces probed with dynamic AFM. *Phys. Rev. B.* **60** (1999) 11051-11061.
16. Anczykowski, B., Gotsmann, B., Fuchs, H., Cleveland, J. P., and Elings, V. B. How to measure energy dissipation in dynamic mode atomic force microscopy. *Appl. Surf. Sci.* **140** (1999) 376-382.
17. Lantz, M. A., O'Shea, S. J., and Welland, M. E. Force microscopy imaging in liquids using ac techniques. *Appl. Phys. Lett.* **65** (1994) 409-411.
18. Dreier, M., Anselmetti, D., Richmond, T., Dammer, U., and Güntherodt, H.-J. Dynamic force microscopy in liquids. *J. Appl. Phys.* **76** (1994) 5095-5098.
19. Wong, T. M. H., and Descouts, P. Atomic force microscopy under liquid – a comparative study of 3 different AC mode-operations. *J. Microsc.* **178** (1995) 7-13.
20. Magonov, S. N., Elings, V., and Whangbo, M.-H. Phase imaging and stiffness in tapping-mode atomic force microscopy. *Surf. Sci.* **375** (1997) L385-L391.
21. Radmacher, M., Tillmann, R. W., and Gaub, H. E. Imaging viscoelasticity by force modulation with the atomic force microscope. *Biophys. J.* **64** (1993) 735-742.
22. Chen, X., Davies, M. C., Roberts, C. J., Tendler, S. J. B., Williams, P. M., Davies, J., Dawkes, A. C., and Edwards, J. C. Interpretation of tapping mode atomic force microscopy data using amplitude-phase-distance measurements. *Ultramicroscopy.* **75** (1998) 171-181.
23. Jourdan, J. S., Cruchon-Dupeyrat, S. J., Huan, Y., Kuo, P. K., and Liu, G. Y. Imaging nanoscopic elasticity of thin film materials by atomic force microscopy: effects of force modulation frequency and amplitude. *Langmuir.* **15** (1999) 6495-6504.
24. Fritz, M., Radmacher, M., Petersen, N., and Gaub, H. E. Visualization and identification of intracellular structures by force modulation microscopy and drug induced degradation. *J. Vac. Sci. Technol. B.* **12** (1994) 1526-1529.

25. Argaman, M., Golan, R., Thomson, N. H., and Hansma, H. G. Phase imaging of moving DNA molecules and DNA molecules replicated in the atomic force microscope. *Nucl. Acids. Res.* **25** (1997) 4379-4384.
26. A-Hassan, E., Heinz, W. F., Antonik, M. D., D'Costa, N. P., Nageswaran, S., Schönenberger, C. A., and Hoh, J. H. Relative microelastic mapping of living cells by atomic force microscopy. *Biophys. J.* **74** (1998) 1564-1578.
27. Nagao, E., and Dvorak, J. A. Phase imaging by atomic force microscopy: analysis of living homoeothermic vertebrate cells. *Biophys. J.* **76** (1999) 3289-3297.
28. Holland, N. B., and Marchant, R. E. Individual plasma proteins detected on rough biomaterials by phase imaging AFM. *J. Biomed. Mater. Res.* **51** (2000) 307-315.

1.2 Quasistatic Force Spectroscopy

1.2.1 Introduction

Understanding the forces at the level of single biomolecules and/or their complexes is a challenging task in molecular and structural biology. The direct and quantitative examination of the bonds holding a molecular structure together on the single molecule level can be achieved, for example, by applying of force to individual molecules locally. Experiments of this kind, taken on individual molecules, have been called force spectroscopy [1-7]. In our study, the force spectroscopy experiments were carried out by AFM. As known, the AFM has several properties that make it an ideal tool for measuring biomolecular forces on the single molecule level: force sensitivity on the pN ($1 \text{ pN} = 10^{-12} \text{ N}$) level with high lateral sensitivity of 0.5-1 nm (which is the realm of molecular dimensions), contact areas as small as 10 nm^2 , ability to operate under physiological conditions, and, of course, relative ease to use and commercial availability. A true milestone in force spectroscopy using AFM was the first measurements of the rupture forces of individual biotin complexes by Gaub's and Colton's groups [1-3a], the measurement of the forces holding together complementary DNA strands [3b] and the measurements of the binding strength between cell-adhesion proteoglycans [4].

In this technique one molecule of interest is attached to the sample surface and the other is anchored to the AFM tip. This put several requirements for tip and sample functionalization. Please note that a proper functionalization of the tip and sample is crucial for force spectroscopy experiments. Designing an appropriate chemistry of our experiments is discussed in details in chapter II describing tip and sample preparation methods.

As discussed in chapter I "AFM principles", the tip deflections are used to record a topographic image. If the probe is moved in z-direction down and up (toward and away from the

surface), the measured tip deflections can be used also to create the so-called force curve (force-distance curve).

1.2.2 Force curves

Force curve is the resultant plot of cantilever deflection versus the separation between the relaxed tip position and the sample (displacement of the z-piezo, z). In the most common analysis, cantilever deflections are converted into forces using Hook's law:

$$F = k_{cantilever} \cdot z_{cantilever}$$

where F - is the force acting on the cantilever, $k_{cantilever}$ - the spring constant of the cantilever, and $z_{cantilever}$ - the cantilever deflection. The accuracy of the cantilever spring constant value is uncertain, unless independent calibration is made [8-10].

A typical force curve (force versus z distance) is shown in fig. 1.

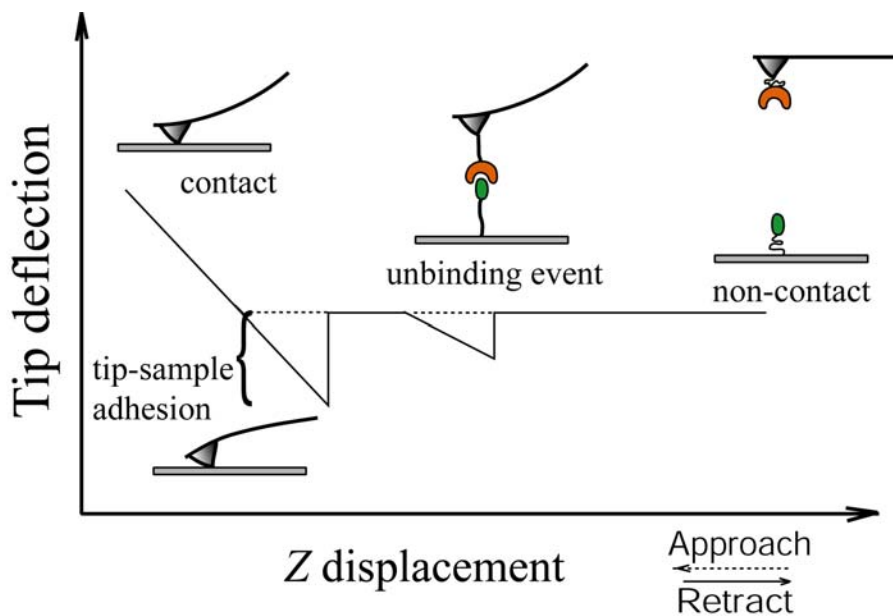


Figure 1. Schematic drawing of a typical force curve.

Initially, when the tip is far from the surface, there is no interaction (non-contact). As the tip-sample separation distance is reduced, forces between atoms/molecules on the two surfaces cause the bending of the cantilever toward the sample, in the case of attractive forces (van der Waals and electrostatic), or away from the sample, in the case of repulsive forces (electrostatic). At each z distance, the cantilever bends until its elastic (restoring) force equals the tip-sample interaction force and the system is in equilibrium. The attractive forces may be sufficient to cause the jump-to-contact of the tip. During the contact with the surface, the tip will feel an increasing repulsive force. In this contact region of the force curve, there may be elastic (reversible) and/or plastic (irreversible) deformations of either or both of the tip and the sample. These deformations provide further additional information about the mechanical properties of the sample [11-16]. When the preset value for the load is reached, the direction of motion is reversed, and the tip is moved away from the surface. During the retraction of the tip, contact adhesion forces may delay tip-surface separation (adhesion), which can be detected in the retraction curve (jump-off-contact). Jump-off contact events occur when the effective elastic constant of the cantilever overcomes all the adhesive interactions between the tip and the sample. This force can be used to compare surface-dependent interactions or specific molecular unbinding events.

1.2.2a Force resolution of the AFM

An AFM cantilever with a given spring constant, $k_{cantilever}$, is agitated by thermal fluctuations. In a simple model, the cantilever can be represented as a system with one degree of freedom, i.e. the cantilever can only vibrate up and down. Therefore, the energy of this thermal vibration will be given by the equipartition theorem of classical thermodynamics as $\frac{1}{2}k_B T$, where k_B is the

Boltzmann constant and T is the absolute temperature. The energy of a vibrating spring can be written as $\frac{1}{2}k_{cantilever} \cdot \langle x^2 \rangle$, where $\langle x \rangle$ is the amplitude of vibration. Both energies are equal, and thus, one can obtain the following equation:

$$\frac{1}{2}k_B T = \frac{1}{2}k_{cantilever} \langle x^2 \rangle$$

Consequently, the cantilever will vibrate thermally with amplitude $\langle x \rangle$, given by

$$\langle x \rangle = \sqrt{\langle x^2 \rangle} = \sqrt{\frac{k_B T}{k_{cantilever}}}$$

This will lead to a fluctuation in force given by:

$$\Delta F = k_{cantilever} \langle x \rangle = \sqrt{k_B T \cdot k_{cantilever}}$$

The dependency of the cantilever thermal vibration amplitude and of the force fluctuation under the given cantilever spring constant at 25 °C, is shown in fig. 2.

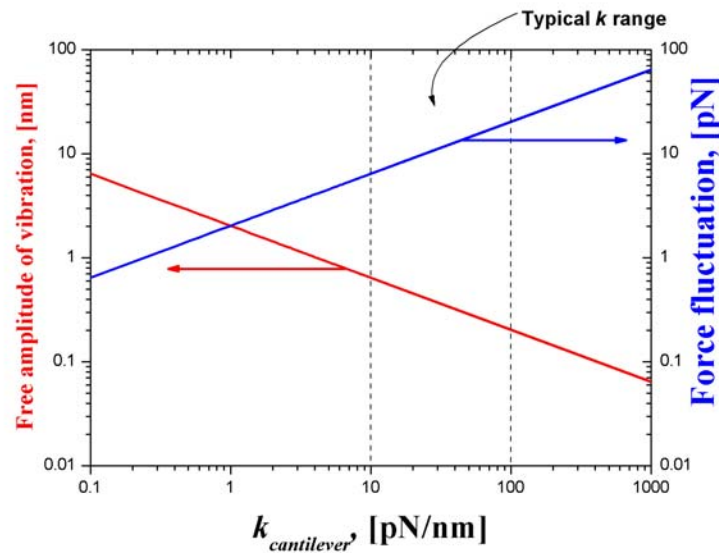


Figure 2. Thermal vibration of AFM cantilevers at room temperature (25 °C). This vibration limits the vertical resolution and the force resolution of the AFM. For typical soft cantilevers (10 to 100 pN/nm), the thermal vibration amplitudes of the free cantilevers varies from 0.64 to 0.2 nm, respectively. These values correspond to force fluctuations between 6 pN and 20 pN, giving a lower limit of force resolution in AFM.

1.2.3 Application of force curves

The interpretation of AFM force curves relies almost entirely on established force laws [17]. These force laws describe force as a function of the tip-sample separation distance, d , rather than as a function of z -piezo displacement. Therefore, the AFM force curves should be transformed into the description of the force as a function of distance, $F(d)$. The transformation to d can be done on the hard surface by subtracting the contact line from the cantilever deflection [18]. A corrected $F(d)$ curve is then called a force-distance curve.

Thus, a complete force curves set consists of successive approach and retraction curves. They are rich in information. For example, the approach curve can contain valuable information about following surface forces: van der Waals force, repulsive electrostatic double-layer force in solution, polymer-brushing forces, and indentation curve on an elastic sample [19]. From the retraction curve, one can observe contact adhesion forces, capillary effect, polymer extension (force-extension curve), and specific molecular bond rupture (unbinding) and/or in some experiments combination of them. Several excellent reviews have been written on the applications of force-distance curves [20-22].

1.2.4 Energies and rates of a molecular reaction

Another interesting question addresses the relationship between the data obtained from single molecule force spectroscopy measurements and the quantities classically obtained in bulk, such as the energies and rates of reaction. From force spectroscopy data one can distinguish two fundamental classes of reactions: first, reactions which proceed at (quasi-)equilibrium and second, those that do not. For both classes, simple models have been developed in order to relate the single molecule force measurements to bulk quantities.

1.3.4a Equilibrium reactions

In equilibrium reactions the system can access all its energy configurational states on the time scale of the experiment and, thus, proceeds on a path along the lowest energy states. If the time scale of the experiment is getting faster than the time scales of the transformation, the equilibrium condition breaks down. Thus, if a force-induced reaction proceeds at equilibrium, the rate at which the force is ramped will not change the force at which the transformations occur. For these equilibrium reactions, the free enthalpy ΔH can be extracted by integrating the area under the force-distance curves. The well-known examples of such reactions are the conformation in polysaccharide chains [23-25], the B-S form transformation of DNA [26, 27], and the unzipping and re-zipping the two strands of double stranded (ds) DNA [6].

1.3.4b Far from equilibrium reactions

This second class of reactions describes the transformation when the application of forces causes a thermodynamically irreversible change. In these reactions, there is usually hysteresis. More important, the force at the bond rupture can depend on the rate at which the force is applied (loading rate). To describe the rupture of weak bonds under a force, a simple transition state model was developed by Bell [28]. This basic approach was further refined by Evans and Ritchie in 1997 [29]. Conceptually, this can be described by treating the unbinding reaction as probabilistic process induced by a thermal kick over the activation barrier. At very slow force rates, the system has simply more attempts to make the transition than at faster force rates, and, thus the bond rupture will occur at lower forces than at higher rates. The unfolding of proteins [30-32], ligand-receptor couples [33-40], unbinding process of adsorbed proteins [41], and the shearing [42] and melting of DNA [26, 27] were successfully described by this model. The

following paragraph will focus in more details on the description of simple model of ligand-receptor separation, where a single energy barrier governs the unbinding process.

1.2.4b/1 Force spectroscopy of simple bonds

Molecular recognition of biomolecules plays a pivotal role in nature. Interactions occur during the formation of double-stranded DNA, in enzymatic reactions, in antigen-antibody (Ag-Ab) recognition events, in hormone-receptor reactions, in signal transduction, in adhesion and migration of cells and etc. The nature of ligand-receptor specific binding forces comes generally from the combination of non-covalent weak bonds: van der Waals, electrostatic, hydrophobic, dipole-dipole interactions, and hydrogen bonding. These binding forces depend on the conditions such as pH and ionic strength. Besides the thermodynamic and kinetic data, the complex interaction of forces is of a paramount interest for understanding the structure-function relationships of biomolecules.

Most systems can be approximated by a simplest system (fig. 3) consisting of only two states, A (bound state) and B (unbound state), which are separated by one transition state characterized by a single energy barrier. To describe the reaction (1),



the following quantities are traditionally determined in bulk:

$$\text{- the dissociation rate constant, } k_{diss} = \nu_{diss} \exp\left(-\frac{\Delta G_{diss}}{k_B T}\right), \quad (2)$$

$$\text{- the association rate constant, } k_{ass} = \nu_{ass} \exp\left(-\frac{\Delta G_{ass}}{k_B T}\right), \quad (3)$$

- the equilibrium constant (or affinity constant), $K_{eq} = \frac{k_{diss}}{k_{ass}}$, (4)

- the free energy of the reaction ΔG° : $\Delta G^\circ = \Delta H - T\Delta S = RT \ln K_{eq}$ (5)

where k_B is the Boltzmann constant, T is absolute temperature, and ν is the pre-exponential factor which denotes the frequency of bond vibrations, and is generally different for the association and dissociation reactions.

Bell first introduced a simple model of bond rupture under an applied external force based on the transition-state theory [28]. The lifetime of non-covalent bonds ($1/k_{diss}(0)$) in the absence of external forces is considerably high. However, pulling long enough at one or the other end with an external force may eventually help the system to overcome the potential barrier by thermal fluctuations, and, thus breaks the bond. From a chemical point of view, pulling a receptor-ligand pair apart can be compared with an infinite dilution of both compounds. The system is far away from thermal equilibrium and from a kinetic viewpoint the rate constant of dissociation is meaningful, the probability of rebinding is zero. According to Bell, if the applied force F is in the direction favoring the unbound state B, the activation energies are changed to $\Delta G^*_{diss} = \Delta G_{diss} - F \cdot x_{diss}$ and $\Delta G^*_{ass} = \Delta G_{ass} - F \cdot (-x_{ass})$. The proportionality factor x has the dimension of length and can be interpreted as the width of the potential. We have to note that x_{ass} is negative if the force is applied in the direction of B state. Thus, the rate constants k_{diss} and k_{ass} change to

$$k_{diss}(F) = \nu_{diss} \exp\left(-\frac{1}{k_B T} \left(\Delta G - \int_0^{x_{diss}} F dx\right)\right) = k_{diss}(0) \exp\left(\frac{F \cdot x_{diss}}{k_B T}\right) \quad (6)$$

and

$$k_{ass}(F) = k_{ass}(0) \exp\left(-\frac{F \cdot x_{ass}}{k_B T}\right) \quad (7)$$

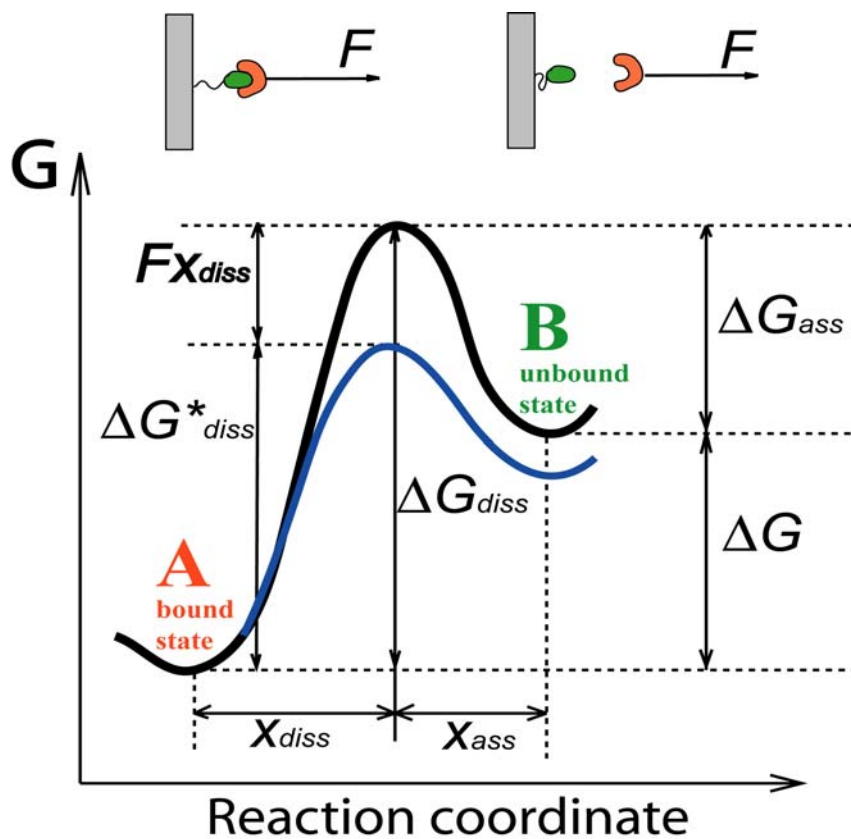


Figure 3. Simple two state model consisting of bound state A and unbound state B. The unbinding reaction proceeds via a transition state with a characteristic energy barrier. An applied force lowers the energy barrier by Fx_{diss} , where x_{diss} is the width of the potential of a particular state (blue line).

The rates change exponentially with the applied force: the dissociation rate, k_{diss} , increases exponentially while the association rate, k_{ass} , decreases exponentially. This is the hallmark of the Bell model.

Assuming that the applied force F increases linearly with a constant loading rate r , (i.e. $dF/dt=r$ and $F=r \cdot t$) the probability $p(t)$ that the system is in the bound state A after time t can be calculated by solving the following equation:

$$\frac{dp(t)}{dt} = -k_{diss}(F) \cdot p(t) \quad (8)$$

with $p(t=0)=1$.

This results in a distribution of unbinding forces (or a probability density ω)

$$\omega(F) = \frac{dp(F/r)}{dF} = \frac{k_{diss}(F)}{r} p(F/r) \quad (9)$$

which results with $p(t=0)=1$ in

$$\omega(F) = \frac{k_{diss}(0)}{r} \exp\left(\frac{F \cdot x_{diss}}{k_B T} + \frac{k_{diss}(0)}{r} \frac{k_B T}{x_{diss}} \left(1 - \exp\left(\frac{F x_{diss}}{k_B T}\right)\right)\right) \quad (10)$$

By definition the most probable unbinding force is the maximum of the distribution (10) and is given by the following equation:

$$\boxed{F^*_{unbinding}(r) = \frac{k_B T}{x_{diss}} \ln\left(\frac{r}{k_{diss}(0)} \frac{x_{diss}}{k_B T}\right)} \quad (11)$$

The equation (11) relates single molecule force measurements with the dissociation rate measured in bulk experiments. It is based on Bell's assumption that the rates of a reaction depend exponentially on the applied force as stated in eq. 6 and 7. Eq. 11 shows that the dissociation kinetics under an applied force are governed by the thermal dissociation rate constant $k_{diss}(0)$ and the length scale x_{diss} , interpreted to be the width of the potential of the bound state. In practical terms, this means that $k_{diss}(0)$ and x_{diss} can be determined by plotting $F^*_{unbinding}$ versus $\ln(r)$.

The width of the distribution (11) depends on the width of the potential x_{diss} and the thermal energy $k_B T$. A more elaborated description of this issue is given by Evans and Ritchie [29]. When the frictional losses, arising from intrinsic and hydrodynamic damping, are considered, the rate of dissociation can be expressed as:

$$k_{diss}(F) = k_{diss}(0) \cdot g(F) \cdot \exp\left(\frac{\Delta\Delta E^*(F)}{k_B T}\right) \quad (12)$$

in which $g(F)$ and $\Delta\Delta E^*(F)$ represent the deformation of the potential under the influence of the external force and molecular friction, respectively. Consequently, increasing the loading rate results in a shift in the distribution (11) to higher unbinding forces and is accompanied by a broadening of the function. Statistical analysis of the unbinding forces provides the rupture force of the non-covalent bond, which is defined as the most probable occurring in the histogram at a certain loading rate. The assumption of a stationary force $F^*_{unbinding}$ is valid, since thermal fluctuations take place within a time scale of 10^{-12} s or shorter, while the mechanical loading in force probe experiences spans periods of about $10^{-3} - 10^{-5}$ s and is therefore extremely slow compared to thermal fluctuations.

In reality, however, not all force spectroscopy measurements can be fitted to a simple two-state model. This is the case of the avidin-biotin [43] and the streptavidin-biotin [44] systems and some others receptor-ligand pairs [45-48] where there is more than one transition state. Some theoretical approaches of complex molecular bonds have been presented [49, 50].

In conclusion, force spectroscopy complements classical methods to determine the kinetics of ligand-receptor pairs and provides new insights into the energy landscape of the bond. Care must be taken when comparing off-rates statically determined to those which are dynamically determined. In certain examples they may agree in the force-zero extrapolation if only a single barrier exists. Another often disregarded issue is the fact that receptor-ligand pairs,

being free in solution, may display different binding properties than those covalently anchored to the tip and substrate and give rise to steric hindrance and, hence, different off-rates.

References

1. Florin, E-L., Moy, V. T., and Gaub, H. E. Adhesion forces between individual ligand-receptor pairs. *Science*. **264** (1994) 415-417.
2. Moy, V. T., Florin, E-L., and Gaub, H. E. Intermolecular forces and energies between ligands and receptors. *Science*. **266** (1994) 257-259.
3. a) Lee, G. U., Chrisey, L. A., and Colton, R. J. Sensing discrete streptavidin-biotin interactions with AFM. *Langmuir*. **10** (1994) 354-357.
b) Lee, G. U., Chrisey, L. A., and Colton, R. J. Direct measurement of the forces between complementary strands of DNA. *Science*. **266** (1994) 771-773.
4. Dammer, U., Popescu, O., Wagner, P., Anselmetti, D., Guntherodt, H. J., and Misevic, G. N. Binding strength between cell-adhesion proteoglycans measured by Atomic Force Microscopy. *Science*. **267** (1995) 1173-1175.
5. Evans, E., Ritchie, K., and Merkel, R. Sensitive force technique to probe molecular adhesion and structural linkages at biological interfaces. *Biophys. J.* **68** (1995) 2580-2587.
6. Essevez-Roulet, B., Bockelmann, U., and Heslot, F. Mechanical separation of the complementary strands of DNA. *Proc. Natl. Acad. Sci. USA*. **94** (1997) 11935-11940.
7. Stout, A. L. Detection and characterization of individual intermolecular bonds using optical tweezers. *Biophys. J.* **80** (2001) 2976-2986.
8. Hutter, J. L., and Bechhoefer, J. Calibration of AFM tips. *Rev. Sci. Instrum.* **64** (1993) 1868-1873.
9. Cleveland, J., Manne, S., Bocek, D., and Hansma, P. K. A nondestructive method for determining the spring constant of cantilevers for scanning force microscopy. *Rev. Sci. Instrum.* **64** (1993) 403-405.
10. Senden, T. J. and Ducker, W. A. Experimental determination of spring constants in AFM. *Langmuir*. **10** (1994) 1003-1004.
11. Engel, A., Lyubchenko, Y., and Müller, D. AFM: a powerful tool to observe biomolecules at work. *Trends Cell Biol.* **9** (1999) 77-80.
12. Ludwig, M., Rief, M., Schmidt, L., Li, H., Oesterhelt, F., Gautel, M., and Gaub, H. E. AFM, a tool for single-molecule experiments. *Appl. Phys. A.* **68** (1999) 173-176.

13. Li, H., Rief, M., Oesterhelt, F., and Gaub, H. E. Force spectroscopy on single xanthan molecules. *Appl. Phys. A.* **68** (1999) 407-410.
14. Fisher, T. E., Marszalek, P. E., Oberhauser, A. F., Carrion-Vazquez, M., and Fernandez, J. M. The micro-mechanics of single molecules studied with AFM. *J. Physiol.* **520** (1999) 5-14.
15. Fisher, T. E., Oberhauser, A. F., Carrion-Vazquez, M., Marszalek, P. E., and Fernandez, J. M. The study of protein mechanics with AFM. *TIBS.* **24** (1999) 379-384.
16. Fisher, T. E., Marszalek, P. E., and Fernandez, J. M. Stretching single molecules into novel conformations using the AFM. *Nature Struct. Biol.* **7** (2000) 719-723.
17. Israelachvili, J. N. Intermolecular and surface forces. Academic Press, New York, 1992.
18. Butt, H-J. Measuring local surface charge densities in electrolyte solutions with a scanning force microscope. *Biophys. J.* **63** (1992) 578-582.
19. Heinz, W. F., and Hoh, J. H. Spatially resolved force spectroscopy of biological surfaces using the AFM. *Trends in Biotechnology.* **17** (1999) 143-150.
20. Cappella, B., and Dietler, G. Force-distance curves by AFM. *Surf. Sci.Rep.* **34** (1999) 1-104.
21. Leckband, D. Force as a probe of membrane protein structure and function. *Curr. Opin. Struct. Biol.* **11** (2001) 433-439.
22. Janshoff, A., Neitzert, M., Oberdörfer, Y., and Fuchs, H. Force spectroscopy of molecular systems-single molecule spectroscopy of polymers and biomolecules. *Angew. Chem. Int. Ed.* **39** (2000) 3212-3237.
23. Rief, M, Oesterhelt, F., and Gaub, H. E. Single molecule force spectroscopy on polysaccharides by AFM. *Science.* **275** (1997) 1295-1297.
24. Marszalek, P. E., Oberhauser, A. F., Pang, Y. P., and Fernandez, J. M. Polysaccharide elasticity governed by chair-boat transitions of the glucopyranose ring. *Nature.* **396** (1998) 661-664.
25. Zou, S., Zhang, W., Zhang, X., and Jiang, B. Study on polymer micelles of hydrophobically modified ethyl hydroxyethyl cellulose using single-molecule force spectroscopy. *Langmuir.* **17** (2001) 4799-4808.
26. Rief, M., Clausen-Schaumann, H, and Gaub, H. E. Sequence-dependent mechanics of single DNA molecules. *Nature Struct. Biol.* **6** (1999) 346-349.
27. Clausen-Schaumann, H., Rief, M., Tolksdorf, C., and Gaub, H. E. Mechanical stability of single DNA Molecules. *Biophys. J.* **78** (2000) 1997-2007.

28. Bell, G. I. Models for the specific adhesion of cells to cells. *Science*. **200** (1978) 618-627.
29. Evans, E., and Ritchie, K. Dynamic strength of molecular adhesion bonds. *Biophys J*. **72** (1997) 1541-1555.
30. Fong, S., Hamill, S. J., Proctor, M., Freund, S. M. V., Benian, G. M., Chothia, C., Bycroft, M., and Clarke, J. Structure and stability of an immunoglobulin superfamily domain from titin, a muscle protein of the nematode *Caenorhabditis elegans*. *JMB*. **264** (1996) 624-639.
31. Rief, M. Gautel, M., Fernandez, J. M., and Gaub, H. E. Reversible unfolding of individual titin immunoglobulin domains by AFM. *Science*. **276** (1997) 1109-1112.
32. Oberhauser, A. F., Marszalek, P. E., Erickson, H. P., and Fernandez, J. M. The molecular elasticity of the extracellular matrix protein tenascin. *Nature*. **393** (1998) 181-185.
33. Fritz, J., Katopodis, F., Kolbinger, F., and Anselmetti, D. Force-mediated kinetics of single P-selectin/ligand complexes observed by AFM. *Proc. Nat. Acad. Sci. USA*. **95** (1998) 12283-12288.
34. Carrion-Vazquez, M., Oberhauser, A. F., Fowler, S. B., Marszalek, P. E., Broedel, S. E., Clarke, J., and Fernandez, J. M. Mechanical and chemical unfolding of a single protein: A comparison. *Proc. Nat. Acad. Sci. USA*. **96** (1999) 3694-3699.
35. Schwesinger, F., Ros, R., Strunz, T., Anselmetti, D., Guntherodt, H. J., Honegger, A., Jermutus, L., Tiefenauer, L., and Plückthun, A. Unbinding forces of single antibody-antigen complexes correlate with their thermal dissociation rates. *Proc. Nat. Acad. Sci. USA*. **97** (2000) 9972-9977.
36. Baumgarthner, W., Hinterdorfer, P., Ness, W., Raab, A., Vestweber, D., Schindler, H., and Drenckhah, D. Cadherin interaction probed by AFM. *Proc. Nat. Acad. Sci. USA*. **97** (2000) 4005-4010.
37. Evans, E., and Ludwig, F. Dynamic strengths of molecular anchoring and material cohesion in fluid biomembranes. *J. Phys. Condens. Matter*. **12** (2000) A315-A320.
38. Dettmann, W., Grandbois, M., André, S., Benoit, M., Wehle, A. K., Kaltner, H., Gabius, H-J., and Gaub, H. E. Differences in zero-force and force-driven kinetics of ligand dissociation from β -Galactoside-specific proteins (plant and animal lectins, IgG) monitored by plasmon resonance and dynamic single molecule force microscopy. *Arch. Biochem. Biophys*. **383** (2000) 157-170.

39. Lee, I., and Marchant, R. E. Force measurement on the molecular interactions between ligand (RGD) and human platelet $\alpha_{IIb}\beta_3$ receptor system. *Surf. Sci.* **491** (2001) 433-443.
40. Yersin, A., Hirling, H., Steiner, P., Magnin, S., Regazzi, R., Hüni, B., Huguenot, P., De Los Rios, P., Dietler, G., Catsicas, S., and Kasas, S. Interactions between synaptic vesicle fusion proteins explored by AFM. *Proc. Nat. Acad. Sci. USA.* **100** (2003) 8736-8741.
41. Gergely, C., Voegel, J.-C., Schaaf, P., Senger, B., Maaloum, M., Hörber, J. K. H., and Hemmlé, J. Unbinding process of adsorbed proteins under external stress studied by AFM. *Proc. Nat. Acad. Sci. USA.* **97** (2000) 10802-10807.
42. Strunz, T., Oroszlan, K., Schäfer, R., and Güntherodt, H.-J. Dynamic force spectroscopy of single DNA molecules. *Proc. Nat. Acad. Sci. USA.* **96** (1999) 11277-11282.
43. Merkel, R., Nassoy, P., Leung, A., Ritchie, K., and Evans, E. Energy landscapes of receptor-ligand bonds explored by dynamic force spectroscopy. *Nature.* **397** (1999) 50-53.
44. Yuan, C., Chen, A., Kolb, P., and Moy, V. T. Energy landscape of streptavidin-biotin complexes measured by AFM. *Biochemistry.* **39** (2000) 10219-10223.
45. Strigl, M., Simson, D. A., Kacher, C. M., and Merkel, R. Force-induced dissociation of single protein A-IgG bonds. *Langmuir.* **15** (1999) 7316-7324.
46. Simson, D. A., Strigl, M., Hohenadl, M., and Merkel, R. Statistical breakage of single protein A-IgG bonds reveals crossover from spontaneous to force-induced bond dissociation. *Phys. Rev. Lett.* **83** (1999) 652-655.
47. Evans, E., Leung, A., Hammer, D., Simon, S. Chemically distinct transition states govern rapid dissociation of single L-selectin bonds under force. *Proc. Natl. Acad. Sci. USA.* **98** (2001) 3784-3789.
48. Bartels, F. W., Baumgarth, B., Anselmetti, D., Ros, R., and Becker, A. Specific Binding of the regulatory protein ExpG to promoter regions of the galactoglucan biosynthesis gene cluster of *Sinorhizobium meliloti* – a combined molecular biology and force spectroscopy investigation. *J. Struct. Biol.* **143** (2003) 145-152.
49. Strunz, T., Oroszlan, K., Schumakovitch, I., Güntherodt, H.-J., and Hegner, M. Model energy landscapes and the force-induced dissociation of ligand-receptor bonds. *Biophys. J.* **79** (2000) 1206-1212.
50. Evans, E. Probing the relation between force-lifetime-and chemistry in single molecular bonds. *Annu. Rev. Biophys. Biomol. Struct.* **30** (2001) 105-128.

Chapter II

Sample and Tip Preparation Methods for Force

Spectroscopy Study

2.1 Sample preparation for force spectroscopy experiments

The first step to the force spectroscopy measurements of receptor-ligand interactions is immobilization of receptor molecules on the AFM tip and ligand molecules on the sample surface or vice versa. Therefore, the chemistry of the AFM tip and sample surfaces, with functionalization procedures, is essential for FS studies. In this chapter we will focus on the description of sample surface, sample and tip preparation methods as well sample characterization with the AFM.

Glass, mica, silicon (Si), gold surfaces and hydrophobic highly oriented pyrolytic graphite (HOPG) are widely used to immobilize samples, allowing biomolecules to be bound strongly or even crosslinked covalently to the support. Mica was selected for our studies because it is the most commonly used support for imaging biological specimens with the AFM.

2.1.1 Mica

Mica is an aluminosilicate mineral with layered structure and reveals after cleavage an atomically flat surface over several hundred μm^2 . Mica consists of negatively charged layers which are bound together by large, positively charged interlayer cations, K^+ in the case of muscovite mica (Na^+ in paragonite mica). Each stratum consists of two hexagonal layers of SiO_4 , which are cross linked by aluminum atoms with incorporated OH^- groups (fig. 1).

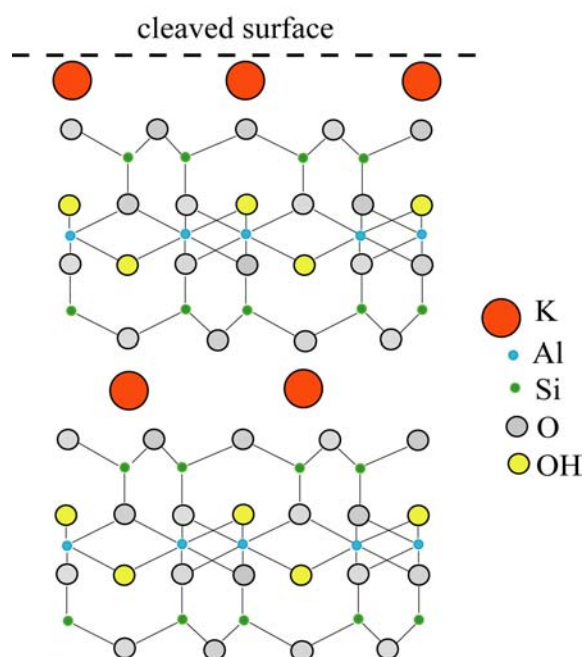


Figure 1. The structure of a vertical slice through freshly cleaved muscovite mica.

The electrostatic bonds, between K^+ ions and basal oxygens from the layer, are weak and easily broken. This layer is disrupted after a simple cleavage procedure with a “scotch” tape, exposing a basal plane covered by K^+ ions, with the density of 0.57 ions/nm^2 [1, 2]. In air, this layer is completely neutralized by

the negative aluminosilicate lattice charge. However, in water some of the K^+ ions dissociate from the surface, which results in a negative surface charge density of $0.015 \text{ charges/nm}^2$ at pH 7.0 (neutral) [3]. The extent of dissociated and partially replaced K^+ ions depends on the electrolyte concentration [3]. Many proteins bind tightly to a clean mica surface because of the large surface charge and hydrogen binding between protein and surface. For our AFM experiments we have been used muscovite mica sheets (Ted Pella, Inc., Redding, USA).

2.1.2 Silanization method (APTES-mica)

The protein immobilization onto a substrate surface was preceded by the silanization procedure. Today, silane coupling is one of the most used coupling methods for preparation of biosensing devices. The alkylsilanes form self-assembled monolayers (SAMs) and have attracted attention because they are capable of covalent attachment to SiO_2 -based oxide surfaces such as glass or oxidized Si, thus making them positively charged [4, 5]. We use 3-aminopropyltriethoxy silane (APTES) (99% purum, Fluka) to functionalize the mica surface, which also contains Si-O bonds.

The amino groups ($-\text{NH}_2$) of APTES after exposing to a water solution become positively charged ($-\text{NH}_3^+$) in a rather broad range of pH (aliphatic amino groups have a pK of around 10.5). It was shown that the silanization of surfaces by chemical-vapor deposition of alkoxy silanes generally produces a smoother and more stable SAM (without “vertical” polymerization [6]) than it was obtained by liquid-phase deposition [7, 8]. In our study we used chemical-vapor APTES deposition in a vacuum chamber. The conditions for uniform and smooth modification of the surface were found. This procedure was first described by Lyubchenko and co-workers [9, 10]. Briefly, this method consists of incubation in 2 L glass desiccator of freshly cleaved mica sheets in the vapor of 30 μl of APTES in the presence of 10 μl N-ethyldiisopropylethylamine (DIPEA) (purum, Fluka) under argon atmosphere during 2h. DIPEA works as a proton scavenger to prevent undesirable polymerization of APTES. APTES molecules are in amine-up configuration and about 50% of these amines are active (protonated, $-\text{NH}_3^+$) [11]. The scheme of modification with APTES (ideal case) is shown in fig 2. APTES-mica substrates are now ready for covalent immobilization of proteins. APTES-mica samples stored under argon show stability and retain their activity for several weeks.

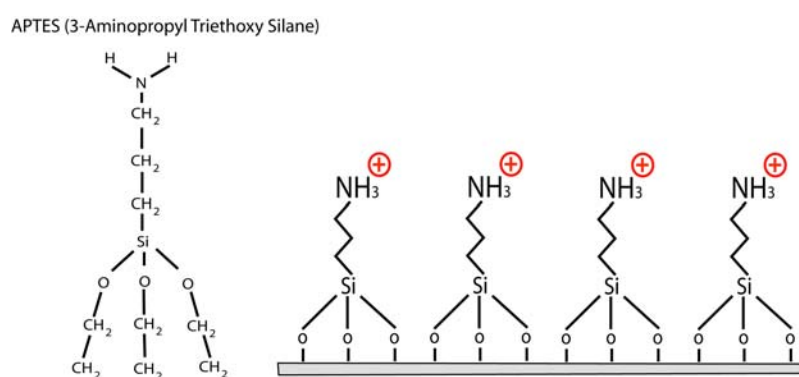


Figure 2. APTES monolayer self-assembled (ideal case) on mica surface.

2.1.2a Characterization of APTES-mica samples by AFM

To check whether APTES was firmly adsorbed on mica surface and to know the thickness of the silane layer, the sweeping method was used. This simple method is widely used for rough and rapid estimation of thickness of adsorbed proteins with the AFM [12]. In this method, the AFM tip first scanned several times a small part of the surface area ($500 \times 500 \text{ nm}^2$) with the increased loading force (several nN) at a scanning speed of 2 Hz. When no further change in the z height of the image was observed, the AFM image was zoomed out a large area ($1.5 \times 1.5 \text{ }\mu\text{m}^2$) and rescanned with normal loading forces and scanning speed of 1.5 Hz (fig. 3). The APTES+glutaraldehyde layer thickness is determined by measuring the height difference between altered and the unaltered area in the image. Thus the layer thickness was roughly estimated and gave a result of about 2 nm. This result is in a good agreement with other experimental data already published [4, 5, 13]. Taking account the length of covalent bond C-C (1.54 \AA) the thickness of APTES+glutaraldehyde layer can be estimated as the length of 13 covalent bonds that gives us the result of 2 nm.

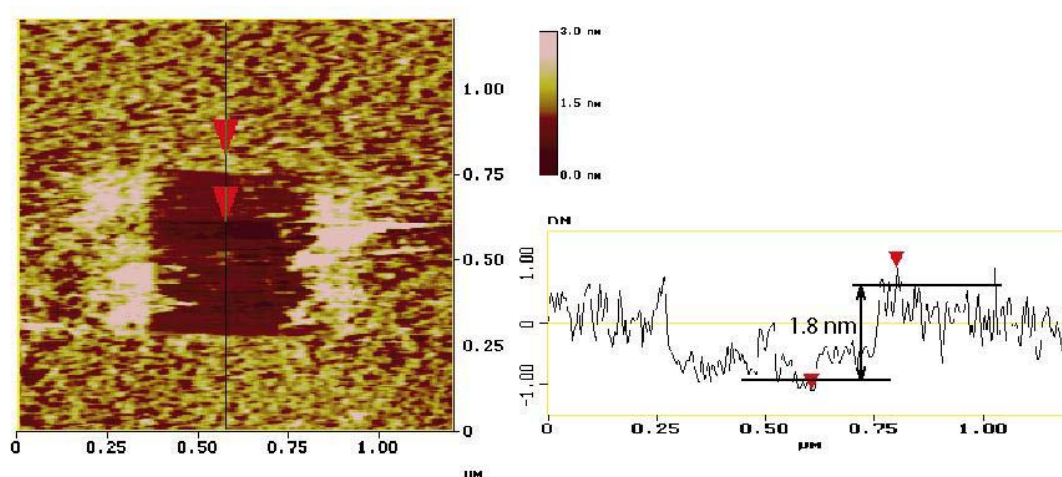


Figure 3. AFM contact image of the APTES+glutaraldehyde-mica surface. In the central surface area of $500 \times 500 \text{ nm}^2$ has undergone scanning at a high loading force.

2.1.3 Functionalization of APTES-mica with proteins

Protonated reactive amino groups of APTES were covalently coupled with protein amino groups via glutaraldehyde molecules (fig. 4). The silanized substrates were reacted with 1% (v/v) glutaraldehyde (Fluka) solution in water for 20 minutes and then rinsed extensively several times with deionized water to remove any unreacted glutaraldehyde molecules. Consecutively, the protein solution drop (1 mg/ml) was deposited onto the sample surface for 20 minutes at room temperature. The unreacted protein molecules were removed by extensive washing with phosphate buffered saline buffer (PBS, 50 mM phosphate, 150 mM NaCl, pH 7.4 at 25 °C) (Sigma). This functionalization method is known to keep proteins functionality intact [14].

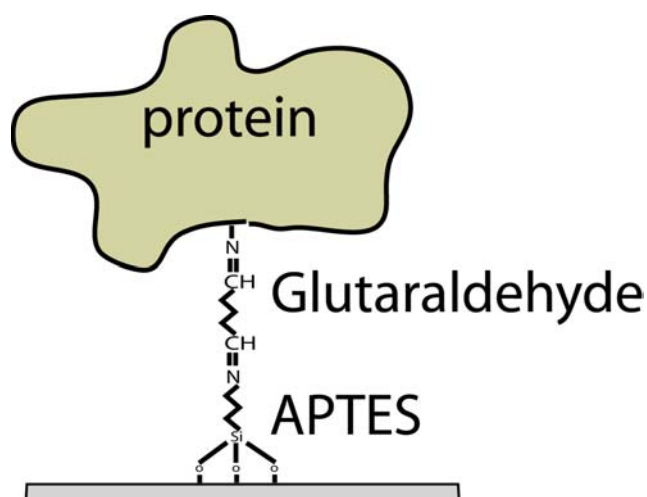


Figure 4. Schematic drawing of protein immobilization onto APTES-mica via glutaraldehyde molecule.

2.2 Tip preparation for Force Spectroscopy experiments

Standard V-shaped Si₃N₄ (silicon nitride) cantilevers (Veeco Instruments, USA), having a length of 200 μm and a nominal spring constant of 0.06 N/m are used for our FS studies.

2.2.1 Tip cleaning

To produce reliable and reproducible results in topographic AFM imaging and in various FS experiences, a perfectly clean AFM tip, or at least AFM tip with a known chemistry is necessary. Cleanliness is also important for the quality and effectiveness of further surface modification on the AFM tip. Thin layers of contaminants may change the reactivity or adsorptive abilities of surfaces so that the desired modifications may not really be carried out on surfaces. Many procedures for cleaning the tip have been developed. Such procedures include ultraviolet (UV) ozone treatment, aggressive acid-based baths [15-17], and plasma etching [12, 14, 18, 19]. Other groups use as-received cantilevers with only simple cleaning methods such as rinsing with detergent and organic solvents or even no cleaning at all.

Three different procedures were used to clean the AFM tips. In the first method, the tips were carefully washed with a very dilute detergent solution, rinsed extensively with deionized ultra high quality (UHQ) (resistivity 18 M Ω cm) water several times, then immersed in acetone for 5 minutes, and finally irradiated with UV light for 30 minutes. The second method comprises the plasma etching. The tips were placed in plasma (2×10^{-2} mbars, 750 V) during 1 min. During this procedure the gold coating on the back of the cantilevers remains intact. The third, and more aggressive method, consists of incubation tips in piranha solution (70% H₂SO₄, 30% H₂O₂) for 30 min. Both sulfuric acid (H₂SO₄) and hydrogen peroxide (H₂O₂) are powerful oxidizing agents which react rapidly with almost any kind of organic compound. One of the products of this type of reaction is hydrogen gas. Immediately after the immersion of tips into piranha solution, visible gaseous bubbles evolved from the cantilevers, indicating the presence of organic contaminants on the surfaces. In some cases, the gold coating on the back side of the tip is peeled away in the course of incubation. After 30 min of incubation, the tips are rinsed with copious amounts of

deionized UHQ water, and dried at 150 ° C. Unfortunately and oppositely to the observations of Lo and coworkers [20], our tips showed not enough laser reflection for subsequent use in AFM, and we were not able to use these tips at all.

All cleaned tips were stored in a cleaned glass Petri dish in air prior to imaging or further functionalization procedure with proteins.

2.2.2 Functionalization of the AFM tips with proteins

The AFM tips have been functionalized with proteins by two different methods: passive adsorption and covalent attachment. *Passive adsorption* is the simplest attachment method. It comprised in to immerse cleaned tip into protein solution during several hours. After adsorption, loosely bound proteins have been removed by extensive washing, leaving behind only those antibodies that were tightly bound to the tip surface. Despite successful and simple use of this method in our experiments, significant tip degradation and low event frequency (number of specific events/total number of cycles, no more than 2%) for specific protein interaction have been observed. Therefore, we have not pursued this method in our study.

To increase event frequency without losing biological activity of proteins during experiment, the *covalent attachment* of proteins on the tip has been performed. For each system studied (antibody-antigen and fibrin(ogen)-fibrin(ogen)) different linkers have been used.

We note that similar results have been obtained with these two methods of the tip functionalization. The results represented in this work have been performed with covalent functionalization procedure of the AFM tips.

2.2.2a Functionalization of the tips with antibodies

1-ethyl-3 (3-dimethylaminopropyl) carbodiimide (EDAC) (Sigma) is used as a coupling agent. The cleaned tips were rinsed with 50 mM PBS and placed in 2-[N-Morpholino] ethanesulfonic acid (MES) buffer (Sigma). Antibody solutions with concentrations of 270 $\mu\text{g/ml}$ (high concentration samples) or 27 $\mu\text{g/ml}$ (low concentration samples) in MES were incubated with the tips at room temperature for 15 minutes. 200 μg EDAC/100 μl reaction volume was added and the reaction was carried out overnight at room temperature. In order to neutralize unreacted EDAC, Glycine (Sigma) was added to give 100 mM in final concentration, and incubated for one hour. The tips then were washed with PBS buffer several times. The antibody functionalized tips were either used immediately for making measurements or stored at 4 °C in PBS in order to avoid denaturation of the bound immunoglobulins. The stored, functionalized tips showed for several days the same level of activity in our experiments.

2.2.2b Functionalization of the tips with fibrinogen molecules

The cleaned tip is immersed in glutaraldehyde aqueous solution (1% v/v) for 20 min, and fibrinogen molecules (1mg/ml) (Haemacure Corporation, Canada; kindly supplied by Prof. André Haeberli) are attached during 20 min of incubation at room temperature. The loosely bound proteins are then removed by extensive washing with PBS buffer. The fibrinogen functionalized tips are used either immediately for making measurements or for further enzymatic reaction with thrombin or Reptilase.

References

1. Stelze, M., Sackmann, E. Sensitive detection of protein adsorption to supported lipid bilayers by frequency dependent capacity measurements and microelectrophoresis. *Biochim. Biophys. Acta.* **981** (1989) 135-142.
2. Müller, D. J., Amrein, M., and Engel, A. Adsorption of biological molecules to a solid support for scanning probe microscopy. *J. Struct. Biol.* **119** (1997) 172-188.
3. Pashley, R. M. Hydration forces between mica surfaces in Li^+ , Na^+ , and Cs^+ electrolyte solutions: a correlation of double layer and hydration forces with surface cation exchange properties. *J. Colloid Interface Sci.* **83** (1981) 531-546.
4. Wasserman, S. R., Whitesides, G. M., Tidswell, I. M., Osko, B. M., Pershan, P. S., and Axe, J. D. The structure of SAMs of alkylsiloxanes of silicon: a comparison of results from ellipsometry and low-angle X-ray reflectivity. *J. Am. Chem. Soc.* **111** (1989) 5852-5861.
5. Vallant, T., Brunner, H., Mayer, U., Hoffmann, H., Leitner, T., Resch, R., and Friedbacher, G. Formation of self-assembled octadecylsiloxane monolayers on mica and silicon surfaces studied by AFM and infrared spectroscopy. *J. Phys. Chem. B.* **102** (1998) 7190-7197.
6. Krasnoslobodtsev, A. V., and Smirnov, S. N. Effect of water on silanization of silica by trimethoxysilanes. *Langmuir.* **18** (2002) 3181-3184.
7. Jönsson, U., Olofsson, G., Malmqvist, M., and Rönnerberg, I. Chemical vapor deposition of silanes. *Thin Solid Films.* **124** (1985) 117-123.
8. Hoffmann, P. W., Stelzle, M., and Rabolt, J. Vapor phase self-assembly of fluorinated monolayers on silicon and germanium oxide. *Langmuir.* **13** (1997) 1877-1880.
9. Lyubchenko, Y. L., Gall, A. A., Shlyakhtenko, L. S., Harrington, R. E., Jacobs, B. L., Oden, P. I., and Lindsay, S. M. Atomic force microscopy imaging of double stranded DNA and RNA. *J. Biomol. Struct. & Dyn.* **10** (1992) 589-606.
10. Lyubchenko, Y. L., Blankenship, R. E., Lindsay, S. M., and Shlyakhtenko, L. S. AFM studies of nucleic acids, nucleoproteins and cellular complexes: the use of functionalized substrates. *Scanning Microscopy.* **10** (1996) 97-109.
11. Shlyakhtenko, L. S., Gall, A. A., Weimer, J. J., Hawn, D. D., and Lyubchenko, Y. L. AFM imaging of DNA covalently immobilized on a functionalized mica substrate. *Biophys. J.* **77** (1999) 568-576.

12. Lee, G. U., Chrisey, L. A., and Colton, R. J. Sensing discrete streptavidin-biotin interactions with AFM. *Langmuir*. **10** (1994) 354-357.
13. Vandenberg, E. T., Bertilsson, L., Liedberg, B., Uvdal, K., Erlandsson, R., Elwing, H., and Lundström, I. Structure of APTES on silicone oxide. *J. Colloid Interface Sci.* **147** (1991) 103-118.
14. Allen, S., Chen, X., Davies, J., Davies, M. C., Dawkes, A. C., Edwards, J. C., Roberts, C. J., Sefton, J., Tendler, S. J. B., and Williams, P. M. Detection of antigen-antibody binding events with the AFM. *Biochemistry*. **36** (1997) 7457-7463.
15. Tsukruk, V. V., and Bliznyuk, V. N. Adhesive and friction forces between chemically modified silicon and silicon nitride surfaces. *Langmuir*. **14** (1998) 446-455.
16. Hinterdorfer, P., Baumgartner, W., Gruber, H. J., Schilcher, K., and Schindler, H. Detection and localization of individual antibody-antigen recognition events by AFM. *Proc. Natl. Acad. Sci. USA*. **93** (1996) 3477-3481.
17. Lo, Y-S., Huefner, N. D., Chan, W. S., Stevens, F., Harris, J. M., and Beebe, T. P. Jr. Specific interactions between biotin and avidin studied by AFM using the Poisson statistical analysis method. *Langmuir*. **15** (1999) 1373-1382.
18. Stuart, J. K., and Hlady, V. Effects of discrete protein-surface interactions in scanning force microscopy adhesion force measurements. *Langmuir*. **11** (1995) 1368-1374.
19. Senden, T. J., and Drummond, C. J. Surface chemistry and tip-sample interactions in AFM. *Colloids Surf. A*. **94** (1995) 29-51.
20. Lo, Y-S., Huefner, N. D., Chan, W. S., Dryden, P., Hagenhoff, B., and Beebe, T. P. Jr. Organic and inorganic contamination on commercial AFM cantilevers. *Langmuir*. **15** (1999) 6522-6526.

Chapter III

Complexes of Bovine Serum Albumin with its different antibodies

3.1 Introduction

When it comes to speak about our proteins and protein complexes, in particular, about their structure and functional properties, a brief general notion of protein structure is needed. Proteins are complex, folded polymers, with the chemical formula $H-(NH-HCR-CO)_n-OH$, consisting of the 20 naturally occurring amino acids; R stands for one of the 20 amino acid residues. There are four levels of structure found in proteins (fig. 1):

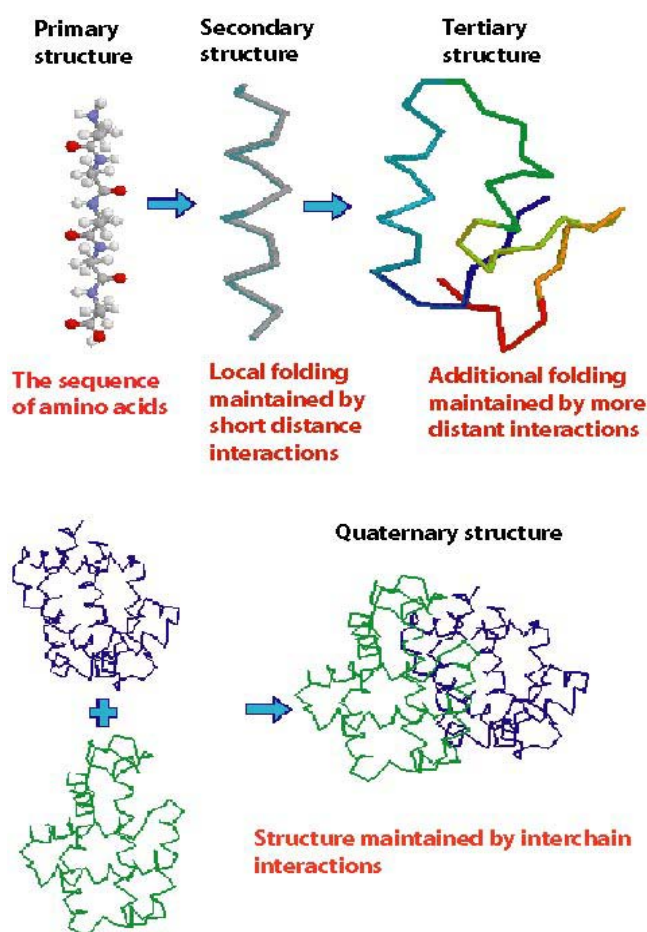


Figure 1. Schematic drawing of the four levels of protein structure.

- Primary structure

The primary structure of proteins is the sequence of amino acids residues along the polypeptide chain with reference to the location of any disulfide bonds. This structure is determined genetically and determines secondary, tertiary and quaternary structures of protein.

- Secondary structure

The secondary structure is the ordered arrangement or conformation of amino acids in localized regions of polypeptide or protein molecule. The two most common local structures are the α -helix and anti-parallel β sheet. Hydrogen bonding plays an important role in stabilizing these folding patterns as well as hydrophobic interaction. A single protein may contain multiple secondary structures.

- Tertiary structure

This is the three-dimensional arrangement of the atoms within a single polypeptide chain. For a protein composed of a single polypeptide molecule, tertiary structure is the highest level of structure that is attained. Tertiary structure is largely maintained by disulfide bonds (also called a disulfide bridge) (S-S) that formed between the side chains of cysteine (Cys) by oxidation of two thiol groups (SH).

- Quaternary structure

This structure is used to describe proteins composed of multiple subunits (multiple polypeptide molecules, each called subunits or monomers). Most proteins with a molecular weight greater than 50 kDa consist of two or more non-covalently-linked polypeptide chains. The arrangement of the multiple polypeptides chains in the three-dimensional protein is the quaternary structure.

In contrast to most other polymers, the position of each atom in a protein molecule is exactly defined – sometimes down to fractions of an Ångström and thus can be determined by X-ray diffraction studies on protein crystals.

3.2 Bovine Serum Albumin, Structure and Properties

Serum albumin is one of the most studied proteins for many years [1]. The Bovine Serum Albumin (BSA) has been chosen for our studies as a model protein. Serum albumin was recognized as a principal component of blood as early as 1839. It is the smallest and most abundant protein in the circulatory system, accounting for about 55% of the total protein in blood plasma with typical blood concentration of 5g/100ml [1]. Albumin provides 80% of colloid osmotic blood pressure and maintains primarily the blood pH. One of the most exceptional properties of albumin is its ability to bind reversibly an incredible variety of ligands such as fatty acids, lysolecithin, bilirubin, warfarin, tryptophan and others [1-6]. It plays also an important role in the transport and deposition of a variety of endogenous and exogenous substances in blood [7]. Up to now, serum albumin is the most known multifunctional transport protein.

3.2.1 BSA structure

Serum albumin is a highly soluble multidomain protein, without prosthetic groups or bulky appending carbohydrates that is very stable and available at high purity and low cost. BSA displays high structural homology (76% sequence identity) with its human counterpart Human Serum Albumin (HSA) [1, 3]. The primary structure of BSA is constituted by a single-stranded polypeptide chain of 582 amino acid residues and its amino acid sequence is well known [8]. The contour length of the denatured (or completely stretched) protein can be calculated from the number of amino acid residues and a peptide bond length of 0.37 nm, $L_{contour}=215\text{ nm}$. The molecular weight is about of 66 kDa. BSA is made up to 100 acidic side chains with 41 Asp and 59 Glu residues and 99 basic side chains with 23 Arg, 59 Lys, and 17 His. Their secondary structure is formed by 67 % of α helix of six turns and 17 disulfide bridges [4]. The three-dimensional structure was also determined [1, 9]. Albumin has three

homologous domains (I, N-terminal; II; III, C-terminal), each domain contains two subdomains dividing up a common helical motif.

The early representation of albumin structure was based on hydrodynamic studies [10, 11] and low-angle X-ray scattering [12], the protein was modeled as a cigar-shaped ellipsoid with dimensions of 14x4 nm and axial ratio of about 3.5, with three domains in line (fig. 2).

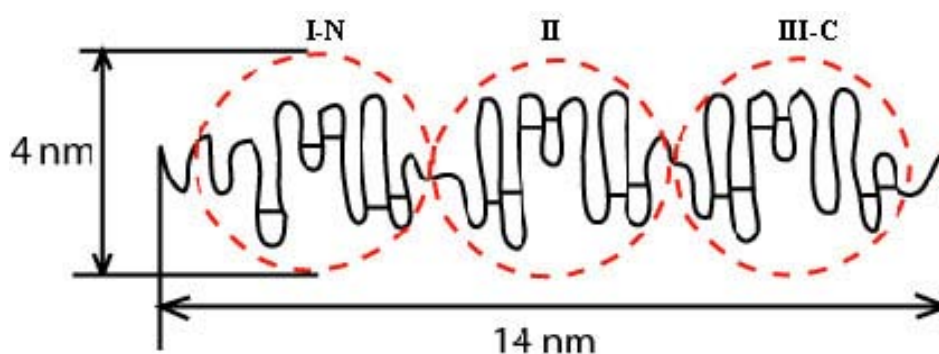


Figure 2. Classical representation of the structure of serum albumin. Reproduced from Peters (1985) [3].

This model was supported by a series of measurements of sedimentation, dielectric dispersion, electric birefringence, and transmission electron microscopy. Some confirmation was found from scanning tunneling microscopy experiences [13]. Interestingly, the “cigar” model is still frequently used [14-16]. Carter and Ho [1] noted that despite the general acceptance of the cigar-shaped model several research groups already provided evidence of the spherical molecule having dimension of ≈ 8 nm [17-19]. These results could only be explained by the current heart-shaped structure determined from X-ray crystallographic data of HSA [9, 20, 21]. Serum albumin is represented by an equilateral triangle with sides of approximately 8 nm each and an average thickness of 3 nm (fig. 3).

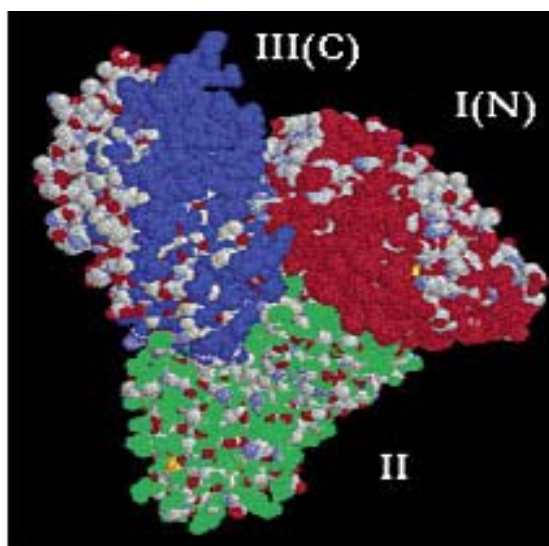


Figure 3. Heart-shaped crystallographic structure of HSA, reproduced from [2].

For a long time, the cigar-shaped model was used to interpret the protein solution hydrodynamics at pH 7-7.4 (neutral-physiological pH). The two different views of serum albumin structure (elongated cigar-shaped and heart-shaped) might be reconciled if the tertiary structure of the protein in the crystal is different from that in solution. To attack this problem, Ferrer et al. [22] investigated and elucidated the conformation of serum albumin using phosphorescence depolarization techniques. They obtained a very good agreement between the predicted and experimental rotational diffusion rate and other hydrodynamic parameters. Based on the detailed computation of the hydrodynamic properties with recently developed bead-model methods they concluded that the conformation of BSA in solution at pH 7.4, as of HSA, should be rigid and very similar to the heart-shaped structure observed in HSA crystals. Through all our studies we use the heart-shaped structure of BSA that was also confirmed by our AFM observations where we detected a globular protein with the diameter of 7-8 nm (see explanation in text below, pages 51 and 52).

3.2.2 BSA conformational transitions

As known, BSA undergoes several well-recognized reversible conformational changes, usually under non-physiological conditions, e.g. by varying pH [23-25]. Foster [26, 27]

classified the forms as N (normal, pH 7.0), F (fast migrating, pH 4.3), E (expanded, pH 2.7), B (basic, pH above 8.0) and A (aged, pH 10) (fig. 4). These five forms are characterized by different content of α helix, β sheets and other structures.

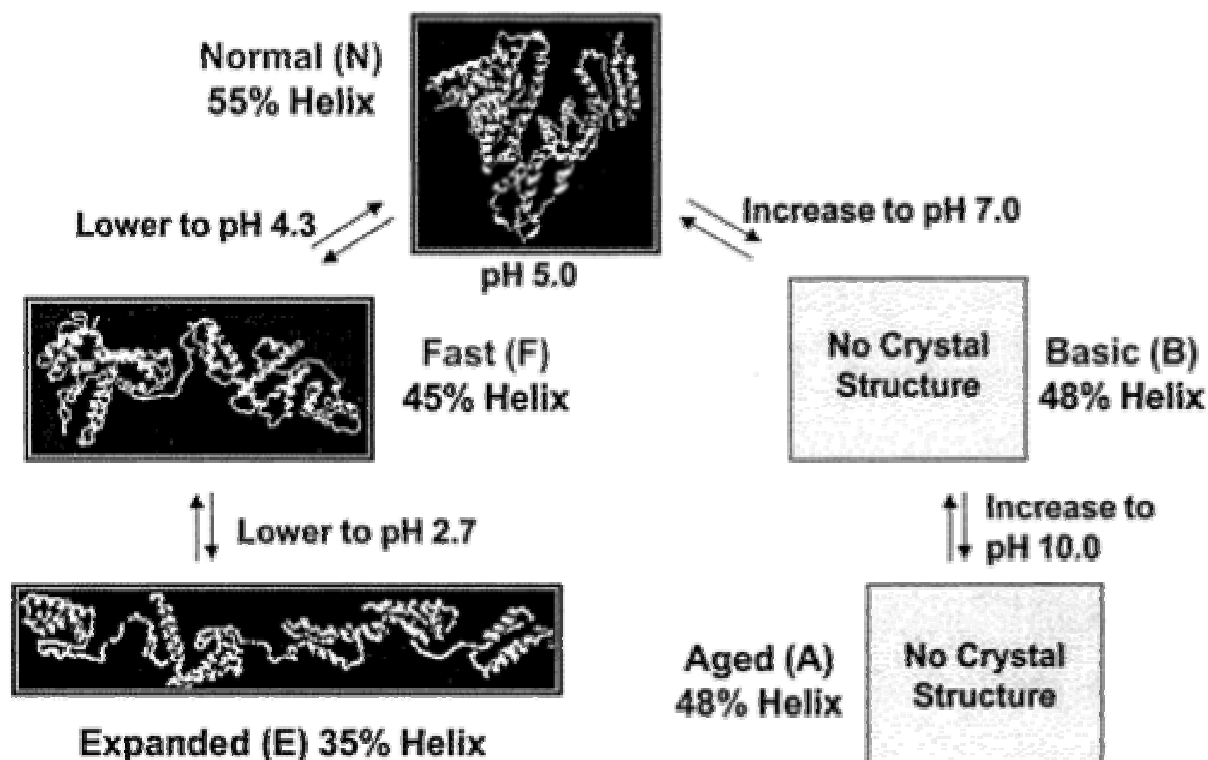


Figure 4. The five conformational forms of BSA molecule, redrawn from [26].

Let us note that expanded (E, 35% helix) form of BSA corresponds to the full extent of the protein allowed by the disulfide bond structures [26].

3.3 Antibodies, their function and general structure

Probably, all of us know or heard that antibodies play an essential role in our immune system. Antibodies defend us against infection by inactivating viruses and bacterial toxins or they can label foreign cells or particles for destruction by macrophages. Antibody molecules have a great affinity for particular proteins and polysaccharides (most of which are foreign). These

foreign proteins and polysaccharides that cause the production of antibodies are called antigens. The antibody function is to first recognize the antigen (millions of different antigens are recognized by antibodies) as foreign substance, then neutralize it and finally prevent it having any dangerous effect on the body. When an antibody recognizes an antigen, the specific bond between an antigen and an antibody (Ag-Ab bond) is created. This binding may be enough to inactivate or neutralize the antigen. The binding of antibody to antigen also helps other cells of the immune system to recognize the foreign antigen. Bound antibody can be detected by macrophages, which are large phagocytotic cells that “eat” foreign and damaged cells. Antibodies are produced exclusively by one type of white blood cells called B lymphocytes and secreted into the blood. Antibodies are also found on the surface of the B lymphocytes. Antibodies are collectively called immunoglobulins and abbreviated as Ig. They account for about 20% of the non-cellular proteins in the blood.

Antibodies are proteins with a particular structure. There are 5 types or classes of antibodies called IgA, IgD, IgE, IgG and IgM. Each class has a different function:

- IgA is the body’s first defense against infection by bacteria and viruses. IgA is found in saliva and tears, in the lungs and digestive tract;
- IgD is membrane bound and found on the surface of cells;
- IgE is involved in reactions to allergens;
- IgG is involved in the immune system’s secondary response to infection and it is found in the blood;
- IgM is involved in the body’s primary response to infection and it is also found in the blood.

All antibodies have the same general structure and they comprise two heavy (H) chains (each usually contains about 440 amino acids) and two light (L) chains (each usually contains about 220 amino acids). These four chains are held together by a combination of non-covalent and covalent (disulphide bridges S-S) bonds. The different classes of antibody

have different heavy chains. The typical antibody molecule is a Y-shaped protein with two identical antigen-binding sites, one at the end of each arm of the Y (the Fab regions) (fig. 5). Molecular weight is about 160 kDa (IgG). Because of their two antigen-binding sites, they are said to be bivalent. Thus, the antibody molecule is composed of two identical halves, each with the same antigen-binding site, and both light and heavy chains usually cooperate to form the antigen-binding surface.

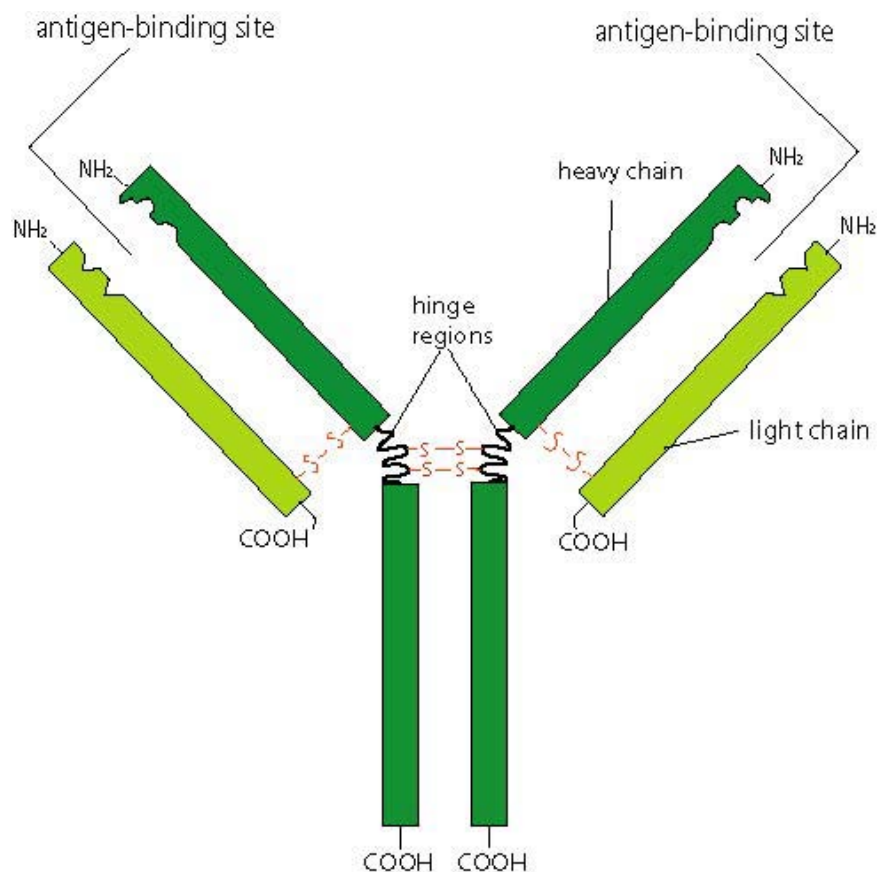


Figure 5. A schematic drawing of a typical antibody molecule. Reproduced from [27].

An antibody also has two functional parts. One is called the constant region (C) (it defines from which animal or human the antibody is produced by) and the other is the variable region (V) (fig. 6). The variable region, containing antigen-binding sites, recognizes a particular antigen and therefore the variable regions are different. Each domain as represented in fig. 6 is roughly a cylinder with dimension of 4x2.5x2.5 nm.

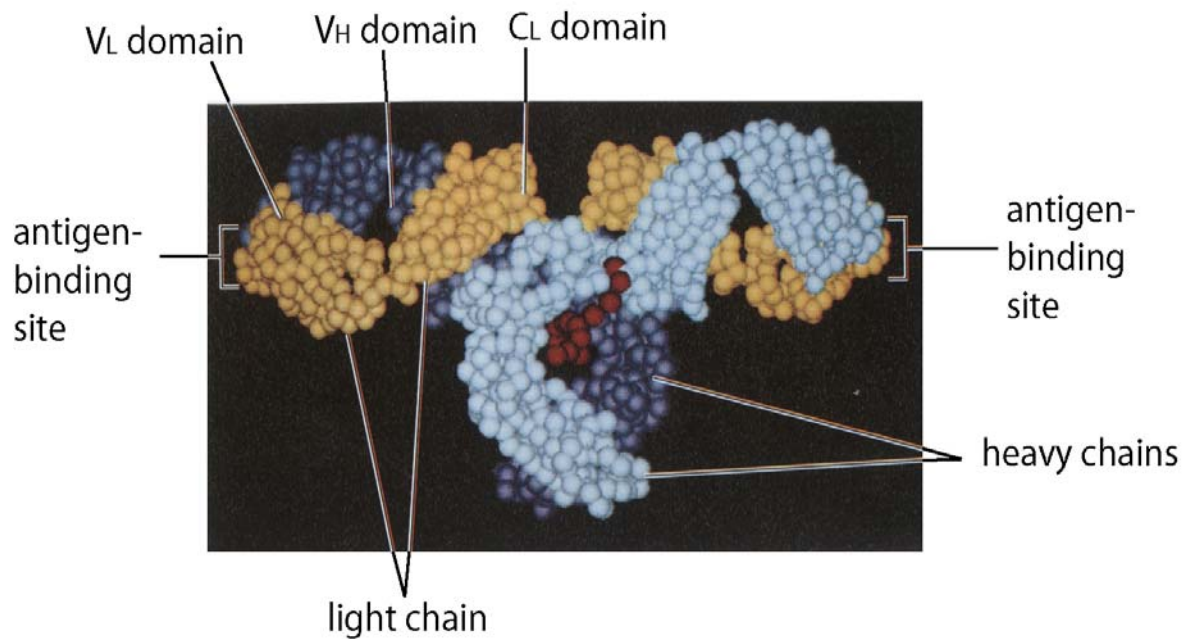


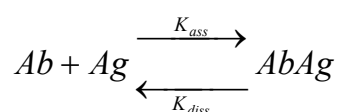
Figure 6. The crystallographic structure of an IgG1 molecule. One heavy chain is drawn in light blue, the other in dark blue, with the light chain in yellow. Reproduced from [27].

3.3.1 Affinity and specificity of antigen-antibody bond

3.3.1a Affinity or tightness of binding

The binding of antibody to antigen is a reversible reaction, involving non-covalent bonds. This process obeys the law of mass action which states that the rate of a reaction is proportional to the concentrations of the reactants. For a bond formation between single antigen-binding site of antibody and a single antigenic determinant (epitope) [27] of antigen, one can describe equilibrium constant (K_{eq}) which describes the tightness of binding, or “affinity”.

Thus, for the reaction:



- the rate of formation of the Ab-Ag complex: $r_{ass} = K_{ass}[Ab][Ag]$, where $[Ab]$ is the concentration of antibody and $[Ag]$ concentration of antigen and K_{ass} is the rate constant of equilibrium of association.

- the rate of dissociation of the Ab-Ag complex: $r_{diss} = K_{diss}[AbAg]$, where $[AbAg]$ is the concentration of the Ab-Ag complex and K_{diss} is the rate constant of equilibrium of dissociation.

The rate constants K_{ass} and K_{diss} depend on temperature, pH and other conditions, as it is explained above in chapter I, paragraph “kinetics of simple bonds”.

At equilibrium, the rate of formation of the Ab-Ag complex, r_{ass} , equals the rate of its dissociation, r_{diss} , and an equilibrium or affinity constant K_{eq} is defined:

$$K_{eq} = \frac{K_{diss}}{K_{ass}} = \frac{[Ab][Ag]}{[AbAg]}$$

Affinity constants for antibodies usually lie in the range to from 10^9 to 10^6 M. We can imagine the affinity constant corresponds to the concentration of antibody at which the antigen is half saturated. This might occur at 0.1 to 100 $\mu\text{g/ml}$.

Because the antibody has multiple binding sites (p. e. two for IgG), real antibody-antigen interactions are more complex than the simplest reaction described above. Once the antibody has bound by one arm, it is possible for the other to bind, which results in an overall increase in the tightness of binding. The second reaction, however, is an internal rearrangement of a single complex and so it is not described by the same rate equations. The extra tightness achieved by binding through multiple sites is called “avidity” or “functional affinity” and it can be considerably greater than the single-site affinity. In practice, when we measure the binding of an antibody to a cell surface antigen, it is a sort of average “functional affinity” which is measured and we do not usually pay much attention to the exact number of binding sites.

3.3.1b Specificity, the relationship between affinity and specificity

By specificity of antibody, we understand the functional ability of an antibody to discriminate between the target antigen and other, chemically similar structures.

During the course of the immune response to a foreign antigen, there is selection for antibodies with increased affinity as a result of somatic mutation. It is wrongly stated that this increase in affinity is accompanied by an increase in specificity of the antibodies. In fact, the opposite is true [28].

3.4 Quasistatic force spectroscopy of polyclonal and monoclonal anti-Bovine Serum Albumin antibodies – BSA complexes

Probably the most informative and interesting force spectroscopy studies are the experiments revealing the molecular recognition events (receptor-ligand interactions) including antigen – antibody (Ag-Ab) systems (see the references below). In this chapter, the results of quasistatic force spectroscopy (FS) measurements for the interaction of the protein bovine serum albumin (BSA) with its polyclonal antibody or with two different monoclonal antibodies are presented. In our experiments, the antibodies are immobilized on the AFM tip and the BSA molecules are covalently bound onto the substrate surface (see chapter II “sample and tip preparation methods for FS study”). Moreover, soft cantilevers are used for higher force sensitivity. Several control experiments are carried out to check the validity of the force measurements. To measure the ability of antibody-functionalized tips to detect specific antigen-antibody interactions, we have used the AFM operated in static force spectroscopy mode. If the force measurement is carried out in air, the cohesive interaction between the thin surface layers of water present on the tip and mica surface is greater than 3 nN [29] and, therefore, dominates the specific molecular interactions (force range is not exceeding 500 pN). It becomes impossible to measure specific molecular forces. Thus, our force experiments have carried out in a buffer solution.

3.4.1 AFM instrumentation

A commercially available AFM (Nanoscope IIIa Multimode Scanning Probe Microscope, Veeco Instruments, Santa Barbara, CA, USA) and standard V-shaped Si₃N₄ (silicon nitride) cantilevers (Veeco), having a length of 200 μm and a nominal spring constant of 0.06 N/m,

were used. All experiments were performed in phosphate-buffered saline (PBS) buffer (50 mM phosphate, 150 mM NaCl, pH 7.4 at 25°C) at 25°C.

The spring constant $k_{cantilever}$ of each cantilever is calibrated by the resonance frequency method [30] and thermal fluctuations method [31]: variations in the spring constant up to 20 % were observed. The “force-volume” option has been used for force spectroscopy measurements. Loading rate-dependent experiments have been performed by varying the retraction velocity from 20 nm/s to 5 000 nm/s. The loading rate has been determined by the slope on the force curve before an unbinding event [32, 33].

3.4.2 Tip and Sample preparation

The following commercial antibodies are used: the rabbit anti-bovine serum albumin (Sigma, B1520); the monoclonal anti-bovine serum albumin clone BSA-33 (Sigma, B2901) and the monoclonal anti-bovine serum albumin clone BSA1 (ANAWA, 0220-1286), called Ab-BSA, mAb-BSA-33 and mAb-BSA-1, respectively. As described in the chapter II “sample and tip preparation methods for FS study”, the antibodies are covalently attached to the AFM tip via EDAC and BSA molecules are immobilized onto the APTES-mica sheets. An example of BSA submonolayer AFM image, in PBS buffer, is represented in fig. 7. To visualize the structure of immobilized BSA molecules, the proteins are further fixed by 10-min incubation in glutaraldehyde (1% v/v). Fig. 7 (left image) shows quite isolated BSA molecules with globular structure of about 7-8 nm in diameter. This image has a large similarity with the one obtained earlier by Gunning (fig. 7 (right image)) [34]. The BSA layer thickness is estimated by the sweeping method described in details in chapter II, and gave a result as about 3.5 nm (fig. 8).

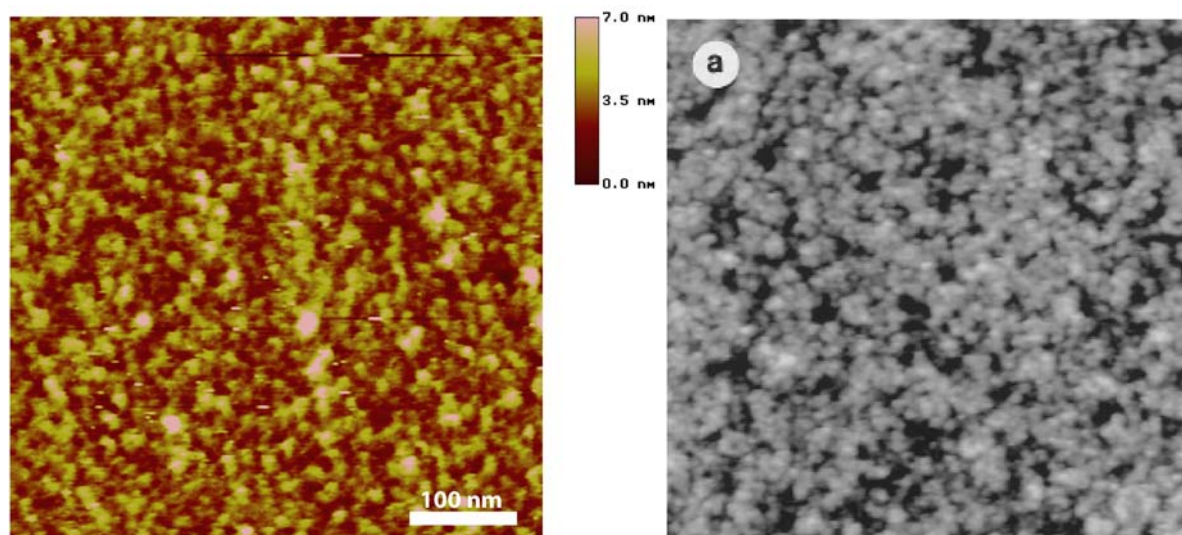


Figure 7. Left image: Tapping mode AFM image in PBS buffer of BSA sub monolayer prepared according to the chemical fixation procedure. Fairly isolated BSA molecules of a globular shape with the size of 7 – 8 nm are seen. Right image: AFM image of BSA film (reproduced from Gunning [34]). Scan size is 500x500 nm². Grey scale (black to white) is 0-7.6 nm.

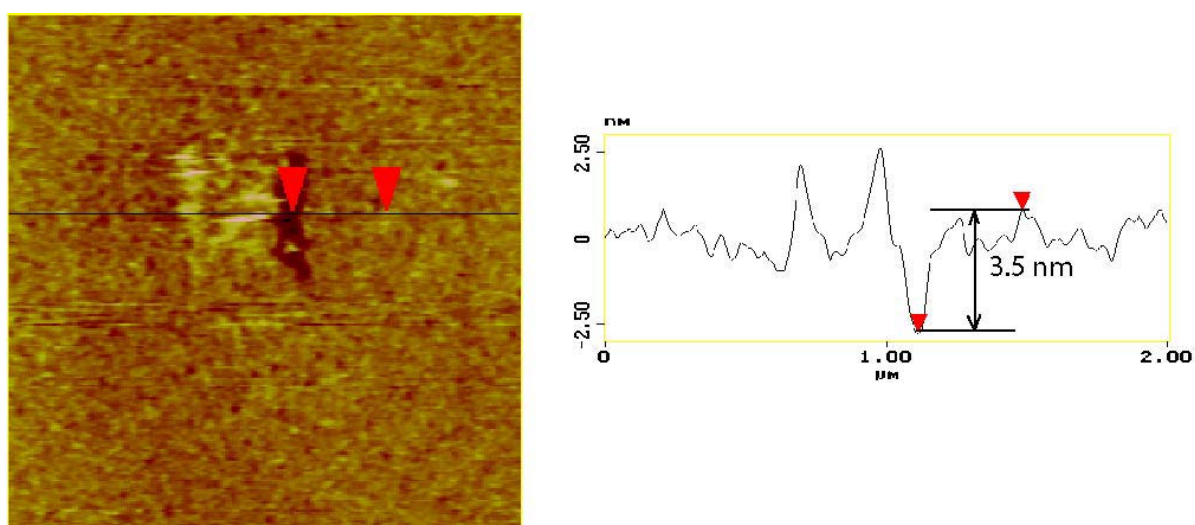


Figure 8. Estimation of BSA layer thickness by sweeping method. The zoomed out scan area is 2x2 µm², the central surface area of 500x500 nm² is scanned at high loading force. The scanning was performed two times just to remove the BSA molecules. The color scale (dark brown to yellow) is 0-5 nm.

3.4.3 Data analysis and control experiments

During force spectroscopy measurements the cantilever moves down (approach to the surface) and up (retraction from the surface) and the deflection of the tip is recorded. Knowing the spring constant of the cantilever and the variation of the deflection signal per nanometer, one can convert deflection signal to force for a given deflection. When the tip enters in contact with sample surface, a specific antigen-antibody (Ag-Ab) bond can be formed. This bond will be ruptured when the tip is pulled away from the substrate surface. So, the specific interaction (unbinding) force can be read directly from the retraction force-distance curves as the difference between the equilibrium position and the bottom of the negative peak (event). One could argue that the measured forces could also come from any non-specific interactions due to the chemical modifications of the tip and sample. Therefore, it is important to measure all possible combinations of the tip-sample treatment in order to exclude artifacts. The following control systems were studied according to the different treatments of the surfaces:

Sample	AFM tip
mica	bare clean tip
mica+APTES	bare clean tip
mica+APTES+Glutaraldehyde	bare clean tip
mica+APTES+Glutaraldehyde+BSA	bare clean tip
mica	tip+antibody
mica+APTES	tip+antibody
mica+APTES+Glutaraldehyde	tip+antibody

These seven control experiments represent all the possible interactions, other than the one under investigation that could occur. The determination of the interaction forces allows us to exclude artifacts for our system. For the above control experiments, the following cases are observed: (1) there are non-specific interactions (adhesions) characterized by the jump-off contact of the tip from the substrate and/or (2) there are strong specific interactions in the

force range 1-3 nN. Case (1) can be easily distinguished because it occurs at the end of the contact line and case (2) also can be easily excluded because the range of specific Ag-Ab interactions does not exceed 500 pN.

Another important control consisted in the analysis of specificity antigen – antibody interaction. It was done by injecting of free BSA molecules in solution (when antigen binding sites of antibodies are blocked). Such an experiment also gave a negative result: specific unbinding forces completely disappeared; they were partially (about 50%) restored when this BSA solution was exchanged again by a PBS buffer (fig. 9). This blocking procedure was repeated after each experiment done with each antigen-antibody pair. These controls give us assurance that the true antigen-antibody interactions were measured and not any unspecific binding process.

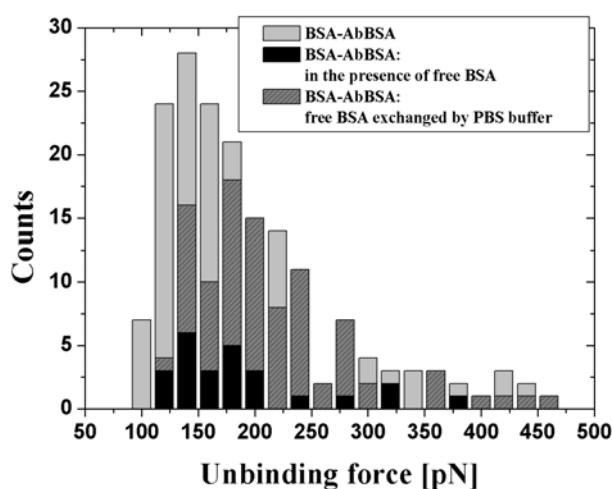


Figure 9. Control of specificity of antigen-antibody interaction. The histogram in light grey presents BSA-Ab-BSA interaction, in black – blocking the antibodies activity with free antigens in solution, and in dark grey – restoring of antigen-antibody interaction after elimination of free antigens from buffer solution.

Fig. 10 shows the typical force-distance (retraction part) curves recorded during one Ag-Ab experiment. We classify the curves as follows: single bond rupture (red), non-specific adhesion of the tip to the sample (black) and no binding events detected (blue). Most of the curves (about 70 %) have not displayed detectable events; sometimes (less than 1% of detected curves) have displayed a non-specific adhesion of the tip to the sample surface.

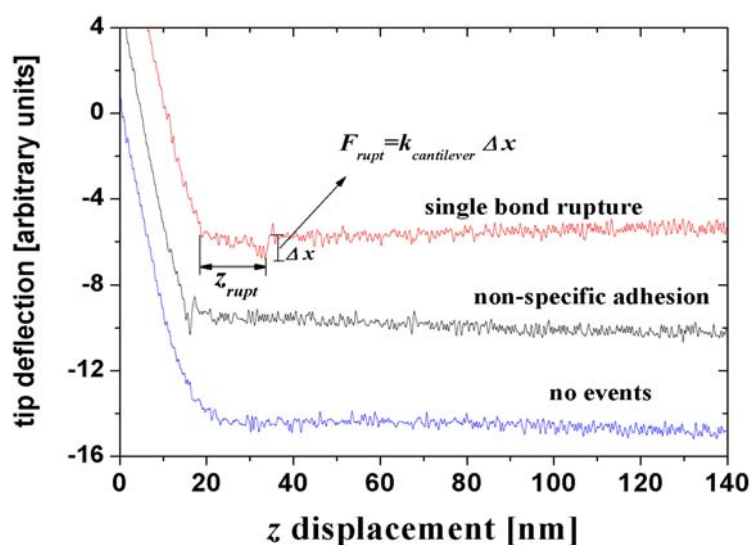


Figure 10. Typical force-distance curves recorded during one antigen-antibody experiment.

Force curves have been analyzed off-line with software developed by Kasas et al. [35]. One can point two disadvantages in the quasistatic pulling experiments: first, molecular interactions can be disrupted by the significant lateral drift and confuse interpretation of force data; and second, the repeated forceful interaction of the tip with the surface may cause tip degradation. So, in order to validate the data interpretation, at least 512 force-distance curves have been detected in a given experiment. Each experiment has been independently made three times or more. The histograms of unbinding forces for each antigen-antibody pair have been constructed and the mean value of the nearly Gaussian distribution has been taken as the most probable unbinding force. To ensure that the mean values are independent of the histogram arrangement, different bin sizes (from 10 pN to 20 pN) have been used to construct the histograms, and no significant differences in the maxima force values have been found.

3.4.4 Experimental results and discussion

It has been shown that the strength of the unbinding force of antigen-antibody complexes, where a single barrier governs the separation process, depends logarithmically upon the

loading rate [32]. This effect does not of course limit the applicability of force spectroscopy measurements. On the contrary, it gives the possibility to interpret the measured force with models in order to extract thermal dissociation and equilibrium constants, and even the reconstruction of the free energy [36]. In order to circumvent the loading rate dependence of the unbinding force, one should perform the FS experiments at a constant loading rate, and compare then between different antibodies in order to detect the homogeneity of the specific interaction of antibodies. The following paragraph presents the results obtained with constant loading rate of about 3.5 nN/s.

3.4.4a Constant loading rate measurements

Three different antibodies to BSA have been used in the experiments in order to study the antigen-antibody interaction: 1) BSA – Ab-BSA (polyclonal antibody), 2) BSA–mAb-BSA-1 (monoclonal antibody), 3) BSA–mAb-BSA-33 (monoclonal antibody) and additional experiments have been carried out between BSA and mixtures of mAb-BSA-1 and mAb-BSA-33 antibodies in order to mimic a polyclonal antibody. The event frequencies (i.e. the relation between the number of curves with specific interactions and the number of all approach-retraction cycles) for the various experiments are summarized in Table 1. The frequency values are comparable to those obtained by other studies [37-40]. However, one has to note that there is a noticeable reduction in the frequency value for the monoclonal antibodies mixtures. This reduction, as we could show by imaging the antibodies deposited on mica, is due to the interaction between the two antibodies. Indeed, the AFM images show (see fig.16) aggregates of the antibodies which inhibit each other and reduce their activity.

<i>Antigen-antibody complex</i>	<i>Specific interactions (%)</i>
BSA – Ab-BSA	30
BSA – mAb-BSA-1	27
BSA – mAb-BSA-33	26
BSA – mixture of mAb-BSA-1 (50%) and mAb-BSA-33 (50%)	10
BSA – mixture of mAb-BSA-1 (20%) and mAb-BSA-33 (80%)	8

Table 1. Interaction event frequencies for experiments done with high antibody concentration (270 $\mu\text{g/ml}$). Antibodies and BSA molecules were covalently bound the tip and sample surface, respectively.

From force-distance curves an average extension for all antigen-antibody pairs has been determined as $z_{rupt} = 14 \pm 4$ nm (figs. 10 and 11).

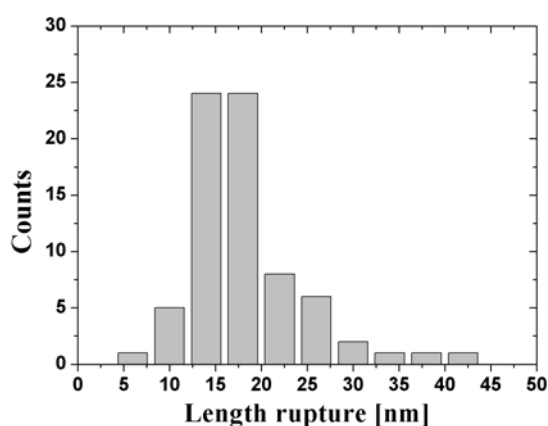


Figure 11. The length distribution (uncorrected z_{rupt} values, see explanation in text below) for one BSA – Ab-BSA pair. 73 specific events detected.

We have used the sample stage displacement z as a measure of such distance. It can be argued that the

antigen-antibody extension is given by the difference of z and Δx cantilever displacement. Δx is a measurable parameter and is determined from the force curve (fig. 10), thus the value of z_{rupt} can be corrected, what we have performed whenever. One can note that this correction is of only minor importance for our experiments. For example, for the typical one bond rupture event ($F_{rupt} = 140$ pN), $\Delta x = 2.3$ nm and, thus, is essentially smaller than the characteristic (uncorrected) z_{rupt} value of 16 nm (fig. 11). This value remained the same for our tips and

sample functionalization methods (covalent immobilization and passive adsorption). Taking into account the BSA size of 6 nm, antibody molecule size of 8 nm and APTES+glutaraldehyde layer thickness of 2 nm, we conclude that essentially an extension of antigen-antibody complex was performed. Different situation was observed for unbinding forces for different antigen-antibody complexes.

Due to the distribution of antigenic determinants (epitopes) [27] on the surface of the antigen (fig. 12 (left)) (BSA molecule has a minimum six different, no repeating, antigenic determinants [41]); the capability of polyclonal antibodies to easily recognize and bind with antigen is not highly dependent on the molecular conformation/orientation. In contrast, the monoclonal antibody can bind with a single antigenic determinant (fig. 12 (right)). So its capability to bind will be much more influenced by molecular conformation and orientation. It is expected that the histograms for polyclonal antibodies should be qualitatively different from those for monoclonal antibodies at high concentration of antibody where more than one antibody molecule is attached to the tip.



Figure 12. Schematic illustration of interaction of polyclonal (left) or monoclonal (right) antibodies with globular protein which has multiple different antigenic determinant on its surface.

Fig. 13 shows the histograms of the unbinding forces for concentrated solutions (270 $\mu\text{g/ml}$) of polyclonal and monoclonal antibodies against BSA. Fig. 13 A represents the histogram for BSA – Ab-BSA complex. One can observe that the spectrum of unbinding forces is broad and spans from 60 pN to 400 pN. This range of unbinding forces is compatible with previous results [37]. All events with a force greater than 1 nN are believed to be the breaking of glutaraldehyde – protein-amine bonds based upon results from the control experiments. In fig. 13 B and 13 C the histograms for BSA – mAb-BSA-1 and BSA – mAb-BSA-33 pairs are reported. In the case of monoclonal antibodies, the histograms are narrow, but with a peak frequency depending upon the monoclonal antibody used. The peak frequency F^* is at 142 ± 16 pN for the mAb-BSA-1 and at 250 ± 18 pN for mAb-BSA-33. From these experiments, one can conclude that the monoclonal antibodies bind to BSA at one specific antigenic determinant with a characteristic unbinding force. This force depends upon the chosen monoclonal antibody. One can clearly distinguish the antibodies. The histograms for the polyclonal antibody are broad, indicating that the attached antibody molecules are different. Each has a different unbinding force or there is one type of antibody molecule with low specificity, and which can bind to different antigenic determinants with different unbinding forces.

In order to discriminate between these two possibilities mentioned above, one has to make experiments where only one or few polyclonal antibody molecules are attached to the tip. In this way, if we observe a broad spectrum of unbinding forces, the second possibility is realized, whereas a narrow spectrum would indicate that single antibody molecules are binding to a specific antigenic determinant with a well-defined unbinding force. To this end, the initial polyclonal antibody solution was diluted ten times to 27 $\mu\text{g/ml}$ while keeping the immobilization protocol unchanged. This should ensure that the concentration of immobilized

antibodies at the tip is strongly reduced. Then, several experiments with a low concentration of polyclonal antibody were made.

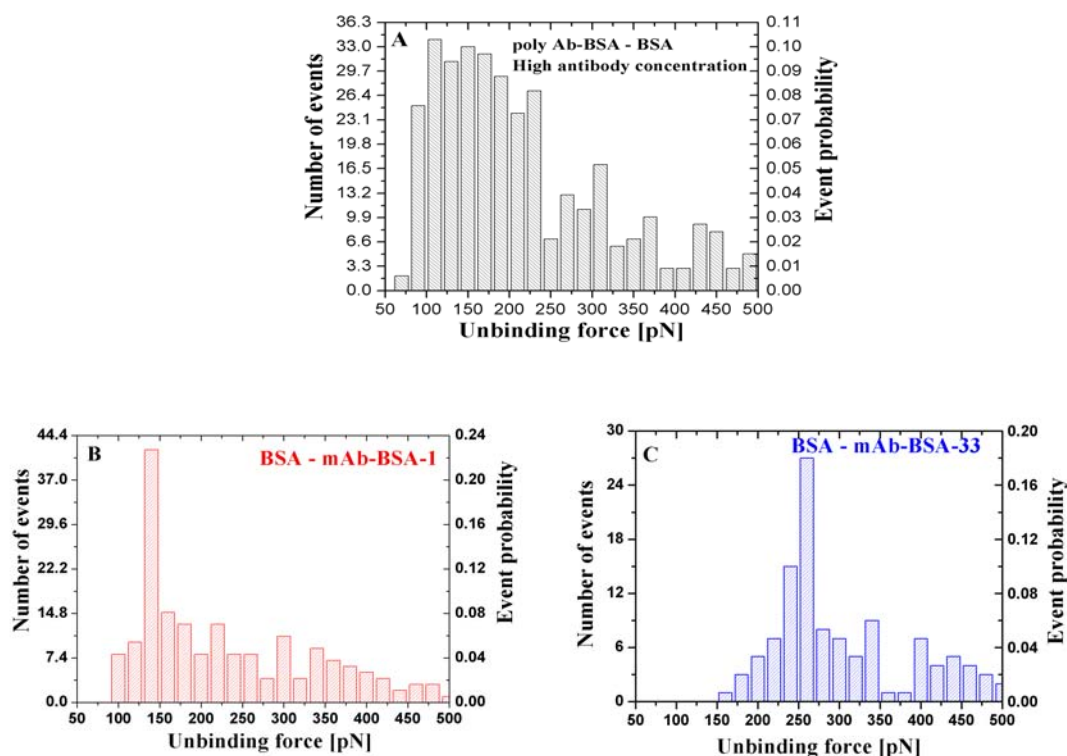


Figure 13. Force histograms for BSA-Ab-BSA (A), BSA-mAb-BSA-1 (B) and BSA-mAb-BSA-33 (C) complexes at high antibody concentration (270 $\mu\text{g/ml}$). Unbinding events were counted at every 20 pN, event probability $P(x)$ was calculated as Nb of x event/Nb of total specific events. The loading rate was 3.5 nN/s.

Because the polyclonal antibody solution can be thought as a mixture of different monoclonal antibodies (fig. 12-left), a different unbinding force can be obtained in each experiment. Therefore, it is possible to characterize each antibody type present via the unbinding force data. Fig. 14 represents the forces histograms for three different experiments (in one experiment one antibody-functionalized tip is used). As one can see, the histograms are narrow and for each tip the histogram peaks at a different unbinding force. This behavior indicates, firstly, that the antibody molecules in a polyclonal antibody solution are different, but each binds in a specific way to the antigen and secondly, that the tips have probably only one antibody molecule that is active for binding. Fig. 14 shows the narrow distributions of unbinding forces measured in each experiment which have peaks at 106 ± 16 pN (peak I), 141

± 15 pN (peak II), 179 ± 16 pN (peak III), and 230 ± 17 pN (peak IV). During each experiment, we have obtained histograms with a maximum of two narrow distributions. This fact indicates that, at this antibody concentration ($27 \mu\text{g/ml}$), still more than one antibody molecule has been attached on the tip. In fact, it is possible that two different antibody molecules have been immobilized on the tip.

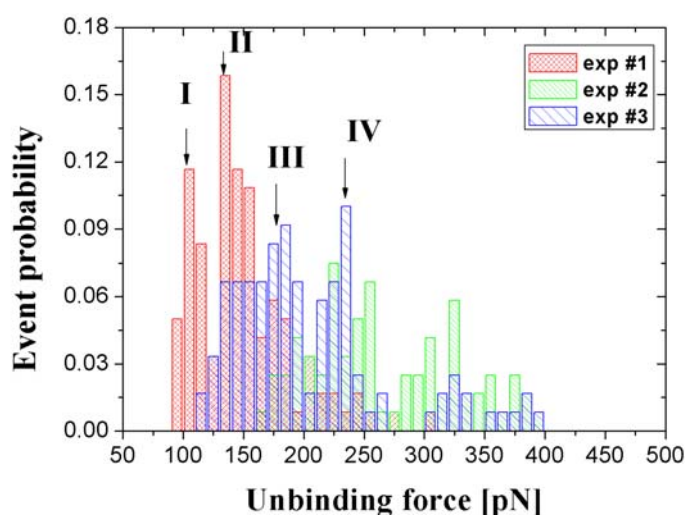


Figure 14. Force histograms (event probability) for data from 3 different experiments with the same BSA – Ab-BSA complex at low antibody concentration ($27 \mu\text{g/ml}$). Unbinding events have been counted at every 10 pN, loading rate is 3.5 nN/s.

It was expected that mixing of two or more monoclonal antibodies having different antigenic determinant specificity would result in a force distribution approaching that of the polyclonal antibody. In order to mimic polyclonal antibodies, mixtures of two different monoclonal antibodies were prepared. Premixed antibodies were obtained by mixing two monoclonal antibodies keeping the total antibody concentration at $270 \mu\text{g/ml}$ before immobilization on the tip. At first, we tested the mixture of mAb-BSA-1 and mAb-BSA-33 at equal molar concentrations. Fig. 15 A shows force histogram detected between BSA and mixture of mAb-BSA-1 (50%) and mAb-BSA-33 (50%). It is seen that the distribution of unbinding forces is broad. The specific event frequency is about 10% (see Table 1). This distribution is more similar to that of mAb-BSA-1 and does not present a peak characteristic of mAb-BSA-33. We suppose that mAb-BSA-1 is preferentially attached on the AFM tip or that there is an interaction among the antibodies. The second possibility is more likely, because aggregates of the two antibodies were observed

by AFM imaging (fig. 16). To detect the presence of mAb-BSA-33 in the mixture, we have tested the following mixture ratio of monoclonal antibodies: 20% of mAb-BSA-1 and 80% of mAb-BSA-33. The force histogram for this system is shown in fig. 15 B.

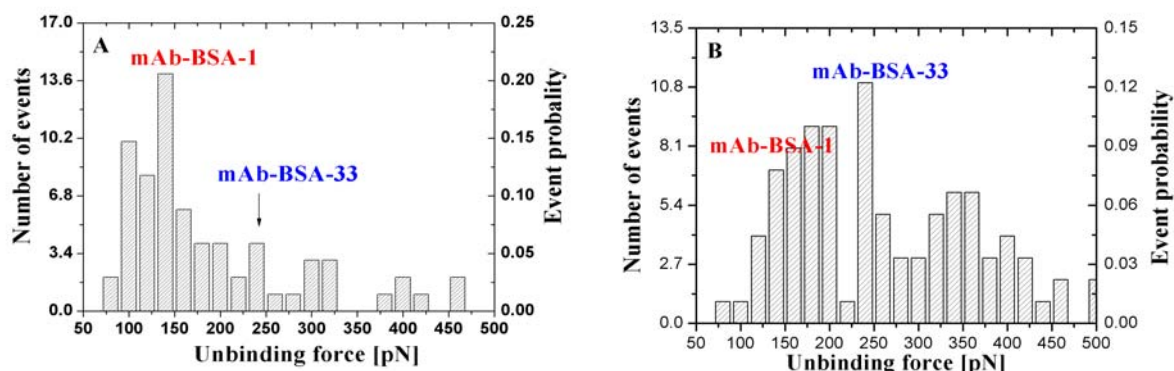


Figure 15. Force histograms observed between BSA and the mixture of mAb-BSA-1 and mAb-BSA-33 monoclonal antibodies at different molar ratios of antibodies: 50:50 (A) and 20:80 (B) where the first number is corresponding to mAb-BSA-1. The total antibody concentration for the mixture has been kept at 270 $\mu\text{g/ml}$ (high antibody concentration). Unbinding events are counted at every 20 pN; loading rate is 3.5 nN/s.

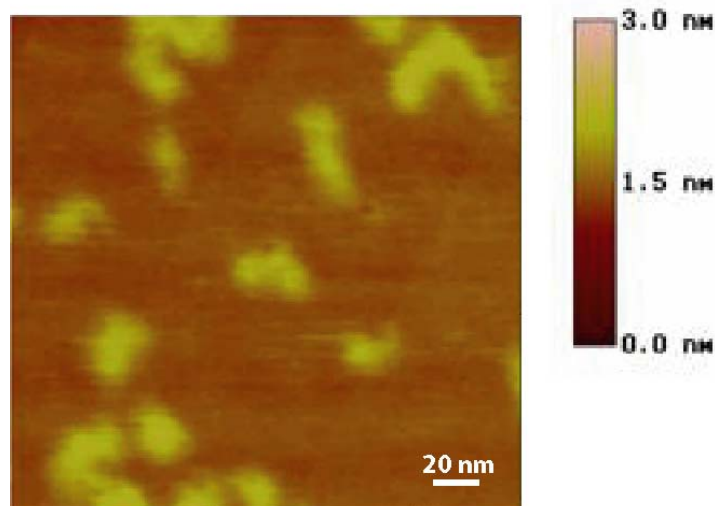


Figure 16. AFM tapping mode images of aggregates formed by mAb-BSA-1 and mAb-BSA-33 antibodies.

One can see that this distribution is broader and similar to the broad force spectrum of the polyclonal antibodies at high antibody

concentration. We note that about 8% of the force curves present a specific event (see Table 1). We conclude that the low event frequency observed in these two experiments is due to antibody aggregation. From force measurements we can also conclude that mAb-BSA-1 probably blocks of mAb-BSA-33. One can argue that there is another possibility to explain the histograms of fig. 15: it is possible, since the antibodies interact among themselves, that

part of the “specific” interaction observed are due to mAb-BSA-1 – mAb-BSA-33 rupture events. If it is the case then the rupture force between two antibodies would not change with the antibody concentration and the force histograms would be same contrary to our observations. Thus, the force histograms shown in fig. 15 represent the specific antigen-antibody interactions.

3.4.4b Loading rate-dependent measurements and dissociation rate estimation

In order to learn more about the mechanisms of the antigen-antibody dissociation in our experimental set-up, the measurements of the unbinding force as a function of the applied mechanical load have been performed for BSA – mAb-BSA-1 and BSA – mAb-BSA-33 pairs. AFM is capable of applying loading rates in the range of 0.2-80 nN/s. It can be achieved by changing the retraction velocity of the tip from 20 nm/s to 5 000 nm/s. The range is limited by thermal drift effects at low pulling velocity and hydrodynamic effects at high pulling velocity. We have found that for BSA – mAb-BSA-1 (fig. 17 A) and BSA – mAb-BSA-33 (fig. 17 B) complexes the most probable unbinding force (F^*) depends linearly on the logarithm of the applied loading rate, showing that the single potential barrier dominates the dissociation for all of the applied loading rates. Fitting the F^* versus the natural logarithm of loading rate ($F^* = A + B \ln r$, see equation 11 in chapter I, part II “ Quasistatic Force Spectroscopy”) permits us to calculate the potential barrier widths ($x_{diss} = \frac{B}{k_B T}$) and the

thermal off-rates (k_{diss} , $A = B \ln \left(\frac{1}{B \cdot k_{diss}} \right)$). The potential barrier widths have been estimated

to be $2.8 \pm 0.6 \text{ \AA}$ for BSA – mAb-BSA-1 and $1.6 \pm 0.5 \text{ \AA}$ for BSA – mAb-BSA-33 complexes. We have obtained the dissociation rate of about $2.4 \times 10^{-2} \text{ s}^{-1}$ for BSA – mAb-

BSA-1 and about $1.5 \times 10^{-2} \text{ s}^{-1}$ for BSA – mAb-BSA-33. Our values of potential widths and dissociation rates are in good agreement with the values measured by the same technique for other antigen-antibody pairs [32].

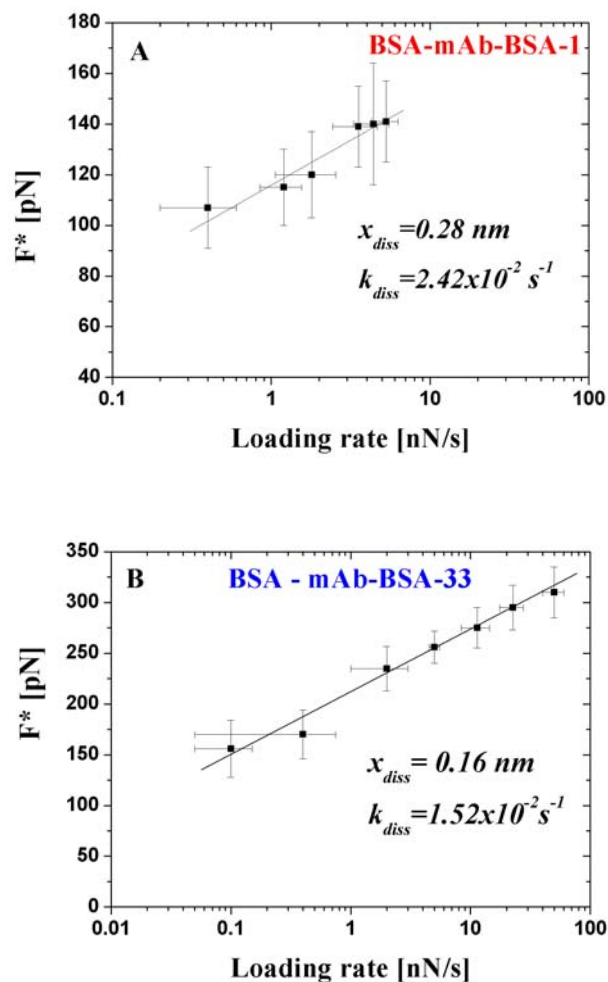


Figure 17. Dependence of the most probable unbinding force (F^*) on the loading rate for BSA – mAb-BSA-1 (A) and BSA – mAb-BSA-33 (B) complexes.

3.5 Conclusion

In this chapter the specific interactions between BSA and poly- or two monoclonal BSA antibodies have been studied using quasistatic force spectroscopy regime of the AFM (without any external modulation of the AFM tip motion). When the measurements have been

performed at constant loading rate one can compare the histograms of unbinding forces for different antigen-antibody complexes. The histograms of the unbinding forces for polyclonal BSA antibodies are broad at high antibody concentrations and narrow at low concentrations, while the histograms for monoclonal antibodies peak at well defined unbinding forces. The peak unbinding force depends on the type of antibody and the antibody concentration. Quasistatic FS could serve as a useful method for characterization of antigen-antibody interactions to measuring the specificity of an antibody or to evaluate the purity of a monoclonal antibody solution, and to distinguish between different antibodies. Loading rate-dependent measurements allow us to learn more about the antigen-antibody complex dissociation. The obvious dependence of the mean value of unbinding forces with the loading rate logarithm has been observed for complexes between BSA and its two different monoclonal antibodies, reflecting that only one single potential barrier is dominant.

References

1. Carter, D. C. and Ho, J. X. Structure of serum albumin. *Advances in Protein Chemistry*. **45** (1994) 153-203.
2. Curry, S., Mandelkow, H., Brick, P., and Franks, H. Crystal structure of HSA complexed with fatty acid reveals an asymmetric distribution of binding sites. *Nature Struct. Biol.* **5** (1998) 827-835.
3. Peters, T. Serum albumin. *Advances in Protein Chemistry*. **37** (1985) 161-245.
4. Narazaki, R., Maruyama, T., and Otagiri, M. Probing the cysteine 34 residue in HSA using fluorescence techniques. *Biochim. Biophys. Acta.* **1338** (1997) 275-281.
5. Chadborn, N., Bryant, J., Bain, A. J., and O'Shea, P. Ligand-dependent conformational equilibria of serum albumin revealed by tryptophan fluorescence quenching. *Biophys. J.* **76** (1999) 2198-2207.
6. Reynolds, J. A., Herbert, S., Polet, H., and Steinhardt, J. The binding of diverse detergent anions to BSA. *Biochemistry*. **6** (1967) 937-947.
7. Kosa, T., Maruyama, T., and Otagiri, M. Species differences of serum albumins: I. Drug binding sites. *Pharm. Res.* **14** (1997) 1607-1612.
8. Holowachuk, E. W. and Stoltenborg, J. K., *Protein Data Bank*, accession M73993.1
9. Carter, D. C., and He, X. M. Structure of HSA. *Science*. **249** (1990) 302-303.
10. Squire, P. G., Moser, P., and O'Konski, C. T. Hydrodynamic properties of BSA monomer and dimer. *Biochemistry*. **7** (1968) 4261-4272.
11. Wright, A. K., and Thompson, M. R. Hydrodynamic structure of BSA determined by transient electric birefringence. *Biophys. J.* **15** (1975) 137-141.
12. Bloomfield, V. The structure of BSA at low pH. *Biochemistry*. **5** (1966) 684-689.
13. Feng, L., Andrade, J. D., and Hu, C. Z. Scanning tunneling microscopy of proteins on graphite surfaces. *Scan. Microsc.* **3** (1989) 399-410.
14. Durchslang, H., and Zipper, P. Calculation of hydrodynamic parameters of biopolymers from scattering data using whole body approaches. *Prog. Colloid Polymer Sci.* **107** (1997) 43-47.
15. Matulis, D., Baumann, C. G., Bloomfield, V. A., and Lovrien, R. E. 1-anilino-8-naphthalene sulfonate as a protein conformational tightening agent. *Biopolymers*. **49** (1999) 451-488.

16. Ladam, G., Gergely, C., Senger, B., Decher, G., Voegel, J-C., Schaaf, P., and Cuisinier, F. J. G. Protein interactions with polyelectrolyte multilayers: interactions between HSA and polystyrene sulfonate/polyallylamine multilayers. *Biomacromolecules*. **1** (2000) 674-687.
17. Slayter, E. M. An electron microscope study of conformational change in BSA at low pH. *J. Mol. Biol.* **14** (1965) 443-452.
18. Luft, A. J., and Lorscheider, F. L. Structural analysis of human and bovine alpha-fetoprotein by electron microscopy, image processing, and circular dichroism. *Biochemistry*. **22** (1983) 5978-5981.
19. Hagag, N., Birnbaum, E. R., and Darnall, D. W. Resonance energy transfer between cysteine-34, tryptophan-214, and tyrosine-411 of human serum albumin. *Biochemistry*. **22** (1983) 2420-2427.
20. He, X. M., and Carter, D. C. Atomic structure and chemistry of HSA. *Nature*. **358** (1992) 209-215.
21. Sugio, S., Kashima, A., Mochizuki, S., Noda, N., and Kobayashi, K. Crystal structure of human serum albumin at 2.5 Å resolution. *Protein. Eng.* **12** (1999) 439-446.
22. Ferrer, M. L., Duchowicz, R., Carrasco, B., de la Torre, J. G., and Acuña, A. U. The conformation of serum albumin in solution: a combined phosphorescence depolarization-hydrodynamic modeling study. *Biophys. J.* **80** (2001) 2422-2430.
23. Luetscher, J.A. Serum Albumin. II. Identification of more than one albumin in horse and human serum by electrophoretic mobility in acid solution. *J. Am. Chem. Soc.* **61** (1939) 2888-2895.
24. Foster, J. F. In “*The Plasma Proteins*” (F. W. Putman, ed) 1st ed, **Vol. 1**, 179-239, (1960) Academic Press, New York.
25. Foster, J. F. In “*Albumin Structure, Function and Uses*” (V. M. Rosenoer, M. Oratz, and M. A. Rotschild, eds.) 53-84 (1977) Pergamon, Oxford.
26. Pereira, L. G. C., Théodoly, O., Blanch, H. W., and Radke, C. J. Dilatational rheology of BSA conformers at the air/water interface. *Langmuir*. **19** (2003) 2349-2356.
27. “Molecular biology of the cell” by Alberts, B., Bray, D., Lewis, J., Raff, M., Roberts, K., Watson, J. D. 3rd ed., Garland Publishing, New York, 1994.
28. Roberts, S., Cheetham, J. C., and Rees, A. R. Generation of an antibody with enhanced affinity and specificity for its antigen by protein engineering. *Nature*. **328** (1987) 731-734.
29. Xu, L., Lio, A., Ogletree, F., and Salmeron, M. Wetting and capillarity phenomena of water on mica. *J. Phys. Chem. B.* **102** (1998) 540-548.

30. Cleveland, J. P., Manne, S., Bocek, D., and P. K. Hansma. A nondestructive method for determining the spring constant of cantilevers for scanning force microscopy. *Rev. Sci. Instrum.* **64** (1993) 403-405.
31. Hutter, J. L., and J. Bechhoefer. 1993. Calibration of atomic force microscope tips. *Rev. Sci. Instrum.* **64**(1993) 1868-1873.
32. Schwesinger, F., Ros, R., Strunz, T., Anselmetti, D., Güntherodt, H. J., Honegger, A., Jermutus, L., Tiefenauer, L., and Plückthun, A. Unbinding forces of single antibody-antigen complexes correlate with their thermal dissociation rates. *Proc. Natl. Acad. Sci. USA.* **97** (2000) 9972-9977.
33. Dettman, W., Grandbois, M., André, S., Benoit, M., Wehle, A. K., Kaltner, H., Gabius, H. J., and Gaub, H. E. Differences in zero-force and force-driven kinetics of ligand dissociation from β -galactoside-specific proteins (plant and animal lectins, immunoglobulin G) monitored by plasmon resonance and dynamic single molecule force microscopy. *Arch. Biochem. Biophys.* **383** (2000) 157-170.
34. Gunnig, A. P., Wilde, P. J., Clark, D. C., Morris, V. J., Parker, M. L., and Gunning P. A. Atomic force microscopy of interfacial protein films. *J. Colloid Interface Sci.* **183** (1996) 600-602.
35. Kasas, S., Riederer, B. M., Catsicas, S., Cappella, B., Dietler, G. Fuzzy logic algorithm to extract specific interaction forces from atomic force microscopy data. *Rev. Sci. Instrum.* **71** (2000) 2082-2086.
36. Hummer, G., and Szabo, A. Free energy reconstruction from nonequilibrium single-molecule pulling experiments. *Proc. Natl. Acad. Sci. USA.* **98** (2001) 3658-3661.
37. Hinterdorfer, P., Baumgartner, W., Gruber, H. J., Schilcher, K., and Schindler, H. Detection and localization of individual antibody-antigen recognition events by AFM. *Proc. Natl. Acad. Sci. USA.* **93** (1996) 3477-3481.
38. Allen, S., Chen, X., Davies, J., Davies, M. C., Dawkes, A. C., Edwards, J. C., Roberts, C. J., Sefton, J., Tendler, S. J. B., and Williams, P. M. Detection of antigen-antibody binding events with the AFM. *Biochemistry.* **36** (1997) 7457-7463.
39. Ros, R., Schwesinger, F., Anselmetti, D., Kubon, M., Schäfer, R., Plückthun, A., and Tiefenauer, L. Antigen binding forces of individually addressed single-chain Fv antibody molecules. *Proc. Natl. Acad. Sci. USA.* **95** (1998) 7402-7405.
40. Harada, Y., Kuroda, M., and Ishida, A. Specific and quantized antigen-antibody interaction measured by AFM. *Langmuir.* **16** (2000) 708-715.

41. Benjamin, D. C., and Teale, J. M. The antigenic structure of BSA. *J. Biol. Chem.* **253** (1978) 8087-8092.

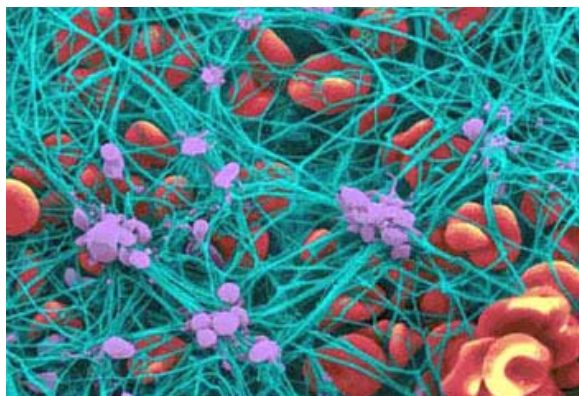
Chapter IV

Fibrinogen and Fibrin

4.1 Fibrinogen and Fibrin

The preceding chapter illustrates the quasistatic force spectroscopy (FS) studies of serum albumin and its antibodies complexes. In this chapter we will focus on the study of another abundant plasma protein, the fibrinogen. First, its structure and their functional properties including the description of fibrin gel formation are given in part I. Some fibrinogen molecules and fibrin strands are visualized with the AFM, and shown in the part II. The possible molecular assembly in fibrin strands is discussed. Until now, not a lot of experimental information about forces involved in the fibrin polymerization process is available. So, in the third part of this chapter, the first standard FS studies of fibrinogen and fibrin complexes are represented.

4.2 Introduction



Scanning electron micrograph of fibrin clot (in blue) and red blood cells (RBC) (in red) [color courtesy of Yuri Veklich and John Weisel, <http://www.med.upenn.edu/cellbio/faculty/weisel/>].

Coagulation of blood is a phenomenon similar for almost all living organisms that have blood and known from the earliest historical times. The philosophers of antiquity tried to give interesting explanations. For example, Aristotle [1] in about 300 BC declared that coagulation of blood was similar to freezing of water. In the end of 17th century, Malpighi (1686) described the structural component of the blood clot as a white

fibrous substance. In the middle of the 19th century, this was identified as a constituent of pathological thrombi and given the name fibrin. Olof Hammarsten (1880) was the first scientist who isolated the fibrinogen, the precursor of fibrin, in a highly purified form and suggested that the first step of fibrin formation was the activation of fibrinogen by the enzyme thrombin.

Fibrinogen is a multifunctional blood protein and it plays a central role in normal hemostasis (coagulation of blood), wound healing and pathological processes, such as thrombosis (blood clotting) and atherosclerosis. Fibrinogen is also known as a very “sticky” protein which adsorbs strongly to a variety of surfaces, for example, fibrinogen is found on medical implants like artificial cardiac valves, etc. Such a multifunctional character of fibrin(ogen) is connected with its complex structure. A comprehensive understanding of its biological functions requires knowledge of its structural organization. Of course, by now, we know and understand many mechanisms at the basis of the fibrinogen-fibrin transformation, but unhappily, many of them remain mysterious. The following part focuses on the molecular structural and functional background of fibrinogen and fibrin.

4.2.1 Molecular structure of fibrinogen

Several models of the structure of fibrinogen were proposed [2-5]. In 1959 Hall and Slayter [2] first described fibrinogen as elongated molecule 47.5 ± 2.5 nm long, featuring three nodules, like “chupa-chups” on a string (fig. 1).

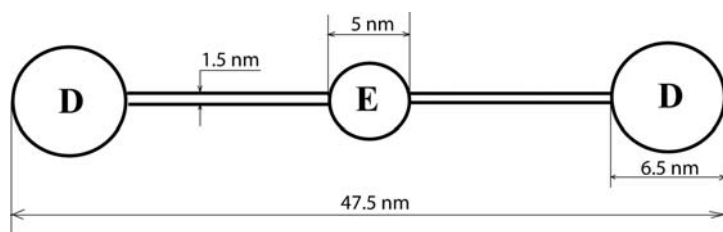


Figure 1. Simplified schematic drawing of the fibrinogen according to Hall and Slayter [2].

The outer two nodules, called terminal

domains (D terminal domains), are 6.5 nm in diameter, and the central domain (E central domain) is 5 nm in diameter. They are joined by a thread less than 1.5 nm thick called the coiled-coil.

By the late 1970s, the molecular structure of fibrinogen was elucidated by Doolittle and the primary sequence of this 340 KDa molecule was completed [3]. According to the current view, fibrinogen consists of two identical subunits, each of which contains three non-identical (but evolutionary related) polypeptide chains named $A\alpha$, $B\beta$ and γ , composed of 610, 461, and 411 amino acids, respectively (fig. 2).

Both the subunits and the chains are linked together by disulfide bonds, and assembled to form at least 20 distinct domains [6-8] grouped into major structural regions: the central E domain, 2 identical terminal D regions, and 2 α C-domains. The central E domain has a dimeric structure and is formed by amino NH_2 -terminals of all 6 polypeptide chains. The slightly thickened NH_2 -terminal ends of the $A\alpha$ and $B\beta$ chains represent fibrinopeptide A (FPA) and fibrinopeptide B (FPB), respectively, which are not present in fibrin molecule. The dimeric halves of the central domain are held together by three of 11 disulfide bonds, the remaining eight are located between the $A\alpha$ and $B\beta$ chains [9] and in the junctions between the central domain and the coiled-coils [10]. These coiled-coils are composed by the single $A\alpha$, $B\beta$, and γ chains super-coiled as α -helices. Six disulfide bonds in each coiled-coil are responsible for the supercoil structure and for the attachment to the central and lateral domains in the form of disulfide rings. The amino acid residue orientation is such that the inside of the coiled-coil is hydrophobic and the outside is polar. The lateral D domains are formed by carboxyl $COOH$ -terminal portions of the $B\beta$ and γ chains and a portion of $A\alpha$ chains, and have a mass of 67.2 KDa each. Most of the bulk in each D domain is represented by random folds of $B\beta$ and γ chains, forming the corresponding β and γ modules.

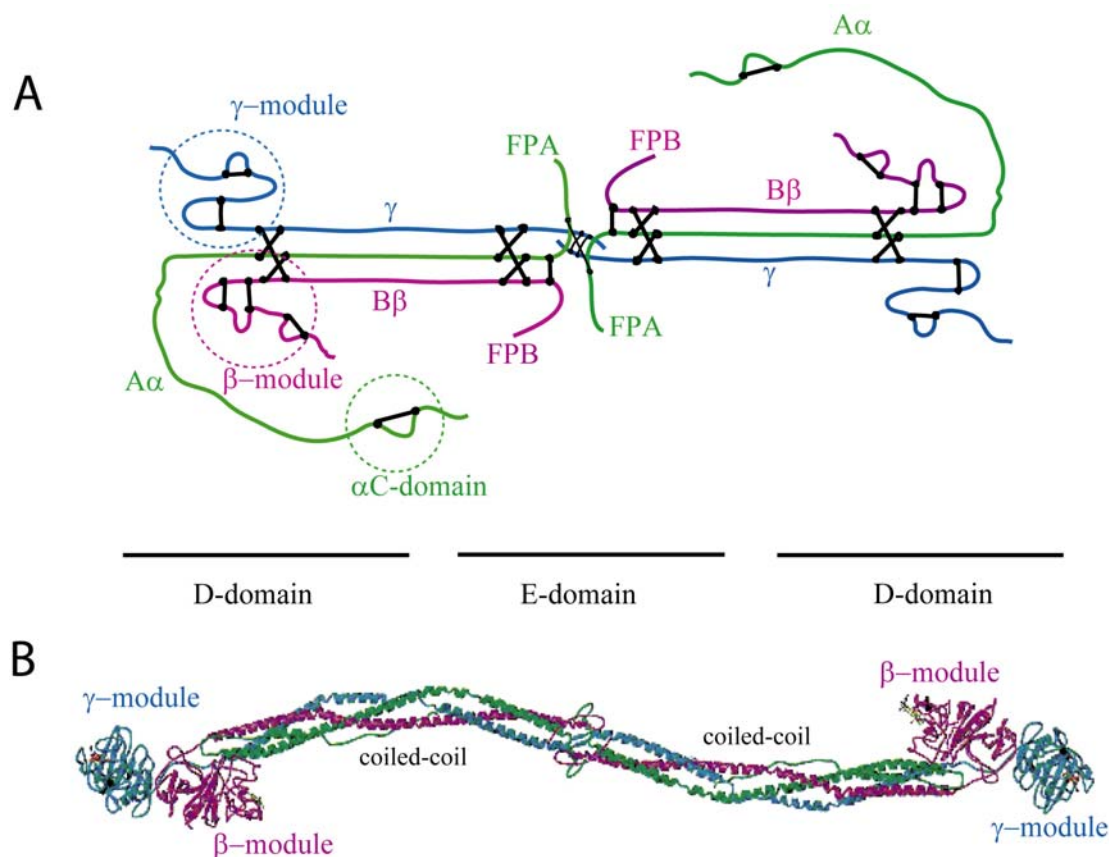


Figure 2. Representation of the fibrinogen molecule. A) The structure (centrosymmetric) of the fibrinogen according to Hoepflich and Doolittle [4]. Polypeptide chain composition and independently folded domains in fibrinogen; $A\alpha$ (green), $B\beta$ (red) and γ (blue) designate individual polypeptide chains; the disulfide bonds are shown by the black bars; FPA and FPB designate the fibrinopeptides A and B in the central E domain. B) Ribbon model of chicken fibrinogen based upon its crystal structure [11]; note that the NH_2 -terminal ends of $A\alpha$ and $B\beta$ were not resolved.

4.2.2 Fibrin polymer formation

Fibrinogen molecule is converted into the insoluble fibrin clot by a series of enzymatic and physical steps. The first step toward fibrinogen polymerization is the formation of fibrin monomers. This is accomplished by the cleavage of peptide material – the fibrinopeptides A and B (FPA and FPB) – from the NH_2 -terminal regions of the $A\alpha$ - and $B\beta$ -chains by an enzyme thrombin [12-14]. This cleavage exposes polymerization sites (knobs) “A” and “B” (in the central

domain E), which include newly generated NH₂-terminal sequences Gly-Pro-Arg (GPR) and Gly-His-Arg (GHR) (fig. 3). The interactions of the knobs “A” and “B” with complementary sites (holes) “a” and “b” located in the lateral D domains of neighboring fibrin(ogen) [15] are crucial for fibrin polymer formation. These two fibrinopeptides (FPA and FPB) are cleaved at different rates [16]. According to the current view [17-19], fibrin formation starts with removal of FPA. This cleavage of FPA enables the formation desA-fibrin monomers and the aggregation of these monomers in desA-protofibrils. The subsequent removal of FPB facilitates the “knob B”-“hole b” interactions. These interactions promote lateral association of protofibrils into thicker fibers which form a three-dimensional network or fibrin clot. The intermolecular association of two α C-domains during fibrin assembly also encourages lateral aggregation of protofibrils (fig. 3) [21, 20]. In addition, thrombin activates factor XIII in factor XIIIa which then covalently cross-links fibrin, reinforcing thus its structure. The cross-linking occurs rapidly between the COOH-terminal ends of the γ chains of the neighboring fibrin D domains (γ - γ cross-linking) and more slowly between the α C-domains in the α C-polymers [22].

Remarkably, small synthetic peptides, modeled on A-knob sequences, with only 3 or 4 amino acids in length can bind to fibrin(ogen) and inhibit fibrin polymerization [23, 24]. Under most circumstances, however, synthetic B-knob sequences do not appreciably interfere with fibrin formation. Synthetic peptides beginning with the sequence GHR are not effective inhibitors of fibrin polymerization [23, 24] and GHRP peptides actually accelerate fibrin formation [23].

It is also well known that fibrin can be formed by the removal of fibrinopeptide A only, as occurs with various snake venom enzymes (e.g. Reptilase) [25]. Nevertheless, such fibrin can be distinguished from fibrin generated by the thrombin-catalyzed removal of both fibrinopeptides A and B, and there must be a physiological basis for removing the B peptide.

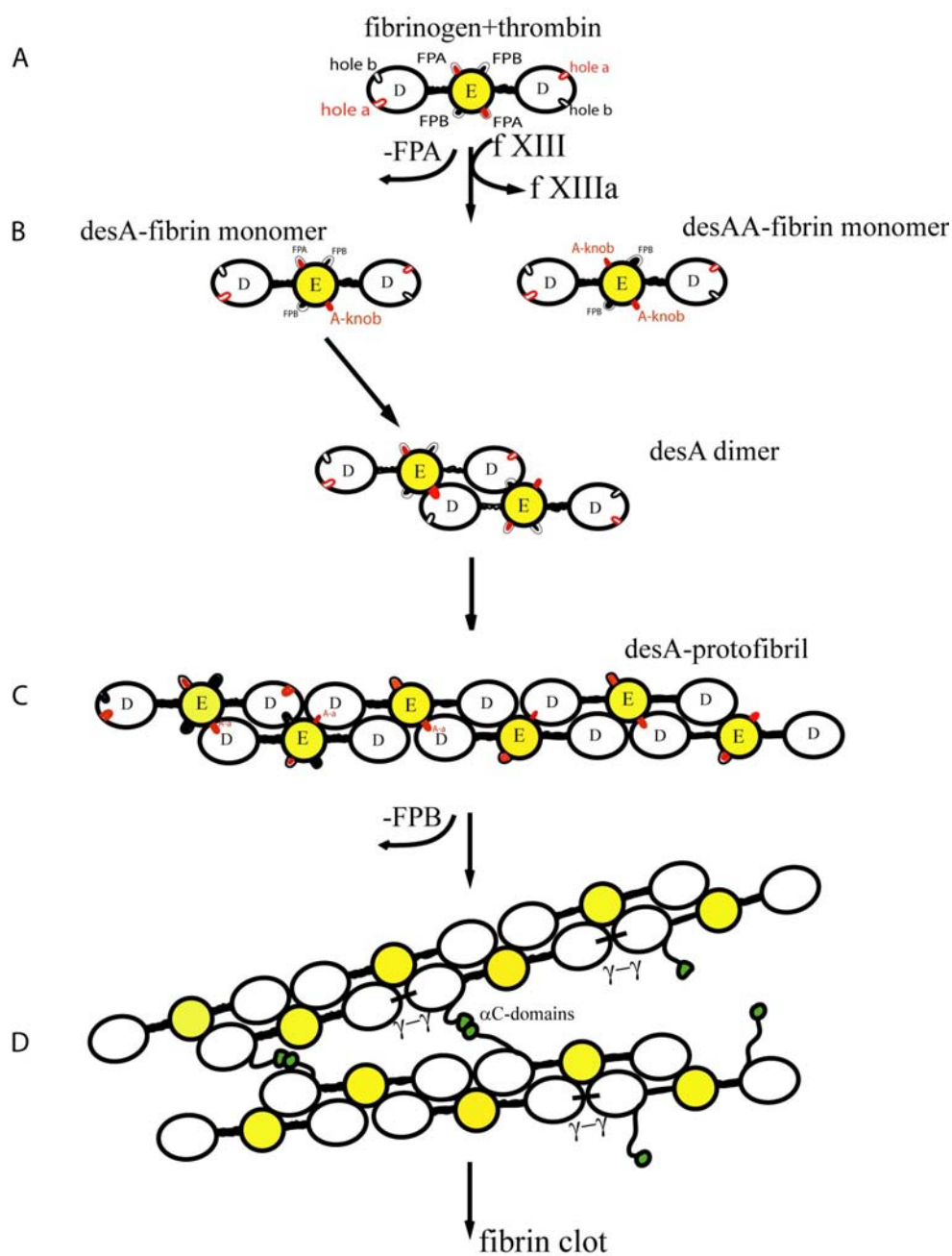


Figure 3. Fibrinogen-to-fibrin polymer formation. A) Activation of fibrinogen molecule by thrombin; the α C-domains in fibrinogen molecule are not shown. B) desA-fibrin and des AA-fibrin monomers; it was assumed that number of desAA-fibrin monomers are neglected in early stage of thrombin action [26]. Knob to hole “A-a” interaction between two desA-monomers yield the desA dimer. C) desA-protofibrils. D) desA-protofibrils and intermolecular the α C-domains upon lateral aggregation of protofibrils. The γ - γ cross-links between the D domains are presented by small black line; they may also occur in a transverse manner [22].

4.2.3 About the symmetry of the fibrinogen molecule

Over the past years and until now, in many reviews and reports, the schematic representation of fibrinogen is shown as a parallel orientation of the half-molecules with symmetry axis (fig. 4). Moreover, both the conversion to fibrin and subsequent polymerization is explained in terms of such structure. Hoeprich and Doolittle [4] were the first who revealed the centrosymmetric (antiparallel) structure of the fibrinogen molecule as presented above (fig 2). Taking into account the antiparallel junction of the two γ -chains at the intermediate fibrin polymer formation [27] and the antiparallel arrangement α -chains cross-linking in fibrin [28], they reported that the fibrinogen is itself dimerized in an antiparallel manner. Dietler and coworkers [26] also supported the centrosymmetric structure of fibrinogen by enzyme kinetics and light scattering studies of fibrin polymerization. They noted that the location of FPAs and corresponding A-knobs must be taken from the Hoeprich's and Doolittle's fibrinogen structure. Interestingly and unfortunately, these conclusions are missed in the biggest amount of literature about fibrinogen and fibrin. One purpose of our study is the revelation of the centrosymmetry of the fibrinogen molecule by AFM experiments.

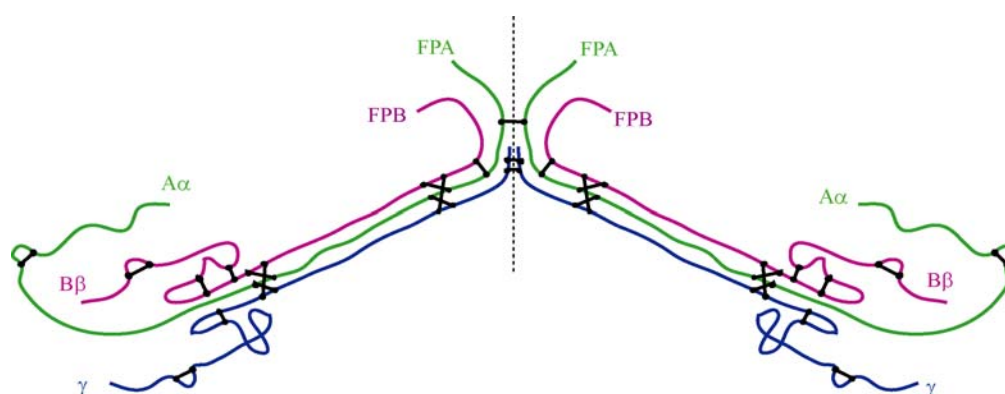


Figure 4. Parallel with axis symmetry presentation of the fibrinogen molecule.

4.3 Fibrinogen to fibrin formation visualized with the AFM

The AFM offers the opportunity to direct visualization of proteins, their structural organization without any treatments of molecules used in the electron microscope (EM), such as negative staining, vacuum or freeze drying that might affect the structural appearance of labile molecules. This paragraph represents the AFM images of fibrinogen molecules and early fibrin polymers (strands or protofibrils) recorded in the tapping mode using the standard non-contact cantilevers (NSC12, Micromasch). First, the AFM images of single fibrinogen molecules are shown in fig. 5. The trinodular structure of this molecule with characteristic length of 45-50 nm is observed.

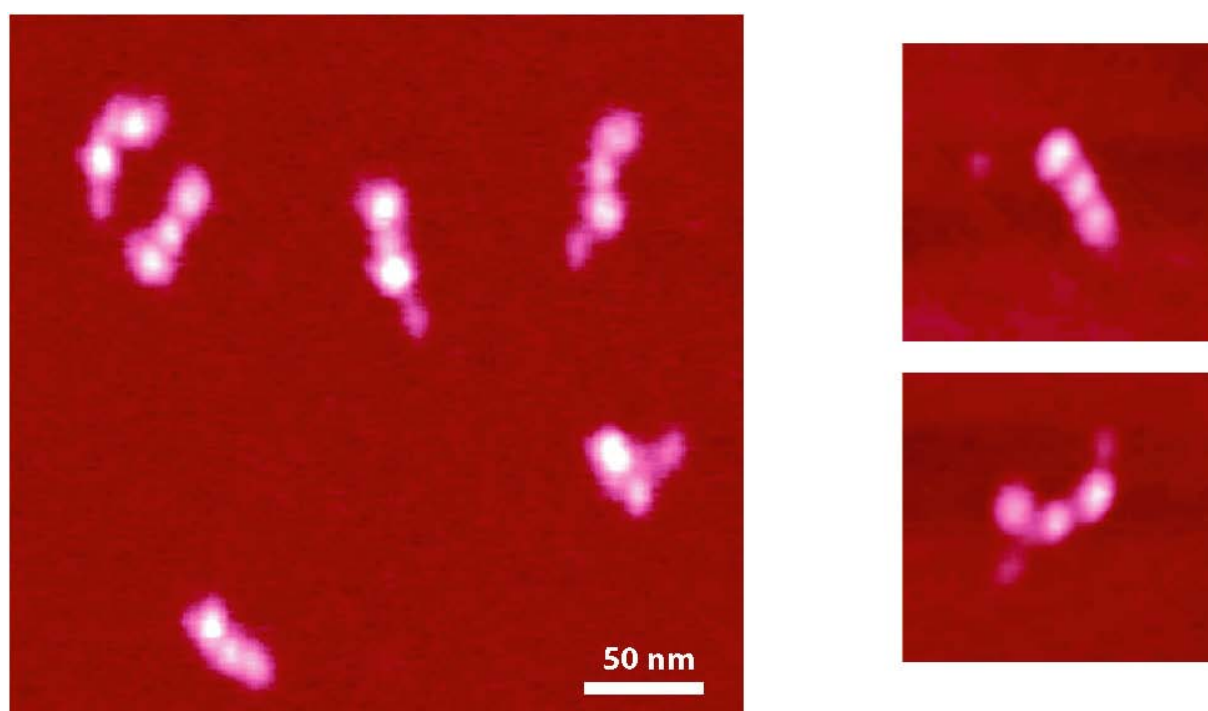


Figure 5. AFM images of fibrinogen molecules adsorbed on freshly cleaved mica. Color scale (dark red to white) is 0 – 3.5 nm.

After that, we were concentrated to find the conditions favorable for the formation of the single long fibrin strands (early fibrin polymers). Fig. 6 illustrates the fibrin strands with lengths of about 1 μm .

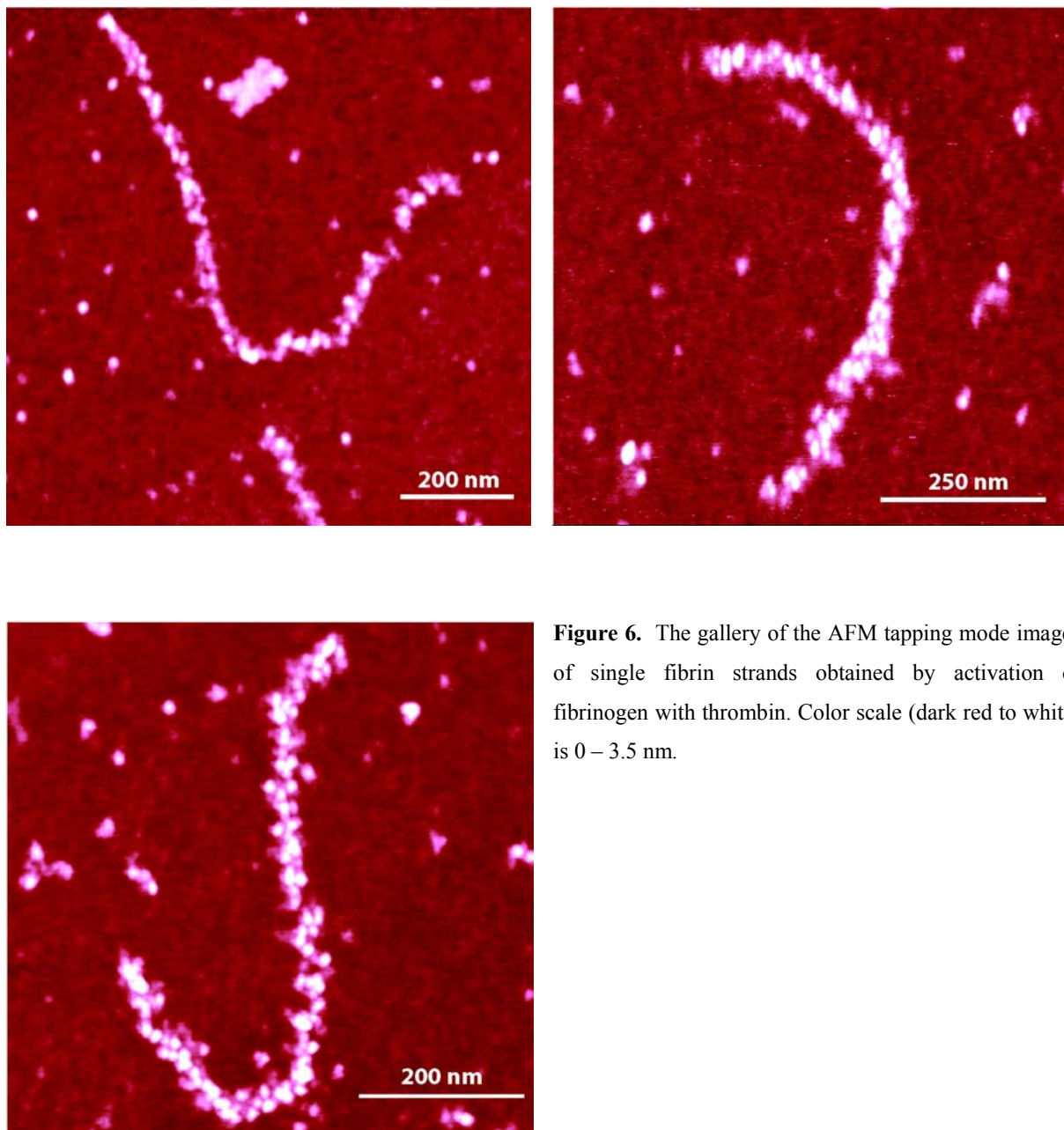


Figure 6. The gallery of the AFM tapping mode images of single fibrin strands obtained by activation of fibrinogen with thrombin. Color scale (dark red to white) is 0 – 3.5 nm.

In these experiments the activation of fibrinogen (25 $\mu\text{g/ml}$ in TRIS buffer, pH 7.4) was achieved by addition of 30 μl of thrombin (0.15 NIH units/ml in TRIS) to the 30 μl of fibrinogen solution. Incubation was carried out in aliquots for about 1 hour at 20 $^{\circ}\text{C}$. 30 μl of solution was deposited on the freshly cleaved mica for 1 min, then the sample was washed with water and air dried prior to AFM imaging. Sometimes smaller fibrin strands are viewed (fig. 7).

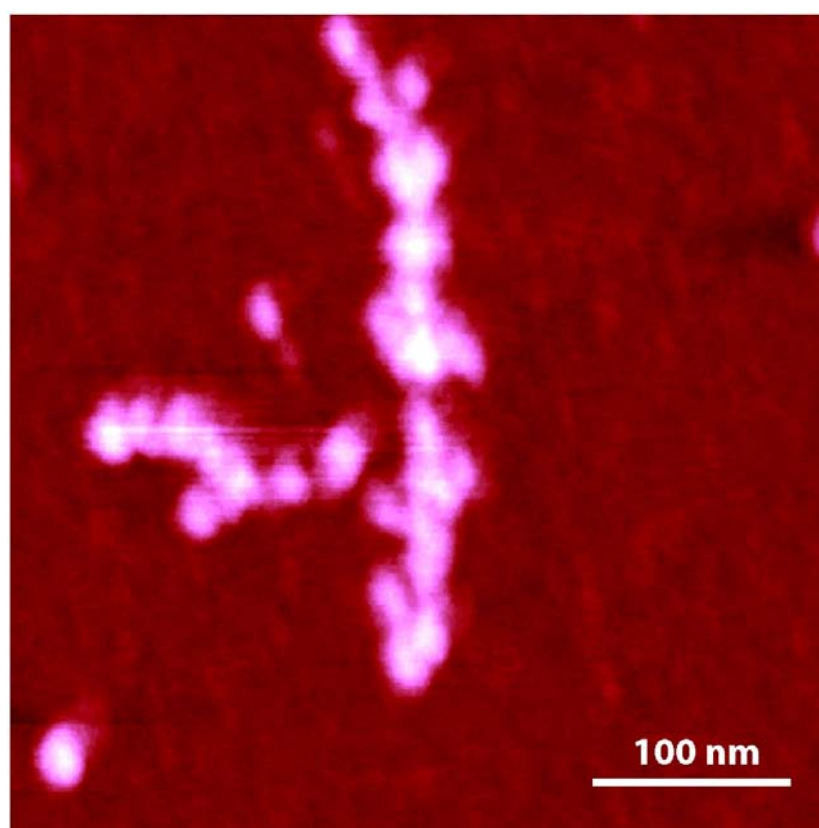


Figure 7. AFM tapping mode image of fibrin strand.

The aggregation of two or more long single strands is also observed (fig. 8). One can see that the strands are twisted; such type of aggregation is never mentioned in the literature.

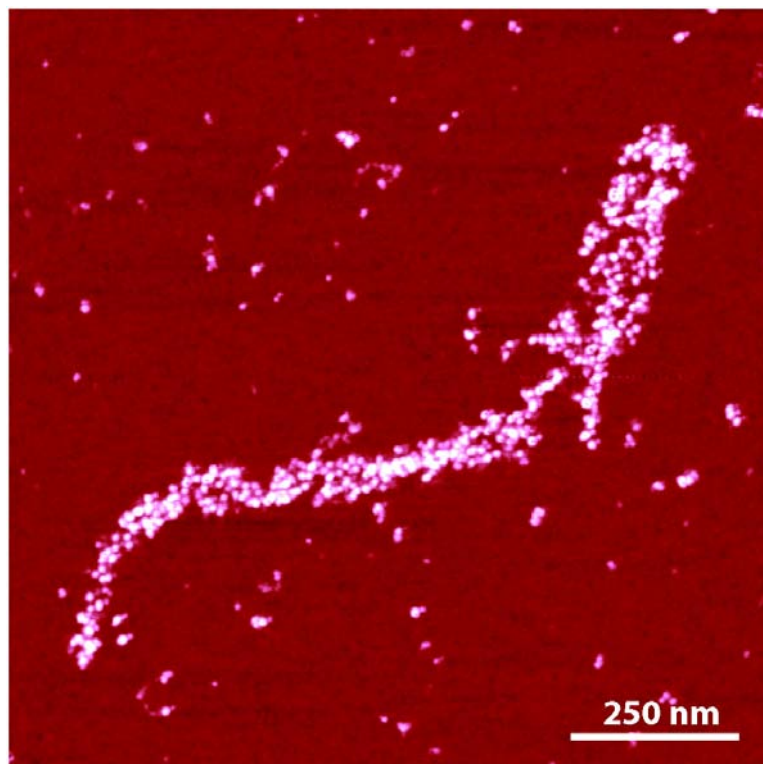
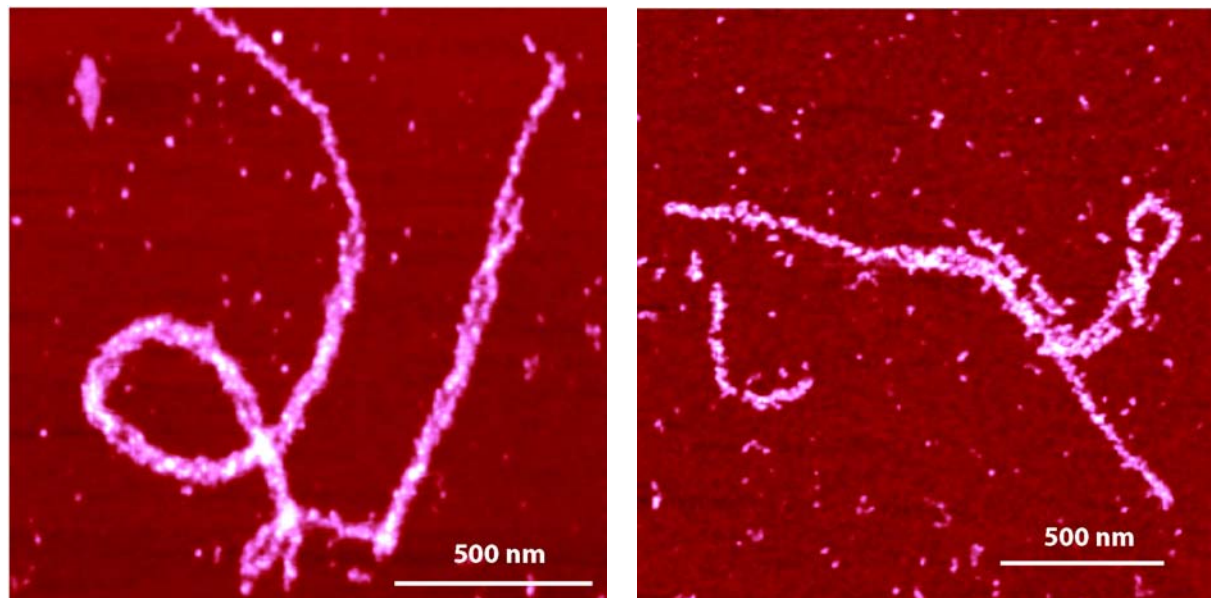
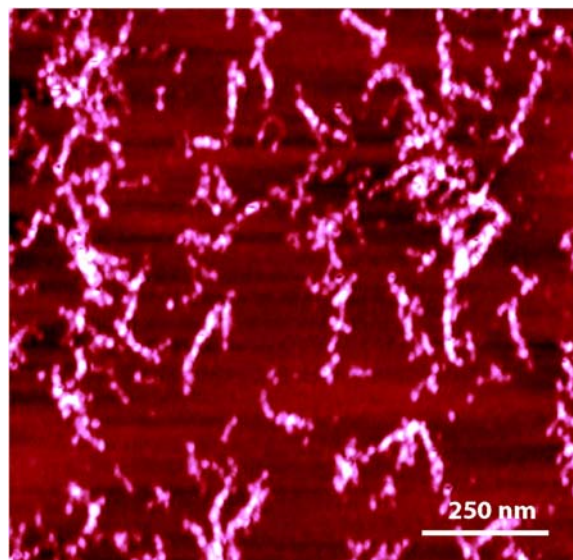


Figure 8. The gallery of the aggregation of two or more single long fibrin strands. The color scale (dark red to white) is 0 – 5 nm.

If the mentioned above concentration ratio is not respected, one can observe the single strands with shorter lengths (fig.9), and their further lateral aggregation in fibrin network (fig.10).



Fibrin 9. The AFM tapping mode images of fibrin strands with the length of about 250 nm. The color scale (from dark red to white) is 0 – 5 nm.

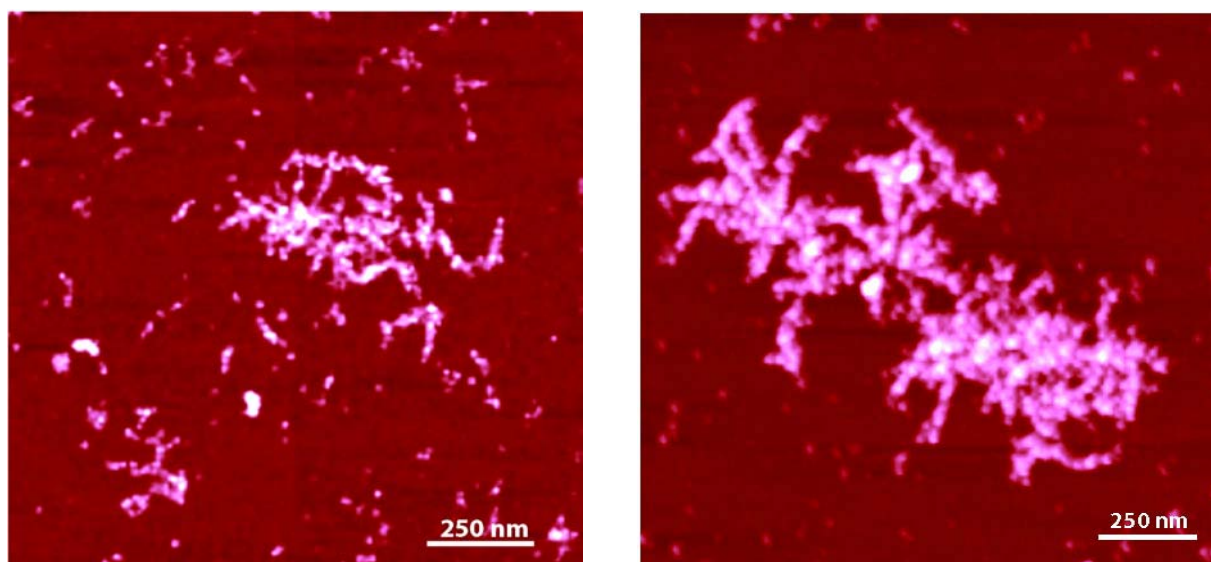


Figure 10. The AFM tapping mode images of fibrin network. The color scale (from dark red to white) is 0 – 10 nm.

Interestingly, the half-staggered double-stranded forms of single fibrin polymers proposed by Ferry [29] have been never observed in our studies. This fact was already mentioned by Hunziker et al [30]. Hunziker and coworkers proposed a new interlocked single-strand mechanism of fibrin formation based on the EM observations of fibrin strands. By using the cantilevers with high aspect ratio (STING, Micromasch) or with the tip curvature < 1 nm (HI'RES, Micromasch) the AFM images of single fibrin strands with better resolution are obtained (fig. 12).

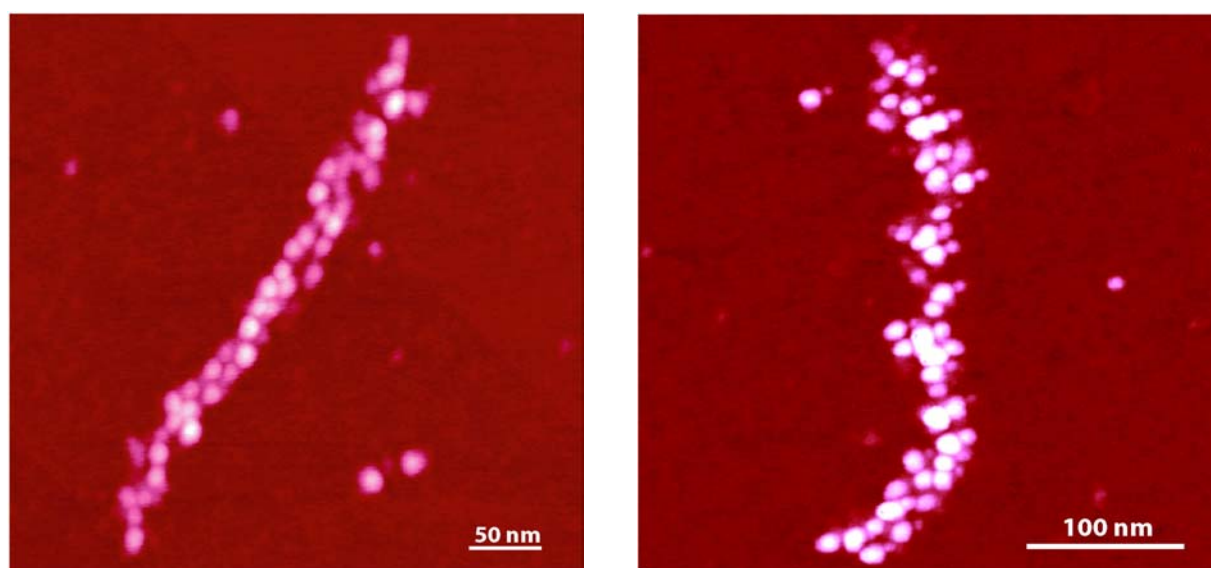


Figure 12. The high resolution AFM images of single fibrin strands obtained with STING (left image) and HI'RES (right image) cantilevers. The color scale (from dark red to white) is 0 – 3.5 nm.

By simple looking at these images, the linear polymer growth can be imaged as a simplified “domino” game (fig. 13) with special rules. Some our imagination of molecular organization in fibrin strand is illustrated in fig. 14.

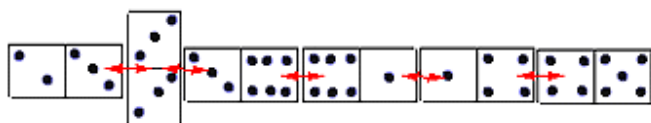


Figure 13. The illustration of domino game.

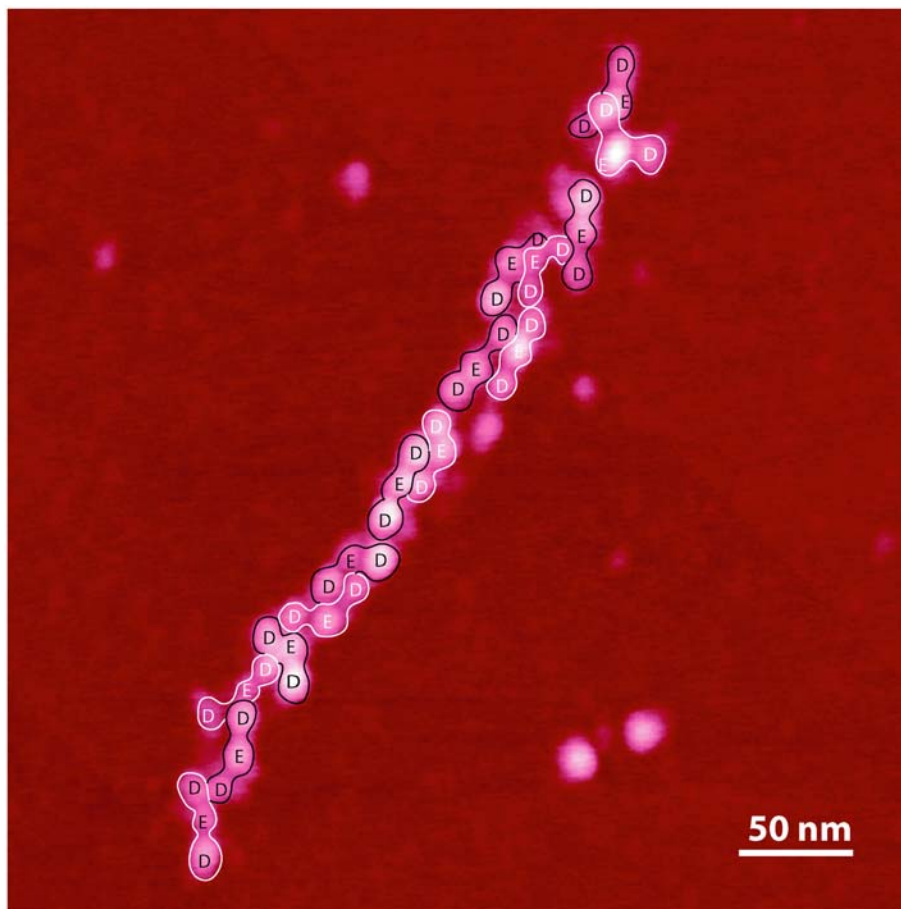


Figure 14. Molecular organization in fibrin strand.

Based on our first AFM observations we conclude that structural organization in fibrin strands is more consistent with centrosymmetric structure of fibrinogen. Of course, in order to confirm this conclusion more detailed and systematic analysis analogous to Hunziker's study [30] should be performed.

4.4 Quasistatic force spectroscopy study of fibrin gel formation

To better understanding the process of fibrin(ogen) aggregation, the possible forces between the molecules involved in gel formation have been measured by AFM operated in quasistatic force spectroscopy mode. The following molecular pairs are considered: fibrinogen-fibrinogen, fibrin-fibrinogen or fibrinogen-fibrin. The activation of the fibrinogen (fibrin monomers) has been performed by two different enzymes, thrombin (cleaves fibrinopeptide A and B) and Reptilase (only cleaves fibrinopeptide A). As an inhibitor of the fibrin gel formation the tetrapeptide *Gly-Pro-Arg-Pro* have been used. In order to improve our experiments, the specific interaction between fibrin(ogen) and longer synthetic peptide beginning by *Gly-Pro-Arg* (*Gly-Pro-Arg-(His)₄*) has been tested. All force forces have been measured by using the AFM operated in static force spectroscopy regime (standard “force-volume” mode) and carried out in PBS buffer solution (50 mM phosphate, 150 mM NaCl, pH 7.4 at 25 °C) at room temperature.

4.4.1 AFM instrumentation, tip and sample preparation, data analysis

AFM instrumentation

The AFM has been described in detail in the “AFM instrumentation” paragraph of chapter III “BSA – Ab-BSA complexes” as well as the cantilever calibration method.

Tip and sample preparation

First, fibrinogen molecules were immobilized on the AFM tip and on the APTES-mica sheet via glutaraldehyde (see Chapter II “Sample ant tip preparation methods for FS study”). To obtain fibrin monomers on the tip and sample surface, fibrinogen-functionalized tips/samples were further activated by thrombin (Sigma, USA) (30 µl of 0.08 NIH units/ml, 30-min incubation at 25°C) or Reptilase[®] (Batroxobin) (Pentapharm LTD, Switzerland) (30 µl of 1 Batroxobin units

(BU)/ml, 30-min incubation at 25°C). The *Gly-Pro-Arg-(His)₄* peptides (0.5 mg/ml) were immobilized on the AFM tip via EDAC. Fibrin(ogen), peptides-functionalized tips/samples were further extensively washed with PBS buffer and used immediately for force spectroscopy study. *Gly-Pro-Arg-Pro* and *Gly-Pro-Arg-(His)₄* peptides were purchased from American Peptide Company, USA. The functionalized tip and samples were immediately used for force spectroscopy study.

Data analysis

Force curves were analyzed following the aforementioned software. For one given experiment, at least 512 force-distance curves were detected and each experiment was independently made three or more times. The histograms of unbinding forces for each studied complex were constructed using different bin sizes (from 10 pN to 20 pN), and no significant differences in the maxima force values were found.

4.4.2 Fibrinogen-fibrinogen interaction

4.4.2a Control experiments

In order to confirm that we really measured fibrinogen-fibrinogen interaction following control experiments were analyzed: bare tip – fibrinogen and fibrinogen-functionalized tip – freshly cleaved mica. No adhesive interactions were detected during approach of the tip to the sample surface, but only on tip retraction.

4.4.2a/1 Bare tip – fibrinogen system

This experiment consists of a measure of the force rupture between a bare AFM tip and fibrinogen immobilized on APTES mica. Fig. 15 shows typical force curves (retraction part) recorded during this measurement.

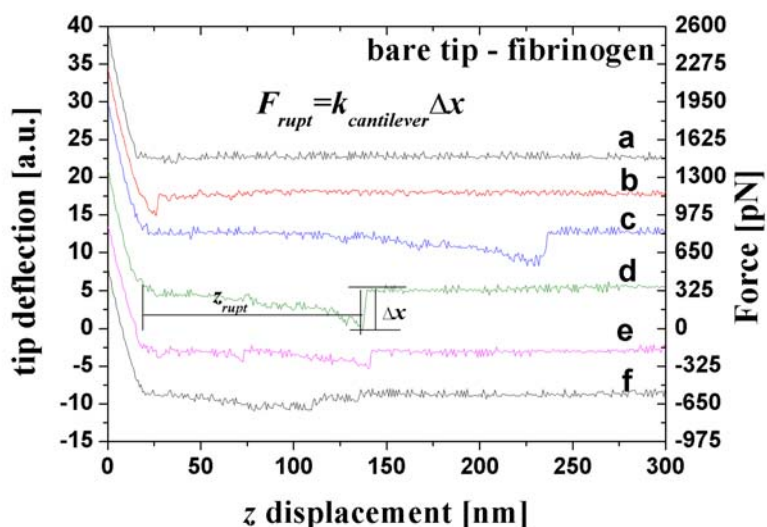


Figure 15. Typical force curves recorded during bare tip-fibrinogen experiment. Curve a) – no rupture events detected; curves b),c),and d) represent single events with different force and length rupture (b - 202 pN, 10 nm; c - 202 pN, 216 nm; d – 336 pN, 118 nm), some times (2% of recorded curves) double rupture events (two well distinguished rupture peaks on the force curve) were observed (curves e – 120 pN, 54 nm; 158 pN, 123 nm and f – 99 pN, 90 nm; 95 pN, 116 nm).

About 35% of all force curves recorded reveal jump-off-contact (rupture) events with characteristic force (F_{rupt}) and length (z_{rupt}) rupture. No dependence between rupture forces and loading rate has been observed. The force and length distributions, measured at constant loading rate of about 3.5 nN/s, are represented in fig. 16 and fig. 17 respectively. Fig. 16 shows a quantization in the force with the peaks at 105 pN, 145 pN, 180 pN, and 225 pN and corresponding period of approximately 40 pN, and force range from 80 pN to 500 pN. The wide distribution of lengths rupture from 5 nm to 400 nm, with the maximum at 20 ± 5 nm, is observed (fig. 17). This broad distribution of lengths can be explained by the random stretching of different chains of fibrinogen, essentially by the α C-chains probably.

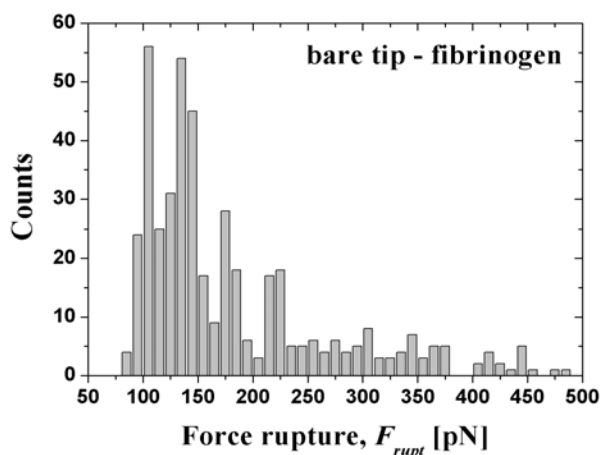


Figure 16. Force histogram for bare tip – fibrinogen experiment. In total 1280 curves are analyzed, 445 curves present rupture events, bin size is 10 pN. The quantization of force is seen with the peaks at 105 pN, 145 pN, 180 pN, and 225 pN.

Figure 17. Lengths rupture histogram for bare tip – fibrinogen experiment. Most of rupture events (13% of all curves analyzed) have the length rupture of about 20-25 nm

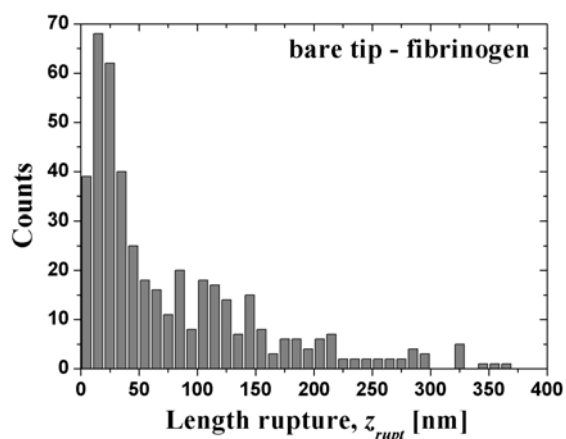


Fig. 18 represents a diagram of forces with corresponding length rupture and schematic representation of the possible interaction between the bare tip and fibrinogen-functionalized mica. As we can see, one part of rupture events (12 % of all curves analyzed) with the lengths not longer than 25 nm (half of the fibrinogen molecule) peaks well at forces of 105 pN, 145 pN, 180 pN, and 225 pN, and another part of events (16 % of all curves analyzed) with the lengths > 25 nm (until 150 nm) peaks also at 105 pN, 145 pN, 180 pN, and 225 pN. A small difference was observed for fibrinogen – mica control system.

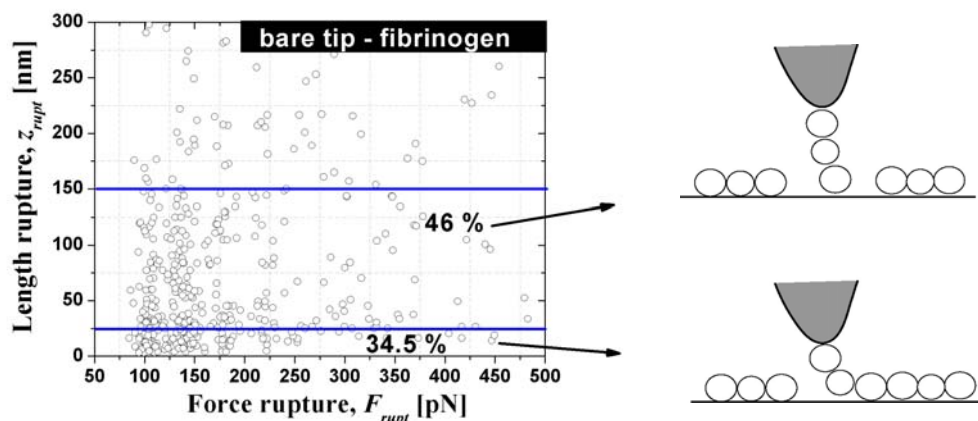
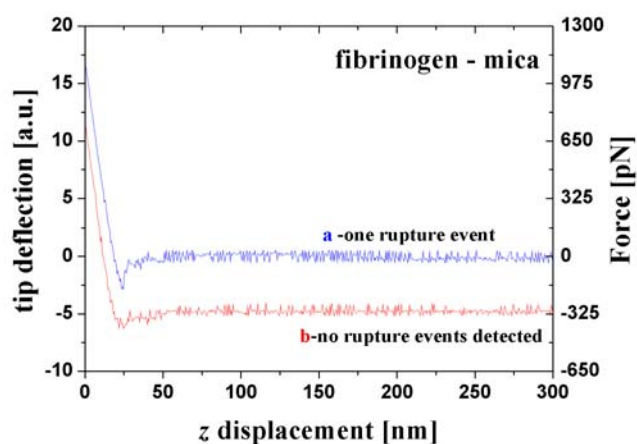


Figure 18. Force-length diagram for bare tip – fibrinogen experiment (left) and illustration of the process of interaction between bare tip and fibrinogen-functionalized mica (right). On the left image 100 % corresponds to all rupture events detected (445 events).

4.4.2a/2 Fibrinogen-functionalized tip – mica system

This experiment consists of a measure of force rupture between fibrinogen-functionalized AFM tip and freshly cleaved mica surface. The typical force curves (retraction part) for fibrinogen-mica system are shown in fig. 19. Most of recorded curves (about 69%) do not represent any rupture events and the 31% have one rupture event with characteristic length, $z_{rupt} = 12 \pm 5$ nm (fig. 20). The values of forces rupture vary from 80 to 150 pN and force distribution peaks at 105



and 145 pN (figs. 21, 22).

Figure 19. Two types of force curves are detected during fibrinogen-mica experiments: a) curves (31%) with only one rupture event and b) curves (69%) do not show any rupture event.

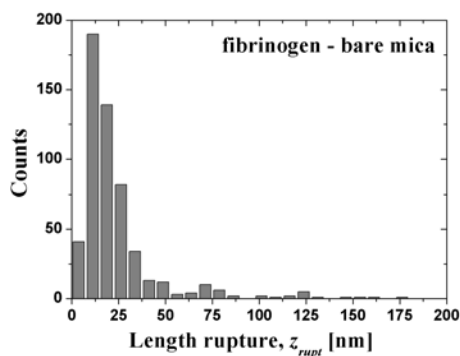


Figure 20. Lengths rupture histogram for fibrinogen - mica experiment. An average length rupture for all rupture events is determined as $z_{rupt} = 12 \pm 5$ nm.

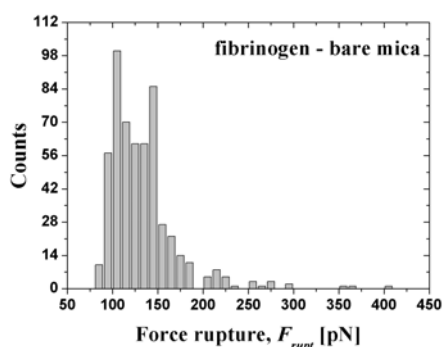


Figure 21. Force histogram for fibrinogen – mica experiment. In total, 1792 curves are analyzed, bin size is 10 pN.

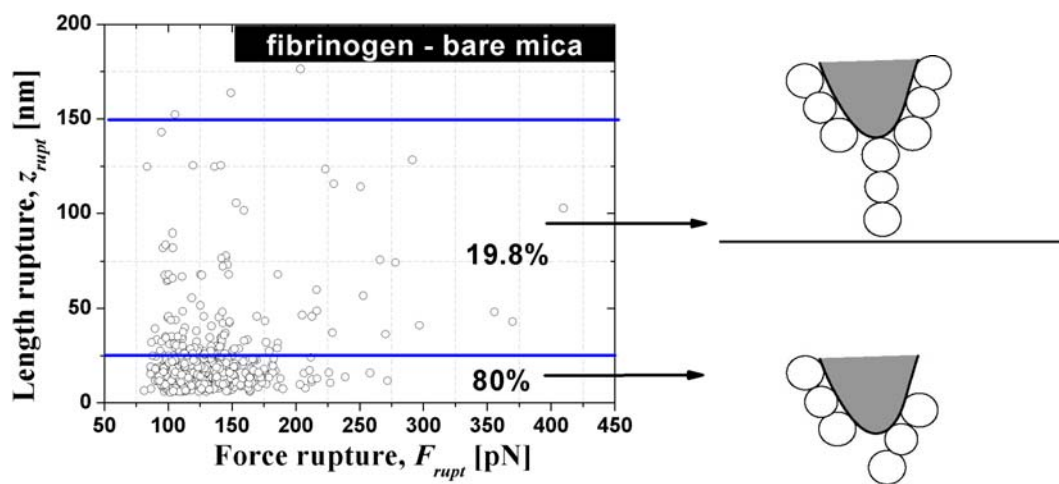


Figure 22. Force-length diagram for fibrinogen – mica experiment (left) and schema of corresponding interaction between fibrinogen-functionalized AFM tip and freshly cleaved mica. On the left image, 100 % corresponds to all rupture events detected (552 rupture events).

The forces rupture between bare tip and freshly cleaved mica were also measured. Indeed, in this case a large number of recorded curves (more than 98%) do not represent any rupture events like illustrated in fig. 19, curve b, and less than 2% of curves have one rupture event similar to the one represented in fig. 19, curve a. Therefore, basing on these control experiments, the rupture events occurring when the tip is still closer than 25 nm (\approx half of fibrinogen molecule) to the surface were assumed to be caused by non-specific adhesion of fibrinogen and were not further considered for the data evaluation.

4.4.2b Fibrinogen-fibrinogen complex

In order to perform this kind of experiment, fibrinogen molecules are immobilized on the tip and on the sample surface, and the rupture forces are measured. The typical force curves are represented in fig. 23. We classify the curves as following: no rupture events detected (40% of all approach-retract cycles, fig.23 A – blue curve); adhesion event with the length $<$ 25 nm (less than 2%, fig. 23 A – red curve); and single rupture events (about 60%, fig. 23 B). As described above we do not consider the adhesion events for fibrinogen-fibrinogen data evaluation.

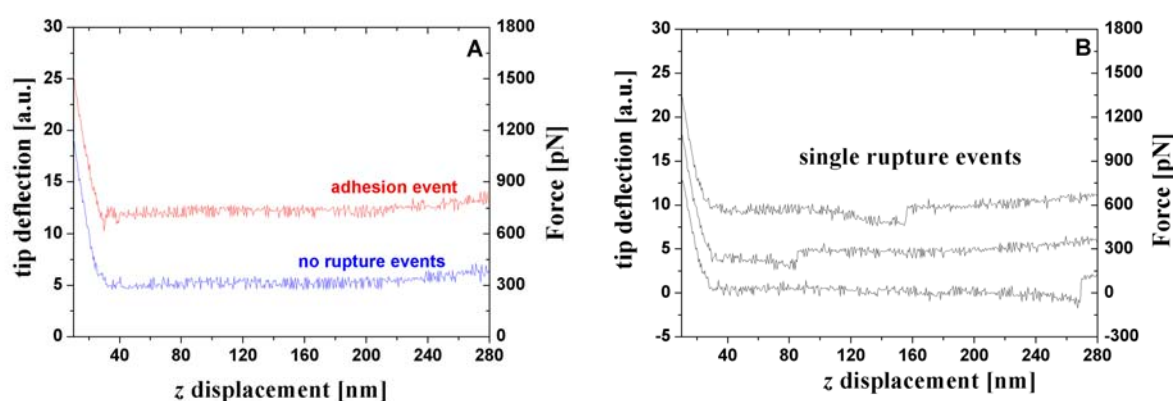


Figure 23. Force curves detected for fibrinogen – fibrinogen system.

Nonetheless, the force distribution (fig. 24) is quite similar to that obtained for bare tip – fibrinogen control system (fig. 16). The force histogram shows also a quantization in the force, with a period of about 40 pN, and the rupture forces range from 80 pN to 500 pN. By deducing the amount of rupture events due to tip – fibrinogen interaction (16% of all curves analyzed, see control data) from total rupture event frequency (about 60%), we estimate the event frequency of real fibrinogen – fibrinogen interaction as to be about 44%. The quantized force is calculated approximately as 40 pN per single fibrinogen – fibrinogen pair. It was not observed any dependence of rupture forces on the loading rate. This fact indicates that a force-induced fibrinogen-fibrinogen interaction proceeds at equilibrium. The length distribution (fig. 25) is broad (from 25 nm to 280 nm). Because our protocols of tip and sample preparation does not assure the well-defined immobilization position of protein on the tip/sample surface, thus, there is high probability that fibrinogen molecules are fixed onto the surface via different amino groups of different peptides chains. This effect can easily explain the wide distribution of length ruptures. The occurrences for lengths from 50 nm to 150 nm are practically the same.

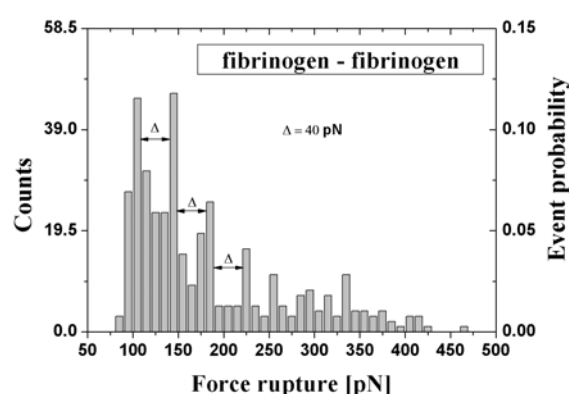


Figure 24. Force rupture histogram for fibrinogen – fibrinogen system, 640 force curves analyzed, 390 rupture events detected.

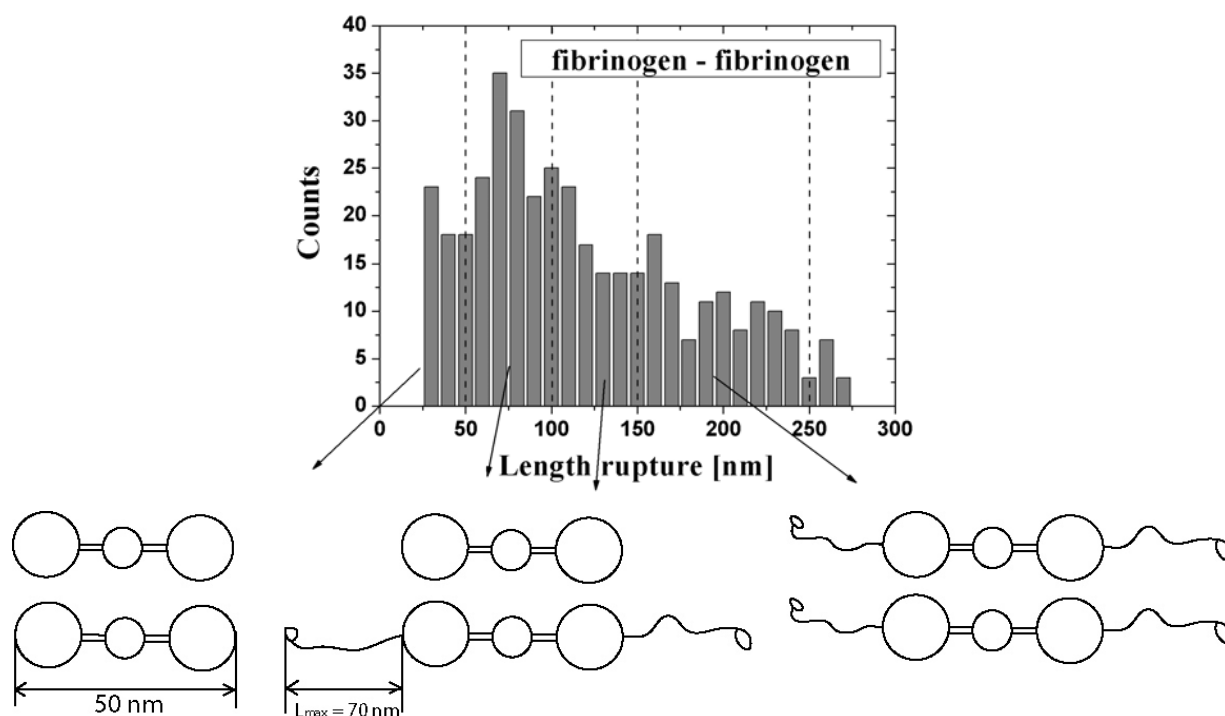


Figure 25. Length rupture histogram for fibrinogen – fibrinogen system and schematic explanation of possible length of interaction pairs. 640 force curves analyzed, 390 rupture events detected.

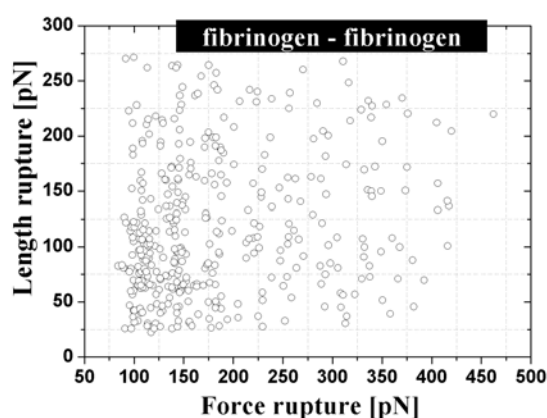


Figure 26. Force-length diagram for fibrinogen-fibrinogen system.

The majority of rupture events with lengths from 50 nm to 150 nm peaks well at 105 pN, 145 pN, 185 pN, and 225 pN (fig. 24). This fact is also indicated for

bare tip – fibrinogen system (fig. 16). There is no correlation between force and length rupture observed (fig. 26). The presence of *Gly-Pro-Arg-Pro* peptide molecules in solution has not a significant influence on the force and length rupture distributions (fig. 27).

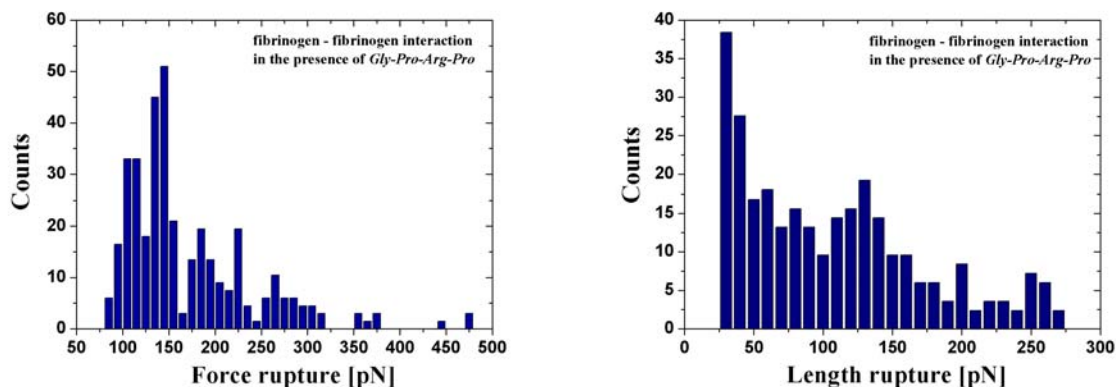


Figure 27. Force (left) and length (right) histograms for fibrinogen-fibrinogen system in the presence of excess (0.5 mg/ml) of *Gly-Pro-Arg-Pro* peptides in buffer solution.

The observed results obviously attest that fibrinogen – fibrinogen interaction is not specific.

4.4.3 Fibrin – fibrinogen complex

First, the AFM tips and APTES-mica sheets were functionalized with fibrinogen molecules. To obtain the fibrin monomers, the fibrinogen was further activated by enzymes, thrombin and Reptilase (for more detailed description see the chapter II “tip and sample preparation methods for FS study”). There was no difference in force and length rupture distributions obtained when the tip or the substrate are activated with enzymes. Molecular interaction parameters such as the activation barrier, x_{diss} , and the zero dissociation rate, k_{diss} , have been obtained from the loading rate-dependent measurements. We present now the results obtained with fibrin-functionalized tips and fibrinogen-functionalized mica samples, recorded at the constant loading rate of ≈ 3.5 nN/s.

4.4.3a Constant loading rate measurements

4.4.3a/1 Fibrin (thrombin) – fibrinogen system

The typical force curves are depicted in fig. 28. No adhesion rupture events (length rupture < 25 nm) have been recorded. We notice the following types of curves: no rupture detected (32% of all curves analyzed, fig. 28 A, black curve); single rupture events (29.5 %, fig. 28 A, red curves); double (two rupture peaks) (21.5%, fig. 28 B) and multiple rupture events (17%, fig. 28 C). As we can observe, contrarily to fibrinogen – fibrinogen system, a large amount of force curves represents double and multiple rupture events, indicating the formation of multiple bonds during the contact.

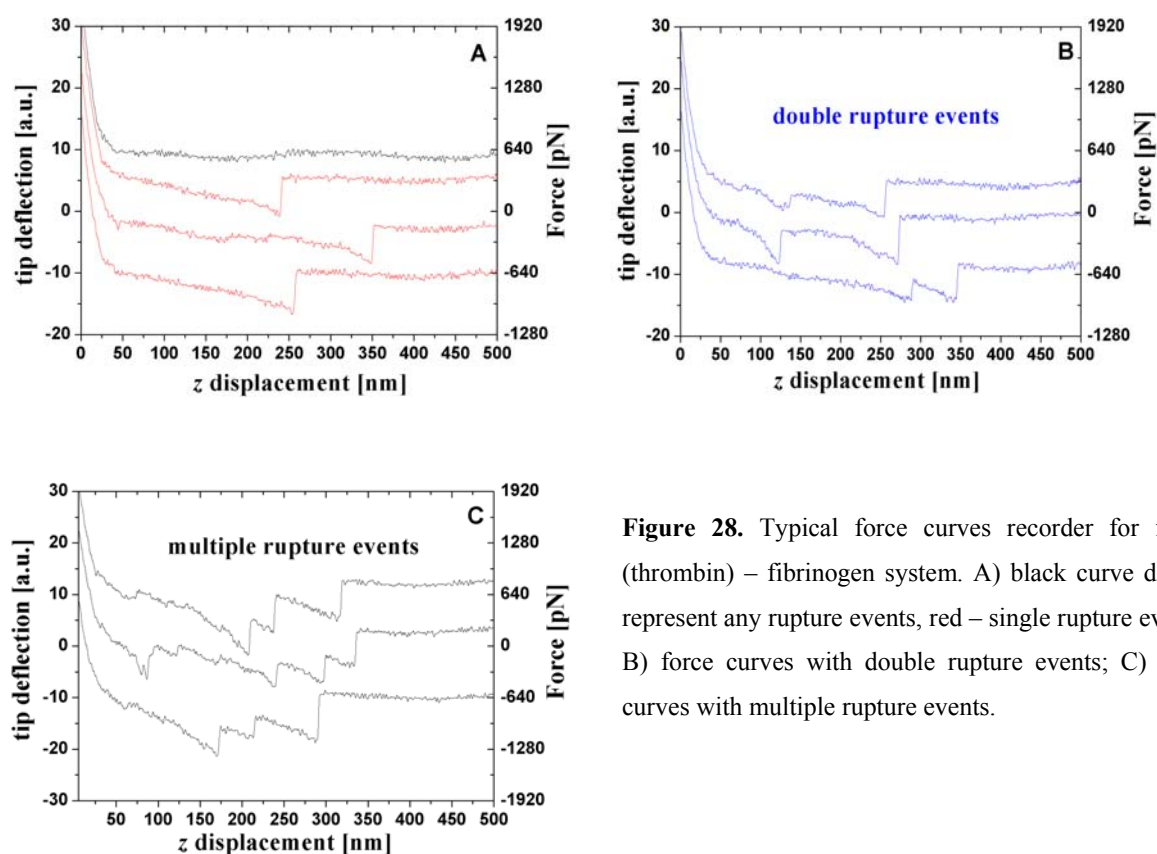
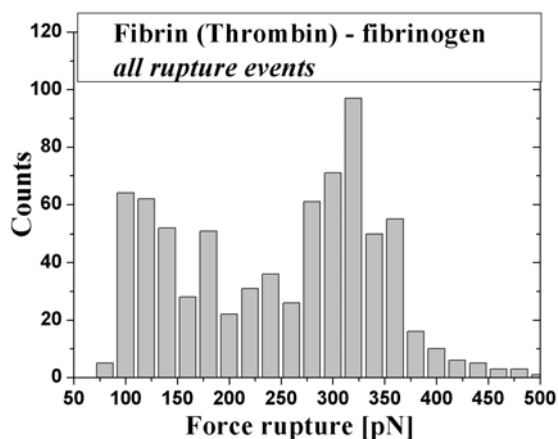


Figure 28. Typical force curves recorder for fibrin (thrombin) – fibrinogen system. A) black curve do not represent any rupture events, red – single rupture events; B) force curves with double rupture events; C) force curves with multiple rupture events.

Construction of force histogram of all rupture events (fig. 29) could lead to misleading of data interpretation. One can note the first domain (domain I) of forces from 80 pN to 200 pN similar to fibrinogen – fibrinogen system and the apparition of the second domain (domain II) with a force peak at ≈ 320 pN.

Figure 29. Force histogram of all rupture events for fibrin (thrombin) – fibrinogen system. 512 force curves analyzed, 754 rupture events detected.



By comparison of force distributions of all rupture events and single rupture events (fig. 30) one can see that domain

I is corresponding for only multiple rupture events while domain II is represented in both histograms. The force distribution corresponding to domain I is similar to those observed for the bare tip-fibrinogen, the fibrinogen-mica and the fibrinogen-fibrinogen systems. This fact can be explained by the multiple and consecutive detachments of fibrin(ogen) molecules. Nevertheless, as we will explain below domain II characterizes the specific interaction between fibrin and

fibrinogen molecules.

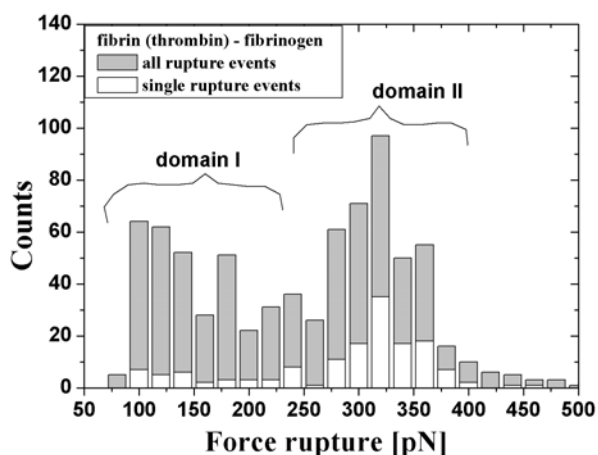


Figure 30. Comparison of force distributions corresponding to all rupture events (light grey) and single rupture event (white).

We consider now only the curves with single rupture events. Force

distribution for single rupture events is narrow and peaks at the well defined force value of 324 ± 28 pN (fig. 31-left). The length rupture histogram (fig. 31-right) is broad and can be explained by uncertainty in immobilization position of fibrinogen (see for comparison fibrinogen – fibrinogen complex).

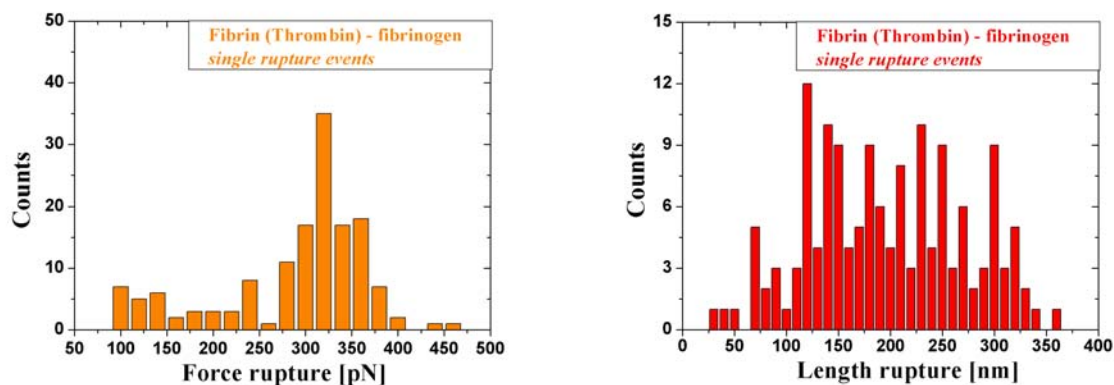


Figure 31. Force (left) and length rupture (right) histograms of single rupture events for fibrin (thrombin) – fibrinogen complex. 512 force curves analyzed, 151 single rupture events detected.

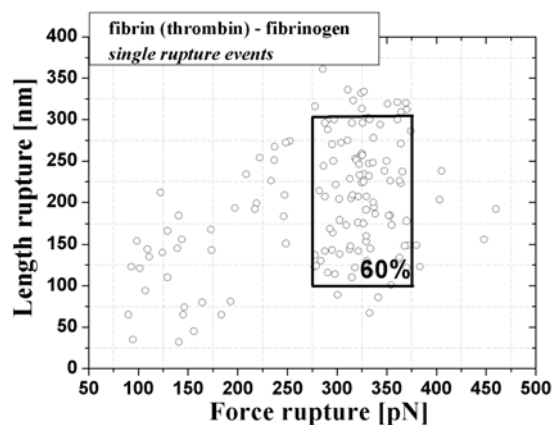


Figure 32. Force-length diagram for fibrin (thrombin) – fibrinogen complex. 100 % corresponds to all single rupture events detected.

The force-length diagram (fig. 32) illustrates that the forces of about 320 pN show characteristic lengths rupture from 100 nm to 300 nm. One can also note that the bigger elongation (300 nm) is only observed for these forces. The specificity of fibrin – fibrinogen interactions has been tested in the presence of excess of strong inhibitor, tetrapeptide *Gly-Pro-Arg-Pro* (when the “a-holes” of fibrin(ogen) are blocked with peptides) (figs. 33 and 34). The number of curves with detected rupture events is

considerably reduced, essentially with double and multiple rupture events. 16.3% of all analyzed curves present single rupture events, 2.7 % - double rupture events, and 2% - multiple rupture events. From the force histogram (fig. 33-left) we can state that the characteristic peak at 320 pN has totally disappeared. The interaction forces, very similar to the fibrinogen – fibrinogen system interaction forces, are observed.

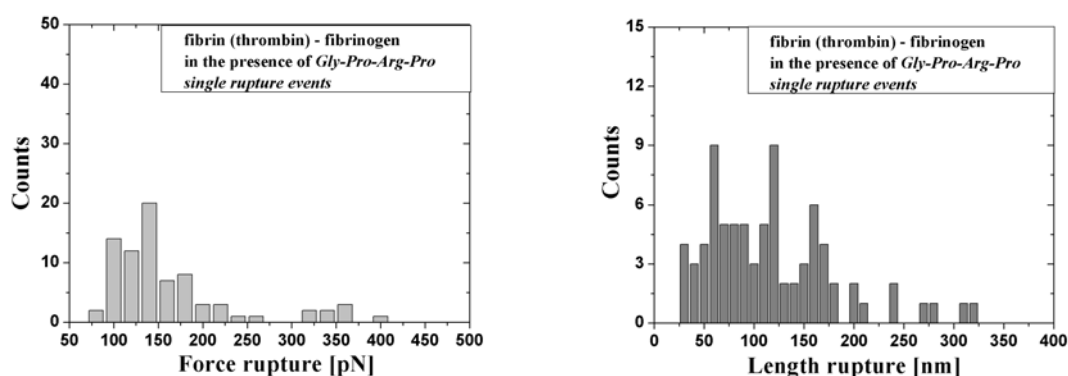


Figure 33. Force (left) and length distributions for fibrin (thrombin) – fibrinogen in the presence of excess of *Gly-Pro-Arg-Pro* peptides in buffer solution. 512 force curves have been analyzed, 83 single rupture events have been detected.

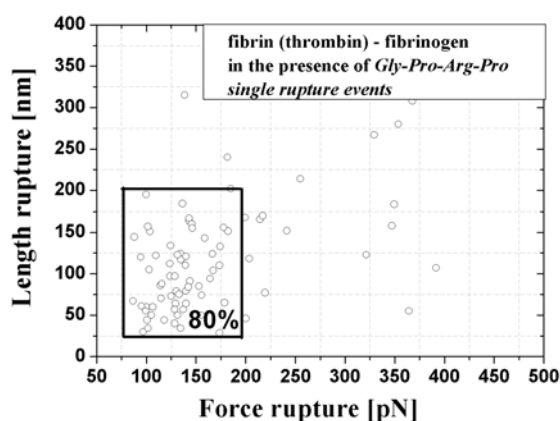


Figure 34. Force-length diagram for fibrin (thrombin) – fibrinogen complex in the presence of *Gly-Pro-Arg-Pro* peptides in buffer solution. 100 % corresponds to all single rupture events detected.

The majority of rupture lengths for these forces vary from 50 nm to 100 nm (fig. 34). The force distribution of single rupture events is basically restored after elimination of *Gly-Pro-Arg-Pro* peptides from buffer solution (fig. 35-left). Interestingly, not so big amount of force curves with double/multiple rupture events

is observed (table 1 at the end of this chapter). The length distribution becomes narrow with a peak at 145 nm (fig. 35-right).

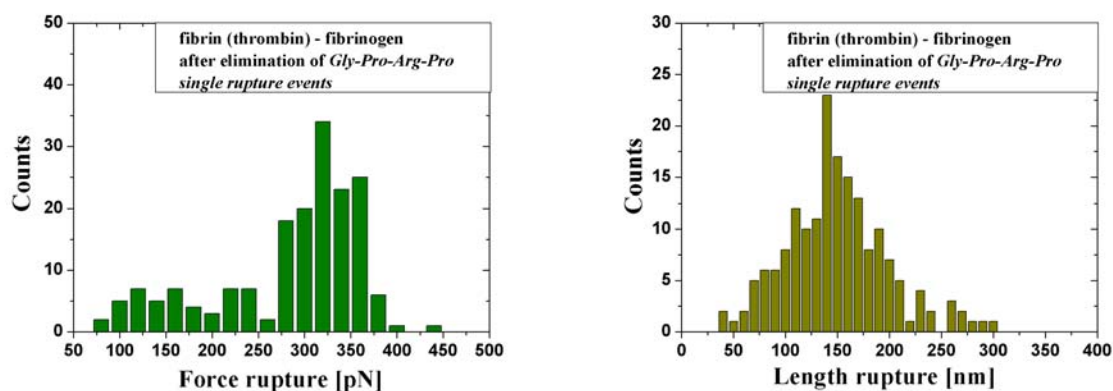


Figure 35. Force (left) and length rupture (right) histograms for fibrin (thrombin) – fibrinogen complex after elimination of *Gly-Pro-Arg-Pro* peptides from buffer solution. 608 force curves analyzed, 181 single rupture events detected.

Forces of about 320 pN are again observed for the characteristic lengths from 100 nm to 300 nm (fig. 36).

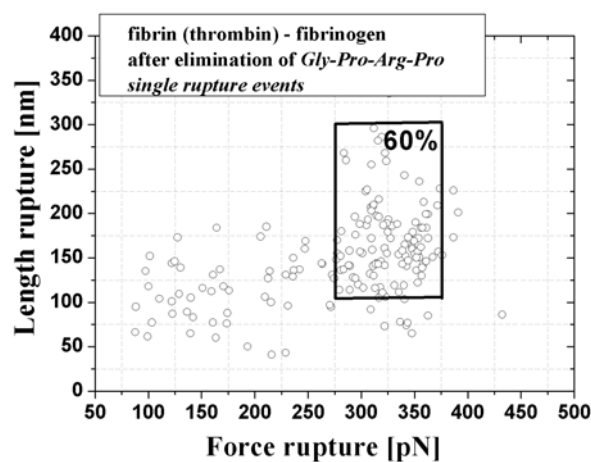


Figure 36. Force-length diagram for fibrin (thrombin) – fibrinogen complex after elimination of *Gly-Pro-Arg-Pro* peptides from buffer solution. 100 % corresponds to all single rupture events detected.

The similar results are obtained when fibrinogen molecules are activated with Reptilase (only release fibrinopeptides A).

4.4.3a/2 Fibrin (Reptilase) – fibrinogen system

The typical force curves are illustrated in fig. 37. No adhesion rupture events have been recorded. We classify the curves in the similar way as described above: without any detected rupture event (22% of all analyzed force curves) (fig. 37 A, black curve); curves with single rupture events (26.4%) (fig. 37 A, red curves); with double rupture events (16%) (fig. 37 B); and with multiple rupture events (35.6%) (fig. 37 C). The remarkable quantity of force curves with double and multiple rupture events (51.6%) are observed indicating complex behavior of interactions between fibrin and fibrinogen molecules.

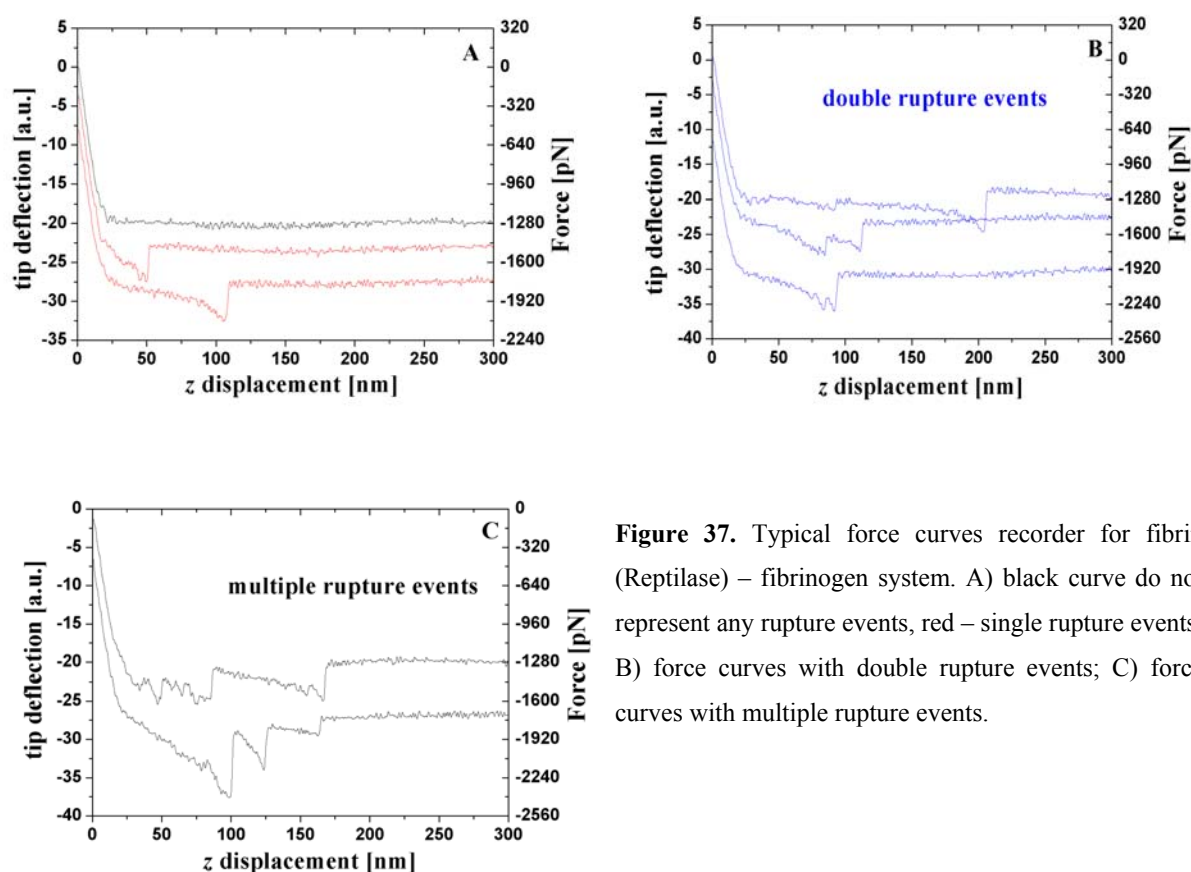


Figure 37. Typical force curves recorder for fibrin (Reptilase) – fibrinogen system. A) black curve do not represent any rupture events, red – single rupture events; B) force curves with double rupture events; C) force curves with multiple rupture events.

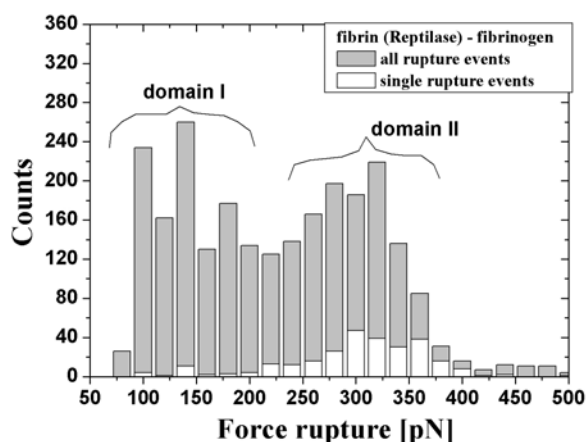


Figure 38. Force histogram of all rupture events (light grey) in comparison with that of single rupture events. 1072 force curves analyzed, 2467 rupture events and 283 single rupture detected.

The force histogram for all rupture events are depicted in fig. 38 (in light grey). Again, the force distribution of multiple rupture events represents

domain I and domain II, on the other hand the force histogram of single rupture events (in white) has only domain II characterizing the specific fibrin-fibrinogen interaction. Below we only take the force curves with single rupture events for data evaluation. Fig. 39 shows the force (left) and length (right) distributions. From the force histogram we can see a well defined peak at 318 ± 45 pN.

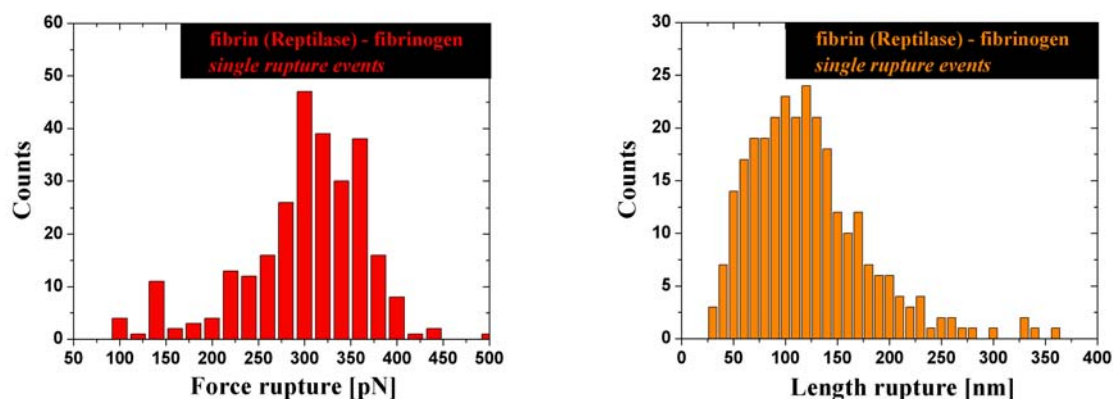


Figure 39. Force (left) and length rupture (right) histograms of single rupture events for fibrin (Reptilase) – fibrinogen complex. 1072 force curves analyzed, 283 single rupture events detected.

From force-length diagram (fig. 40) we can evaluate the correlation between force and length rupture. Majority of single rupture events with forces at about 320 pN shows characteristic rupture lengths from 50 nm to 150 nm.

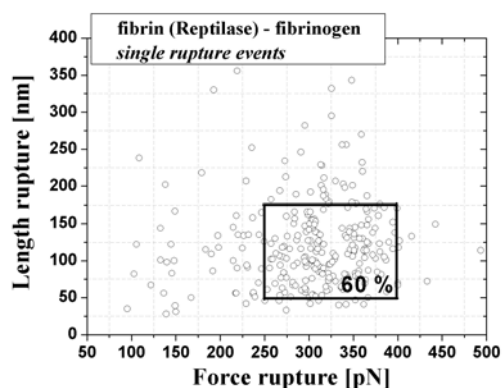


Figure 40. Force-length diagram of single rupture events for fibrin (Reptilase) – fibrinogen complex. 1072 force curves analyzed. 100 % corresponds to all single rupture events detected (283).

The specificity of fibrin (Reptilase)–fibrinogen interaction has been successfully probed with the same inhibitor used, the tetrapeptide *Gly-Pro-Arg-Pro* (fig. 41). The number of total rupture events is considerably reduced with a strong decrease of the number of the force curves with double/multiple rupture events (see table 1 at the end of this chapter). The force histogram (fig. 41-left) of the single rupture events does not show anymore a peak at 320 pN, but at around 130 pN.

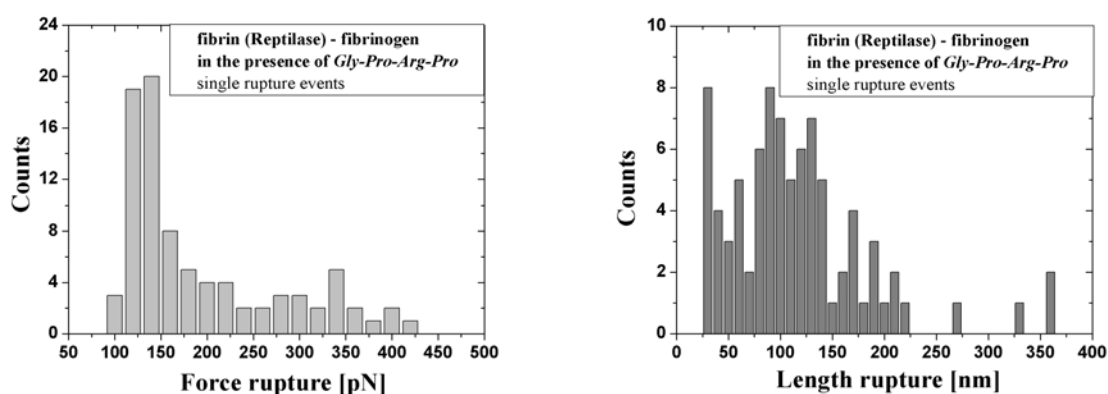


Figure 41. Force (left) and length (right) histograms of single rupture events for fibrin (Reptilase) – fibrinogen complex in the presence of excess of strong inhibitor, *Gly-Pro-Arg-Pro* peptides. 768 force curves analyzed, 86 single rupture events detected.

The typical lengths corresponding to this force maximum vary from 25 to 130 nm (fig. 42).

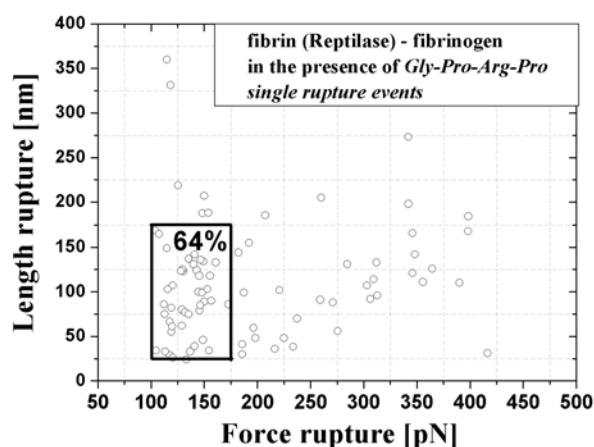


Figure 42. Force-length diagram of single rupture events for fibrin (Reptilase) – fibrinogen system in the presence of *Gly-Pro-Arg-Pro*. 100 % corresponds to all single rupture events detected (86).

The specific force distribution with a peak at ≈ 320 pN has been partially

restored (fig. 43 and table 1 at the end of this chapter). A domain of weak interaction forces from 100 pN to 250 pN (fig. 43) with corresponding characteristic length rupture of about 50 nm (fig. 44) is also present in the force histogram. Similar domain is not observed in the case of fibrin (thrombin) – fibrinogen and is probably due to incomplete elimination of *Gly-Pro-Arg-Pro* peptides from buffer solution.

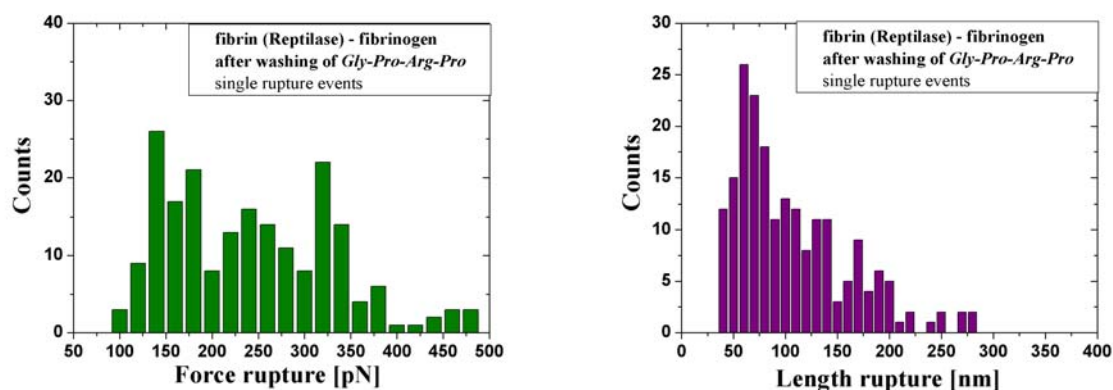


Figure 43. Force (left) and length (right) histograms of single rupture events for fibrin (Reptilase) – fibrinogen system after washing of *Gly-Pro-Arg-Pro*. 864 force curves analyzed, 203 single rupture events detected.

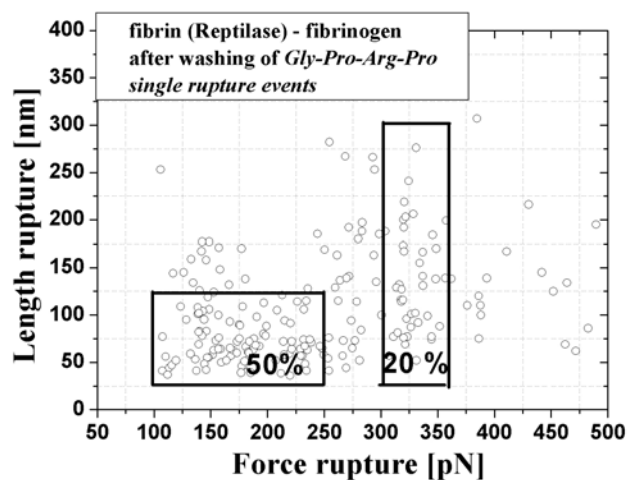


Figure 44. Force-length diagram of single rupture events for fibrin (Reptilase) – fibrinogen system after washing of *Gly-Pro-Arg-Pro*. 100 % corresponds to all single rupture events detected (203).

Forces of about 320 pN illustrate the characteristic lengths from 75 nm to 250 nm.

In order to show that exactly *Gly-Pro-Arg* ending of knob-A which is involved directly in specific interaction with hole-a, forces between synthetic peptide, *Gly-Pro-Arg-(His)₄* and fibrinogen molecules were measured .

4.4.3a/3 *Gly-Pro-Arg-(His)₄* – fibrinogen interaction

Gly-Pro-Arg-(His)₄ peptides (0.5 mg/ml) are covalently attached to the AFM tip via EDAC permitting the peptide immobilization by *His* residues. Fibrinogen molecules (1 mg/ml) are covalently attached to APTES-mica sample. The force spectroscopy measurements have been performed at the same constant loading rate used for other systems. By the same reasons indicated for the fibrin-fibrinogen complexes we consider single rupture events for data evolution. Numbers of force curves with different types of rupture events are represented in Table 1. A very similar force distribution to fibrin-fibrinogen systems with a peak force at about 320 pN is observed (fig. 45-left). The length distribution (fig. 45-right) is still broad with a peak length rupture at about 30 nm.

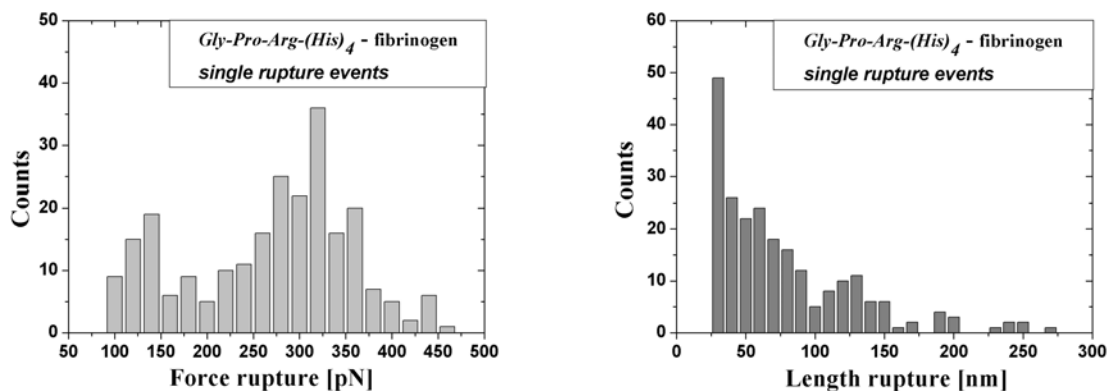


Figure 45. Force (left) and length (right) histograms for *Gly-Pro-Arg-(His)₄* – fibrinogen system 1280 force curves analyzed, 243 single rupture events detected.

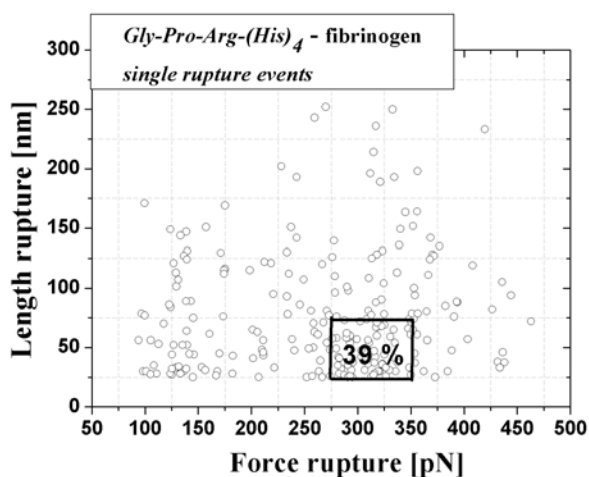


Figure 46. Force-length diagram for *Gly-Pro-Arg-(His)₄* – fibrinogen system. 100 % corresponds to all single rupture events detected (243).

The forces at around of 320 pN have a narrower distribution of the rupture lengths from 25 to 75 nm (see the square in the force-length diagram, fig. 46).

Table 1. The comparison of number of force curves (in %) with different types of rupture events observed for fibrinogen – fibrinogen and fibrin – fibrinogen complexes. Abbreviation for f. c. – force curve.

	f. c. with all rupture events	f. c. with adhesion events	f. c. with single rupture events	f. c. with double rupture events	f. c. with multiple rupture events
fibrinogen - fibrinogen	60	<2	58	<1	0
fibrin (thrombin) – fibrinogen in the presence of <i>Gly-Pro-Arg-Pro</i> after elimination of <i>Gly-Pro-Arg-Pro</i>	68	0	30	21	17
	21	0	16.3	2.7	2
	46	0	30	9	7
fibrin (Reptilase) – fibrinogen in the presence of <i>Gly-Pro-Arg-Pro</i> after elimination of <i>Gly-Pro-Arg-Pro</i>	78	0	26.4	16	35.6
	15.5	0	11	2.5	2
	40	0	23.6	10	6.4
<i>Gly-Pro-Arg-(His)₄ - fibrinogen</i>	44.7	4.4	19	5.8	15.5

4.4.3b Loading rate dependence of the unbinding force and dissociation rate estimation for the fibrin – fibrin(ogen) complex

The unbinding forces for the fibrin – fibrin(ogen) complex were measured at loading rates in the range of 0.2 to 20 nN/s. The force curves with only single rupture events have been considered for the data evaluation. The fig. 47 reveals that the mean unbinding force increase linearly, when plotted against the logarithm of the loading rate. The zero kinetic off-rate, k_{diss} , and the distance of the transition state, x_{diss} , have been estimated as $3.78 \times 10^{-4} \text{ s}^{-1}$ and 0.16 nm, respectively.

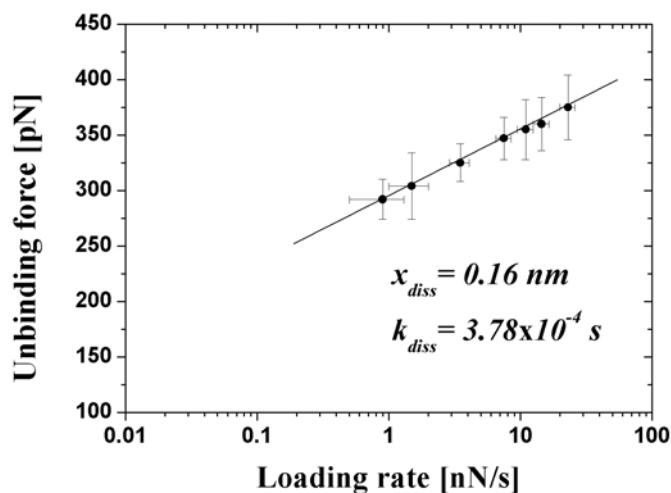


Figure 47. Dependence of the most probable unbinding force (F^*) on the loading rate for fibrin – fibrinogen complex (single rupture events considered).

4.5 Conclusion

In summary, based on our force spectroscopy results we conclude that:

- The interaction between two fibrinogen molecules is a non specific interaction with a force of about 40 pN and a wide distribution of rupture lengths ranging from 25 nm to 250 nm.
- The interaction between fibrin and fibrinogen molecules is a specific interaction. The mean unbinding force, F^* , is determined to be 320 pN at loading rate of 3.5 nN/s. This specific interaction is much stronger than the interaction between fibrinogen molecules. The length distribution is a little bit narrower but remains still broad, the majority of rupture lengths take place from 50 nm to 150 nm. The dependence of the mean value of unbinding forces with the loading rate logarithm has been observed for the single molecular complex between fibrin and fibrinogen (or fibrin), indicating that only one single potential barrier is dominant.
- There is not a big difference in the value of rupture forces observed when the fibrinogen molecules are activated by different enzymes: thrombin (both cleavage of fibrinopeptides A

and B) or Reptilase (only cleavage of fibrinopeptides A). This indicates that just the specific interaction between the *knob-A* of the fibrin molecule and the *hole a* of fibrin(ogen) takes place in our experiments. For our experimental conditions, the *knob-B – hole b* interaction is not seen. The *knob A – hole a* interaction has been successfully tested by using the tetrapeptide *Gly-Pro-Arg-Pro* as a strong inhibitor of the fibrin formation.

- The wide distribution of rupture lengths for fibrinogen – fibrinogen and fibrin – fibrinogen complexes can be explained by various lengths stretching of the peptide chains. This is probably caused by uncertainty in the immobilization position of fibrinogen molecules on the tip and on the substrate surface.
- The responsibility of the *Gly-Pro-Arg* for the specific interaction with the fibrinogen molecule is revealed.

References

1. Beck, E. A. The discovery of fibrinogen and its conversion to fibrin. *In* Fibrinogen. K. Laki, ed. Marcel Dekker, Inc., New York, 1968.
2. Hall, C. E., and Slayter, H. S. The fibrinogen molecule: Its size, shape, and mode of polymerization. *J. Biophys. Biochem. Cytol.* **5** (1959) 11-15.
3. Doolittle, R. F. Fibrinogen and fibrin. *Sci. Am.* **245** (1981) 92-101.
4. Hoepflich, P. D. Jr., and Doolittle, R. F. Dimeric half-molecules of human fibrinogen are joined through disulfide bonds in an antiparallel orientation. *Biochemistry.* **22** (1983) 2049-2055.
5. Weisel, J. W., Stauffacher, C. V., Bullitt, E., and Cohen, C. A model for fibrinogen: domains and sequence. *Science.* **230** (1985) 1388-1391.
6. Privalov, P. L., and Medved, L. V. Domains in the fibrinogen molecule. *J. Mol. Biol.* **159** (1982) 665-683.
7. Medved, L. V., Gorkun, O. V., and Privalov, P. L. Structural organization of C-terminal parts of fibrinogen α -chains. *FEBS Lett.* **160** (1983) 291-295.
8. Medved, L., Litvinovitch, S., Ugarova, T., Matsuka, Y., and Ingham, K. Domain structure and functional activity of the recombinant human fibrinogen γ -module (γ 148-411). *Biochemistry.* **36** (1997) 4685-4693.
9. Watt, K. W., Takagi, T., and Doolittle, R. F. Amino acid sequence of the beta chain of human fibrinogen: homology with the gamma chain. *Proc. Natl. Acad. Sci USA.* **75** (1978) 1731-1735.
10. Doolittle, R. F., Goldbaum, D. M., and Doolittle L. R. Designation of sequences involved in the "coiled-coil" interdomainal connections in fibrinogen: constructions of an atomic scale model. *J. Mol. Biol.* **120** (1978) 311-325.
11. Yang, Z., Kollman, J. M., Pandi, L., and Doolittle, R. F. Crystal structure of native chicken fibrinogen at 2.7 Å resolution. *Biochemistry.* **40** (2001) 12515-12523.
12. Bailey, K. Bettelheim, F. R., Lorand, L., and Middlebrook, W. R. Action of thrombin in the clotting of fibrinogen. *Nature.* **167** (1951) 233-234.
13. Di Cera, E., Dang, Q. D., and Ayala, Y. M. Molecular mechanisms of thrombin function. *Cell. Mol. Life Sci.* **53** (1997) 701-730.

14. Becker, R. C., and Spencer, F. Thrombin: structure, biochemistry, measurement, and status in clinical medicine. *J. Trombosis and Thrombolysis*. (1998) 215-229.
15. Doolittle, R. F., Yang, Z., Mochalkin, I. Crystal structure studies on fibrinogen and fibrin. *Ann. NY Acad. Sci.* **936** (2001) 31-43.
16. Vindigni, A., and Di Cera, E. Release of fibrinopeptides by the slow and fast forms of thrombin. *Biochemistry*. **35** (1996) 4417-4426.
17. Higgins, D. L., Lewis, S. D., and Shafer, J. A. Steady state kinetic parameters for the thrombin-catalyzed conversion of human fibrinogen to fibrin. *J. Biol. Chem.* **258** (1983) 9276-9282.
18. Lewis, S. D., Shields, P. P., and Shafer, J. A. Characterization of the kinetic pathway for liberation of fibrinopeptides during assembly of fibrin. *J. Biol. Chem.* **260** (1985) 10192-10199.
19. Ng, A. S., Lewis, S. D., and Shafer, J. A. Quantifying thrombin-catalyzed release of fibrinopeptides from fibrinogen using high-performance liquid chromatography. *Meth. Enzymol.* **222** (1993) 341-358.
20. Gorkun, O. V., Veklich, Yu. I., Medved, L. V., Henschen, A. H., and Weisel, J. W. Role of the α C-domains of fibrin in clot formation. *Biochemistry*. **33** (1994) 6986-6997.
21. Weisel, J. W., and Medved, L. the structure and functions of the α C-domains of fibrinogen. *Ann. NY Acad. Sci.* **936** (2001) 312-327.
22. Mosesson, M. W., Siebenlist, K. R., and Meh, D. A. The structure and biological features of fibrinogen and fibrin. *Ann. NY Acad. Sci.* **936** (2001) 11-30.
23. Laudano, A. L., and Doolittle, R. F. Synthetic peptide derivatives that bind to fibrinogen and prevent the polymerization of fibrin monomers. *Proc. Natl. Acad. Sci. USA.* **75** (1978) 3085-3089.
24. Laudano, A. P., and Doolittle, R. F. Studies on synthetic peptides that bind to fibrinogen and prevent fibrin polymerization. Structural requirements, number of binding sites, and species differences. *Biochemistry*. **19** (1980) 1013-1019.
25. Blombäck, B., Blombäck, M., Nilsson, I. M. Coagulation studies on "Reptilase," an extract of the venom from *Bothrops jararaca*. *Thromb. Diath. Haem.* **1** (1957) 76-86.
26. Dietler, G., Känzig, W., Häberli, A., and Straub, P. W. Experimental tests of a geometrical abstraction of fibrin polymerization. *Biopolymers*. **25** (1986) 905-929.

27. Chen, R., and Doolittle, R. F. γ - γ cross-linking sites in human and bovine fibrin. *Biochemistry*. **10** (1971) 4486-4491.
28. Cottrell, B. A., Strong, D. D., Watt, K. W. K., and Doolittle, R. F. Amino acid sequence studies on the α chain of human fibrinogen. Exact location of cross-linking acceptor sites. *Biochemistry*. **18** (1979) 5405-5409.
29. Ferry, J. D. The mechanism of polymerization of fibrinogen. *Proc. Natl. Acad. Sci. USA*. **38** (1952) 566-569.
30. Hunziker, E. B., Straub, P. W., and Haerberli, A. A new concept of fibrin formation based upon the linear growth of interlacing and branching polymers and molecular alignment into interlocked single-stranded segments. *J. Biol. Chem.* **265** (1990) 7455-7463.

Chapter V

Force Spectroscopy with Modulation of the AFM tips

5.1 Introduction

Chapters III and IV present the technique of single molecule and single molecular complex force spectroscopy operated in contact mode, i.e. with no external dithering applied to the cantilever/tip assembly. In our days, this technique becomes a well established one and a very promising research field, which attracts attention of tens of research groups all over the world. At the same time, practically all applications of the standard quasistatic force spectroscopy are limited with the measurements of (quasi)static effects: only is used the information, which can be extracted from the (quasi)static deflection of a cantilever. In chapter I we have briefly described the *dynamic AFM mode of operation* where the tip oscillates near its resonance frequency while it is moved to and from the surface. The measured parameter in this force recording regime is the reduction of the amplitude of oscillation that is caused by the interaction of the tip and the surface. This dynamic AFM mode of operation presents several advantages over the contact mode (i.e. lateral forces between tip and the sample are minimized and it becomes possible to image sticky or/and soft biological surfaces). In order to analyze the conditions advantageous for measurement, one needs the help of an adequate theoretical model [1, 2]. However, at present, there is no complete theoretical description of the cantilever oscillations in liquid environment near the surface of a sample in a wide range of excitation frequencies; a reasonable approach have been published recently for a cantilever far from the sample [3].

Very recently it has been proposed to slightly modulate the distance between the cantilever and the sample at a driving frequency ω [4-7]. To this aim, in a magnetically

oscillated dynamic force microscope (DFM) (also known as MAC mode AFM) magnetically coated tips are directly excited by an alternating magnetic field. Which additional information could be obtained from this kind of experiments where the tip is oscillated at the same time as it is moved to and from the surface? Recording the topography and the recognition images at the same time enables fast and reliable molecular recognition mapping on a nanometer scale [5]. Measuring the amplitude of the tip vibrations at this driving frequency leads to the improved molecule recognition fidelity [6]. The possibility to measure the dynamical properties of single molecules using this method has been also demonstrated for a short polymer molecule of poly(ethylene glycol) [7].

This chapter reports our development of this methodology for direct and continuous measurement of the spring constant of a single stretched molecule or a molecular complex. Mainly, the complex of bovine serum albumin (BSA) with polyclonal antibody to BSA (Ab-BSA) have been studied, additionally the potentialities of this method are illustrated in the case of fibrinogen – fibrinogen complex.

5.1.1 AFM instrumentation

A schematic diagram of our elaborated experimental setup is given in Fig. 1. A commercially available AFM (Nanoscope IIIa Multimode Scanning Probe Microscope, Veeco Instruments, Santa Barbara, CA, USA) and standard V-shaped Si₃N₄ (silicon nitride) cantilevers (Veeco), having a length of 200 μm, with a nominal spring constant of 0.06 N/m are used. All experiments are performed in phosphate-buffered saline (PBS) buffer (50 mM phosphate, 150 mM NaCl, pH 7.4 at 25°C) at 25°C. The Nanoscope IIIa “force-volume” option is used but a small sine wave modulation voltage is applied to the piezocrystal normally used for the “tapping-mode”. This dithering voltage, U_{mod} , has a peak-to-peak amplitude of 20 – 80 mV at a frequency of $\omega = 2\pi \cdot 3.2$ kHz. This modulation is equivalent to the application of a driving

force f_ω at the frequency ω onto the cantilever which makes the tip dither with an amplitude of 0.5 – 2 nm. This leads to the modulation of the photodiode current at the same frequency and its signal is measured using a digital lock in amplifier (SR750, Stanford Research Instruments, Stanford, USA). Thus, two signals are recorded simultaneously, using a dedicated Labview program (see appendix I): a) standard force-distance curves, i.e. dependence of the interaction force on the z -displacement of the substrate, and b) the dependence of the amplitude of forced cantilever vibrations on the same z -displacement. No noticeable dependence of the results on the dithering amplitude has been observed, provides that the excitation remains in the range given above. The smallest reasonable pull off rate of 11 nm/s (0.7 nN/s) has been used.

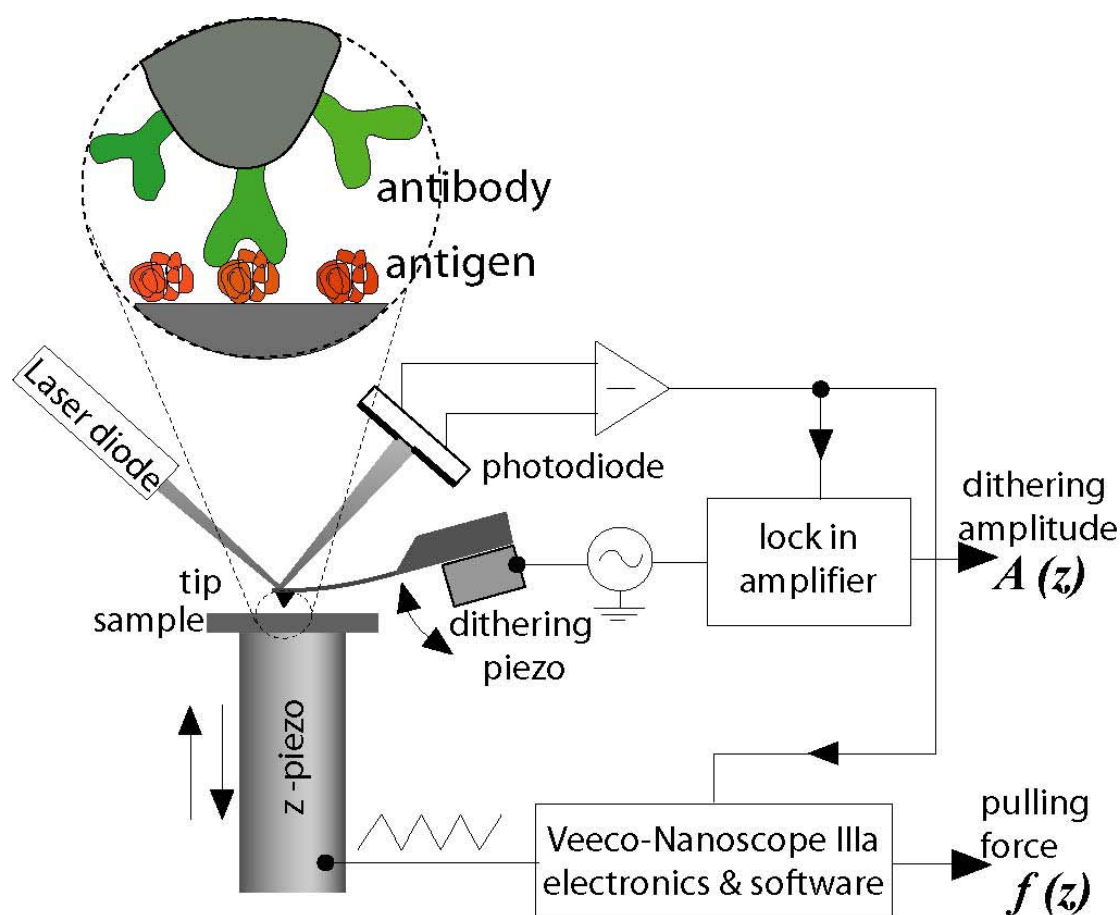


Figure 1. Schematic of the experimental setup.

5.1.2 Tip and sample preparation, control experiments

The functionalization of the AFM tips and mica samples with proteins are followed by the same receipt described in more details in chapter II. All the earlier control experiments have been repeated and have given similar negative results.

5.2 Experimental results and discussion

Typical amplitude and force-distance curves, obtained for the BSA – Ab-BSA complex, are shown in fig. 2.

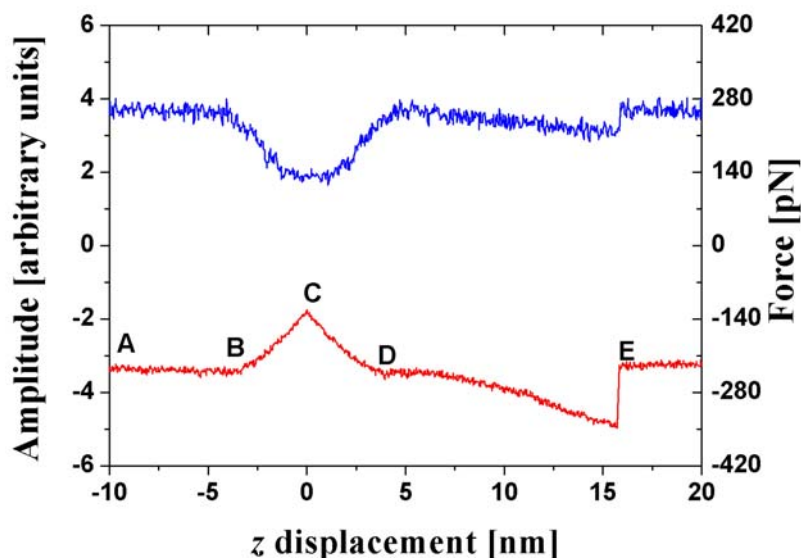


Figure 2. Experimental dependencies of the pulling force (red curve) and lock in output signal used to measure the spring constant (blue curve) on the sample stage z displacement.

The recording of the data starts when the tip and the substrate are far apart (A to B in fig. 2). Then, as the tip approaches, it enters into contact with the substrate (segment B to C). At point C the tip is retracted till point D where it loses contact with the substrate. Between D and E the tip is further retracted from the substrate with the extension of molecular complex. Point E corresponds to the rupture of the molecular bond and the unbinding force is measured at this moment. The calibration of the absolute value for the force has been performed basing on the linear part of the contact line (B - C and C - D) and using the known tip spring constant.

5.2.1 Calculation of spring constant of tip – sample complex

The following procedure is used to extract, from the recorded data, the value of the spring constant, characterizing the tip – sample complex, $k_{complex}$.

The process of exciting the cantilever vibrations in a liquid, is very complex to describe and is not yet fully understood. Nevertheless, for small vibration amplitudes, it can be still described as forced vibrations of a nonlinear oscillator [1, 3, 6, 7]. Introducing the variable δz , which describes the deviation of the cantilever from its equilibrium position, z_0 , produced by a (quasi)static pulling force f_{pul} , one can write down:

$$m_{eff} \frac{\partial^2(\delta z)}{\partial t^2} + \gamma \frac{\partial(\delta z)}{\partial t} + k_{eff} \delta z = f_{\omega} \cos(\omega \cdot t) \quad (1)$$

Here, the parameters m_{eff} and γ characterize the vibrations of the cantilever in liquid and k_{eff} is the sum of the spring constant of the cantilever and the one of the stretched complex. Note that the differential spring constant of the complex $k_{complex} = \left. \frac{df}{dz} \right|_{z=z_0}$, rather than its static spring constant f/z_0 , is relevant for this equation, containing δz as the variable. (Here $f(z)$ is the force – extension characteristic of the BSA – Ab-BSA complex; see below).

The solution of Eq. 1 is well known [1 or any textbook with an introduction to oscillatory motion]. This equation describes the forced vibrations $\delta z = a \cos(\omega \cdot t + \varphi)$ which amplitude is given by:

$$a = \frac{f_{\omega}}{\sqrt{(k^2 - m_{eff} \omega^2)^2 + \gamma^2 \omega^2}} \quad (2)$$

and the phase shift by:

$$\sin \varphi = \frac{\gamma \omega}{\sqrt{(k^2 - m_{eff} \omega^2)^2 + \gamma^2 \omega^2}} \quad (3)$$

If the driving frequency ω is much lower than the value of $\omega_0 = \sqrt{k_{eff} / m_{eff}}$, which, for the rather small quality factor $Q \geq 2$, is already very close to the resonance frequency of the

system $\omega_{res} = \omega_0 \sqrt{1 - (1/4Q^2)}$ then, evidently, the vibration amplitude can be well approximated by the value of

$$a = f_\omega / k_{eff}$$

because $m_{eff}\omega^2 / k_{eff} = (\omega / \omega_0)^2 \ll 1$ and $\gamma\omega / k_{eff} = (1/Q)(\omega / \omega_0) \ll 1$ for this case. The amplitude of the forced oscillation is measured with a lock in amplifier while recording force-distance curves. Three intervals are interesting for the force-distance curve as indicated in fig. 2 A: 1) *A-B* where the lever oscillates freely; 2) *D-E* where the molecular complex is extended under the action of the pulling force f_{pul} ; and 3) after *E* where the molecular bond is ruptured and the cantilever oscillates again freely. From the oscillation amplitude in these three regions, one can obtain the reciprocal spring constants k^{-1} , $(k + k_{complex})^{-1}$ and k^{-1} respectively. The value of k is known, that makes possible to determine the spring constant $k_{complex}$ of the single molecular complex as a function of z and f_{pul}^{-1} .

In our case, the resonant frequency of cantilevers in liquid is measured to be in the range from 8.5 to 10 kHz. The driving frequency of 3.2 kHz is a trade off between the necessity to have this value as small as possible for the better interpretation of data as discussed above and the necessity to have a sufficient number of oscillations per averaging time for the proper performance of the lock in amplifier.

5.2.2 BSA – Ab-BSA complex

We can classify events presented in Fig. 3 as follows: single bond rupture (Fig. 3 A; the value of the unbinding force is 135 pN), double bond rupture denoted as one peak with a double force value (Fig. 3 B; 295 pN), and “no specific event” (Fig. 3 C). The last example is a

¹ In principle, the measured value of $k_{complex}$ can be further refined if the parameters of the oscillatory system (m_{eff} and γ) are well known. This is, however, a very difficult problem, especially given the fact that the acting force value f_ω in itself depends on the frequency for our excitation method since the piezodriver is a source of displacement (of the cantilever base) rather than directly the force.

demonstration of the utility of the measurement of the spring constant for the interpretation of results of pulling off experiments. While the standard force-distance curve (lower) in Fig. 3 C looks like a single bond rupture event, the upper curve has no peculiarities (i.e. no decrease of dithering amplitude during the pulling off) and clearly demonstrates that non specific interaction takes place. This is a really useful addition to all approaches, designed to distinguish between different events in this type of experiments [8]. In some experiments, forces even larger than 1 nN have been observed. These events are believed to be due to multiple ruptures of glutaraldehyde – amine bonds, and we will not discuss them below.

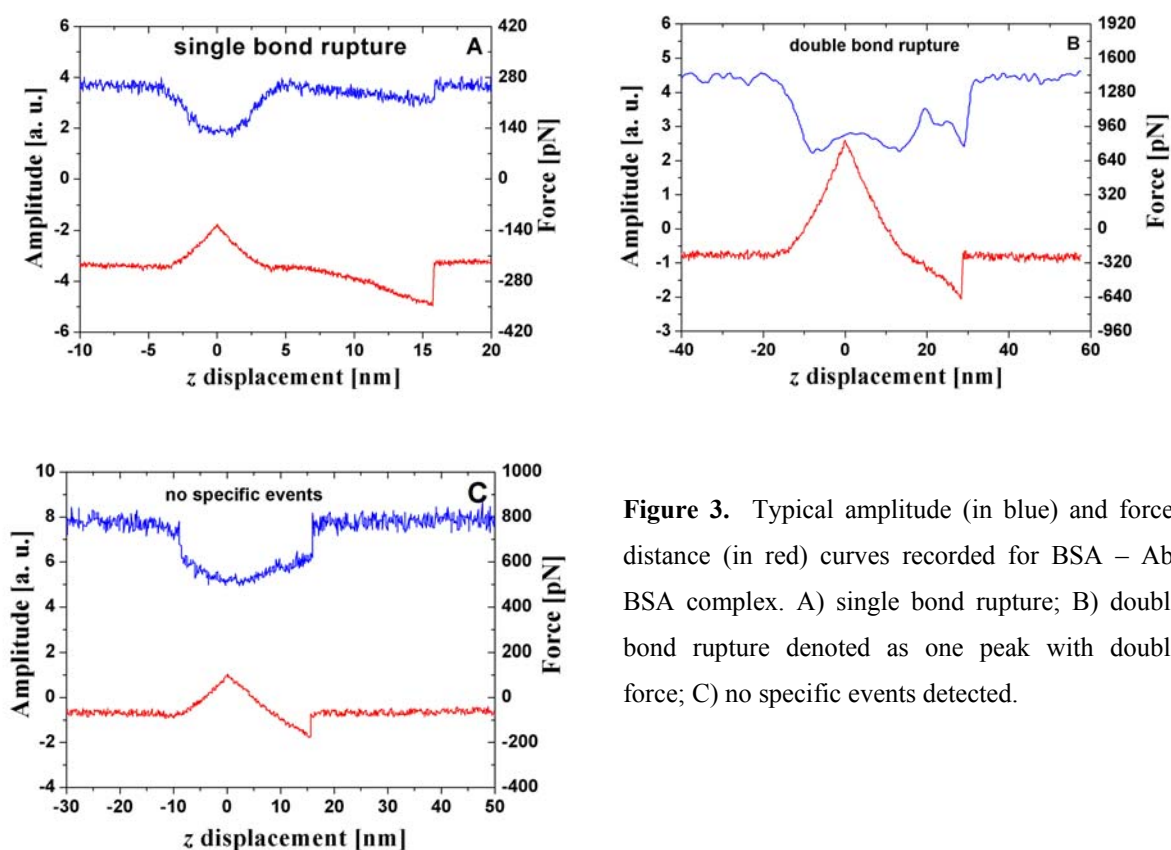


Figure 3. Typical amplitude (in blue) and force-distance (in red) curves recorded for BSA – Ab-BSA complex. A) single bond rupture; B) double bond rupture denoted as one peak with double force; C) no specific events detected.

Fig. 4 presents typical experimental dependencies of $k_{complex}(z)$ (A) and $f_{pul}(z)$ (B) for the case of single bond rupture. The linear approximation of the experimental dependence $k_{complex}(f)$, derived from Fig. 4 A and Fig. 4 B, is given in Fig. 4 C. Prior to plotting Fig. 4 C, fig. 4 A has

been fitted to a straight line in the region from 4.23 nm to 15.72 nm and curve 4 B to a second degree polynomial in the same interval.

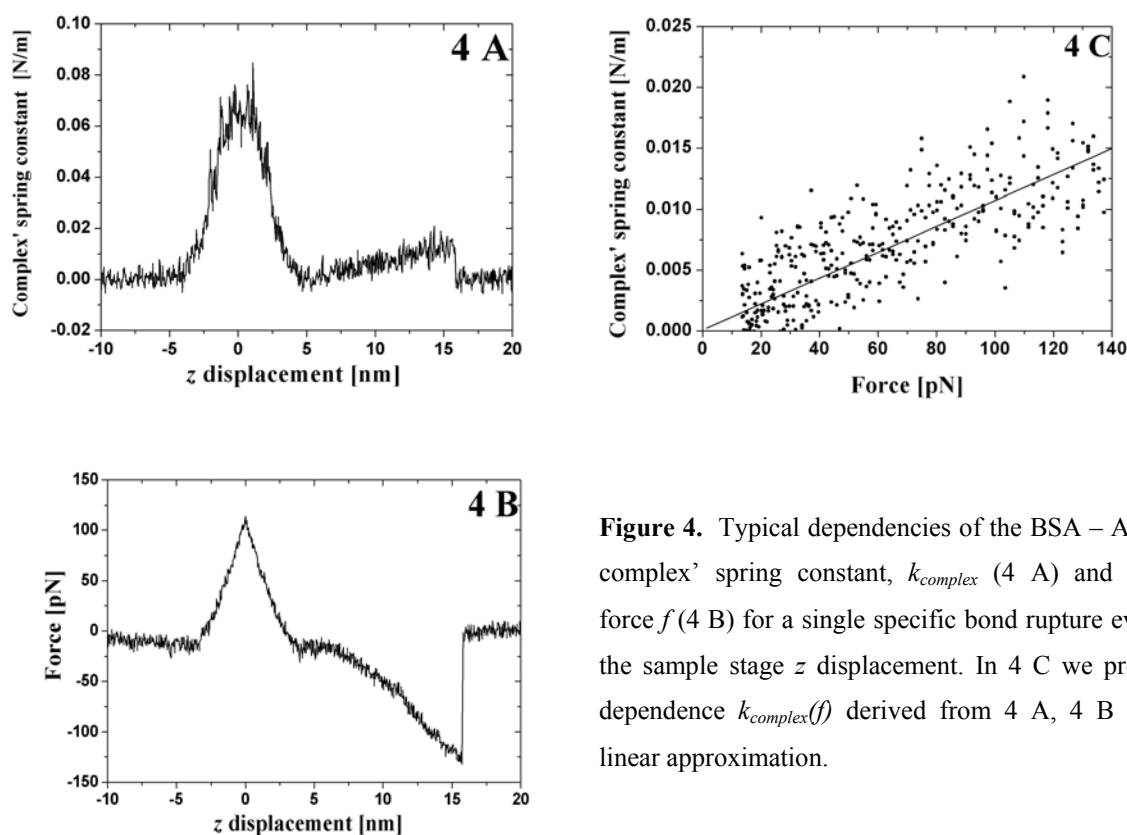


Figure 4. Typical dependencies of the BSA – Ab-BSA complex' spring constant, $k_{complex}$ (4 A) and pulling force f (4 B) for a single specific bond rupture event on the sample stage z displacement. In 4 C we present a dependence $k_{complex}(f)$ derived from 4 A, 4 B and its linear approximation.

The spring constant of the individual (and double) BSA – Ab-BSA complex always increases together with the increase of the pulling force and attains the maximal value at the moment of the bond rupture. A good correlation between the value of the specific interaction force, the simultaneously measured spring constant of the complex and the value of tip – sample distance at this moment is observed. The average value of the complex' spring constant at the moment of the single antigen-antibody bond rupture is measured to be 0.017 ± 0.003 N/m (average over 50 events). The majority of the events corresponding to the double bond rupture gives $k_{complex}$ values ranging from 0.03 to 0.04 N/m (10 events). However, values as large as 0.053 N/m have been also sometimes measured.

5.2.2a Interpretation of data

In order to interpret of the experimental results (only the case of single bond rupture is considered here), we should take into account the following aspects. The force f is the derivative of the free energy of the system with respect to the value of the distance between the molecule's end-points, i.e. the fragments of BSA – Ab-BSA complex are fixed on the tip and on the substrate surface [9]. The sample stage displacement z is the measurement of a such distance². Molecular dynamics calculations, for the extension curves for antigen – antibody complexes [10-17], show that the range of extension is of a few Ångströms and very close to the point of rupture. It is during that period that the details of the antigen – antibody interaction are important. For typical experimental conditions, this corresponds to a characteristic time scale of the order of few milliseconds or less. These values are beyond the reach of our experimental technique, so only the usual “entropy-related” contribution to the antigen – antibody complex' spring constant [9, 18] is observable.

As described in chapter III, BSA has different conformational forms (N, F, B, A and E) [19]. Transitions between these forms can be caused either by a stretching (“mechanical denaturation”) or pH – change. For our experiments, the possibility of BSA – Ab-BSA complex stretching should be limited exactly by attaining the “disulfide bond structures limited” E-form. Relatively weak antigen – antibody bond will be ruptured before the rupture of disulfide bonds will occur, which would allow further stretching. (For different experimental conditions, essentially where larger forces could be applied, the stretching of

² It can be argued that the complex' extension is given by the difference of z and cantilever displacement y . The latter can be determined from the $f_{pul}(z)$ curve, $y = f_{pul}/k$, and, thus, the value of z can be corrected which we did whenever relevant. Note that this correction is of only minor importance for our experiments. For example, for the typical one bond rupture event ($f_{pul} = 130$ pN) $y = 2.4$ nm and, thus, is essentially smaller than the characteristic (uncorrected) z value of 16 nm.

human serum albumin (HSA) molecule until “the full contour length” of ca. 200 nm has been observed by Rixman et al. [20], fig. 5).

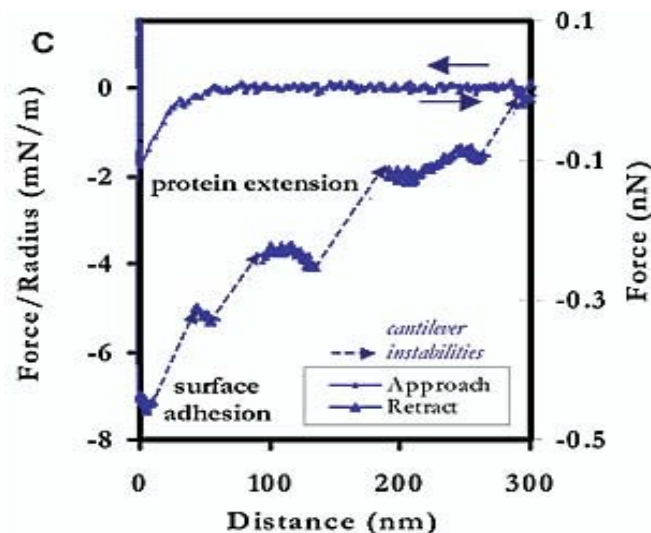


Figure 5. The reproduction of full extension of HSA molecule, fig. 12 C from [20].

Using the data about the sizes of antibody and relevant conformational forms of BSA molecules, together with the ≤ 2 nm thickness of linker layers, one could anticipate the maximal

attainable stretching of the BSA –Ab-BSA complex to roughly 15 nm. This value is very close to the one which has been indeed observed in our experiments. We have determined an average extension $z = 14 \pm 3$ nm (the correction for the cantilever displacement y is taken into account) at the moment of specific bond rupture.

Detailed interpretation of our data using the Worm-Like Chain (WLC) or some other more sophisticated statistical polymer model would be somewhat premature at the current stage of experiments. In fact, such a detailed interpretation seems to require a comparison between analogous data for different Ag-Ab complexes and (possibly) careful characterization of the protein binding sites. Nevertheless, we would like to underline the following: for long flexible molecules having numerous conformational degrees of freedom (linear polymers, DNA, etc.) force – extension dependence is given by a quasiuniversal function, relatively insensitive to the chemical composition of the molecule. Indeed, in all theoretical treatments using the WLC model, the chain is considered as a homogeneous line with no microscopic structure. The only parameter appearing in this model is the persistence length p , which measures the length over which the chain loses its orientational correlation

and, as a heuristic parameter, takes the microscopic details of the real chain into account. In the frame of the WLC model, it was shown that a force can be approximated by the Marko-Siggia's formula [18]:

$$f(z) = \frac{k_B T}{p} \left(\frac{1}{4(1-z/L)^2} - \frac{1}{4} + \frac{z}{L} \right) \quad (4)$$

Here k_B is the Boltzmann constant, T - the temperature, p - the persistence length and L is the maximal attainable length of a stretched polymer. Of course, a polypeptide chain is not a good linear polymer in the sense that there is not a single monomer unit and hence, not a well defined persistence length. Moreover, the WLC model does not allow for the secondary and tertiary structure of the complex. Nevertheless, Eq. 4 is often used to approximate experimental data of single protein stretching [20-26]. For our case, where both the force f and the spring constant are simultaneously and *independently* measured, the following consideration seems to be of great interest. The value of the spring constant for the WLC model is given by the derivative of Eq. 4

$$k_{complex} = df/dz = \frac{k_B T}{2pL} \left(2 + (1-z/L)^{-3} \right) \quad (5)$$

For the case of $z=0$ in this model, one has $k_{complex} = k_0 = 3k_B T / 2pL$. Now it is worthwhile to note that, in the frame of the WLC model, a simple analytical dependence between the pulling force and the spring constant can be deduced. For this, one needs to solve Eq. 5 for z/L and then to insert the obtained expression in Eq. 4, which results in

$$f = \frac{k_B T}{p} \left(\frac{\xi^{2/3}}{2^{4/3}} + \frac{3}{4} - 2^{-1/3} \xi^{-1/3} \right) \quad (6)$$

Here $\xi \geq 0.5$ is a dimensionless parameter, $\xi = \frac{3k_{complex}}{2k_0} - 1$. The inverse function, i.e. the

dependence $k_{complex}(f)$, can be derived from Eq. 6 but this requires a solution of cubic equation.

This renders the resulting expression not so practical. Thus, the inverse function of Eq. 6 is plotted in fig. 6.

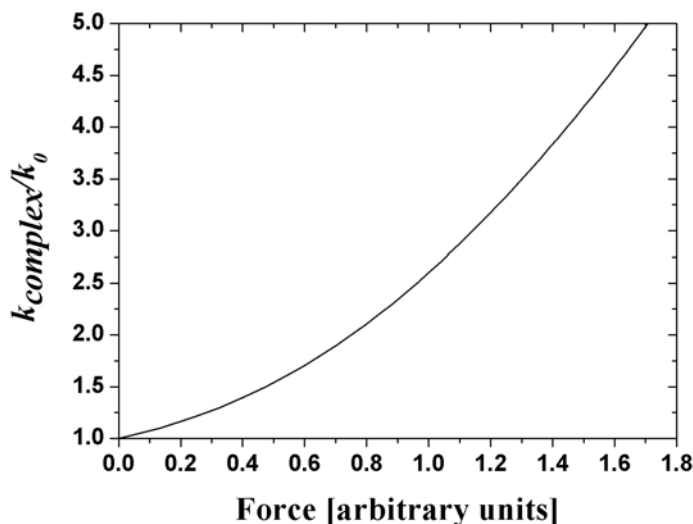


Figure 6. Universal dependence of the spring constant $k_{complex}$ of a polymer molecule (measured in units of the spring constant k_0 of this molecule at $z=0$) on the pulling force for the WLC model of polymer elasticity. Here shown for $k_B T / p = 1$.

Therefore, the WLC model predicts a monotone increase of the single polymer molecule spring constant with the increase of the pulling force and extension. As it has been mentioned above, only such monotone increase has been observed for all single bond rupture events in our experiments. (Note that a non – monotone dependence $k_{complex}(f)$ has been observed in our experiments for some multiple glutaraldehyde – amine bonds rupture events. These data are not considered here). At the current stage of experimental precision and statistics, we were not able to approximate the observed dependencies $k_{complex}(f)$, similar to the one shown in Fig. 4 C by this function. Only a linear approximation turns out to be sufficiently reliable and statistically sound. Nevertheless, we are sure that this will be very interesting to investigate in the nearest future.

The lack of direct measurements of spring constants of stretching antigen – antibody complexes in the literature makes the comparison of our data with other experiments rather difficult. First, usually it is not possible to determine reliably the relevant differential df/dz from the published results. Surprisingly, even to simply calculate the characteristic force – displacement ratio f/z at the moment of rupture of the antigen-antibody bond, turned out to be

virtually impossible. This is because the average value of the complex extension at the moment of rupture, z , is rarely accurately reported in the literature. In some cases, it also turns out that this is the stretching of linkers rather than of an Ag – Ab complex which is responsible for the observed z and k values. This takes place, for example, in Hinterdorfer's et al. experiments [27] with the complex of a human serum albumin (HSA) and polyclonal antibody to HSA (Ab-HSA). These measurements have been performed using 8 nm–poly(ethylene glycol) linkers. No correlation between z and specific interaction value has been reported. This observation is opposite to our data, where, as it was stated above, good correlation between the values of unbinding force, force constant k and extension z has been obtained.

5.2.2b Estimation of the elasticity of linkers

Essentially different df/dz values have been measured for systems other than antigen – antibody complexes. We can use sufficiently detailed data of Sakai et al. [28] to estimate the possible effect of the linkers on our k – measurements. Sakai et al. worked with polystyrene molecules whose stretching data could be a model for the chemicals used to attach the proteins molecules onto the tip and the substrate surface in our experiments (all our chemicals are simple short molecules for which, as for the polystyrene, ordinary C-C, Si-C and similar bonds are the only component). For long polystyrene molecules ($L = 50$ nm, that is ca. 200 styrene monomers and 400 C – C bonds), Sakai et al. obtained for stretching forces of 100 – 140 pN (this is exactly the forces which are of interest to us), a value of $k = df/dz$ close to 0.02 – 0.03 N/m (fig. 7).

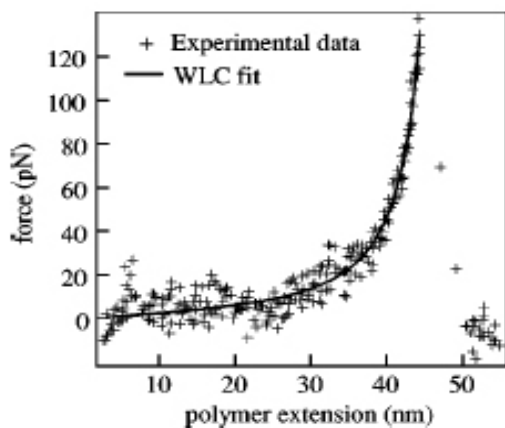


Figure 7. Reproduction of fig.1 from [28].

For our linkers, which contain no more than 10 C–C bonds, and have a length $L_l \sim 1.5$ nm, we have obtained, from the WLC model, the value of k which is L/L_l times larger (see eq.

(5)), that is around 0.8 N/m. Therefore, the short linkers used in our experiments are rigid and practically not stretchable. The value of 0.8 N/m is much larger than the spring constant of 0.017 N/m measured for Ag – Ab complex. We believe thus that the elasticity of rigid linkers does not contribute significantly to the measured value of $k_{complex}$.

5.2.3 Fibrinogen-fibrinogen complex

For comparison and further illustration of our method to measure spring constant, fig. 8 presents typical experimental dependencies of the spring constant (fig. 8 A) and pulling force (fig. 8 B) on the sample stage z -displacement for the fibrinogen-fibrinogen complex. Hence, fig. 8 contains data analogous to that of Fig. 4 but obtained for a completely different system. The fibrinogen – fibrinogen interaction is obviously a non specific interaction as explained in details in chapter IV. This interaction defines much broader distribution in the force values at the moment of the bond rupture, f_{rupt} , and corresponding values of z at this moment, z_{rupt} , in comparison with the single BSA – Ab-BSA complex. Indeed, experimental values of f_{rupt} ranges from 50 to 250 pN, while the corresponding values of z_{rupt} ranges from 50 to 130 nm for the fibrinogen – fibrinogen complex.

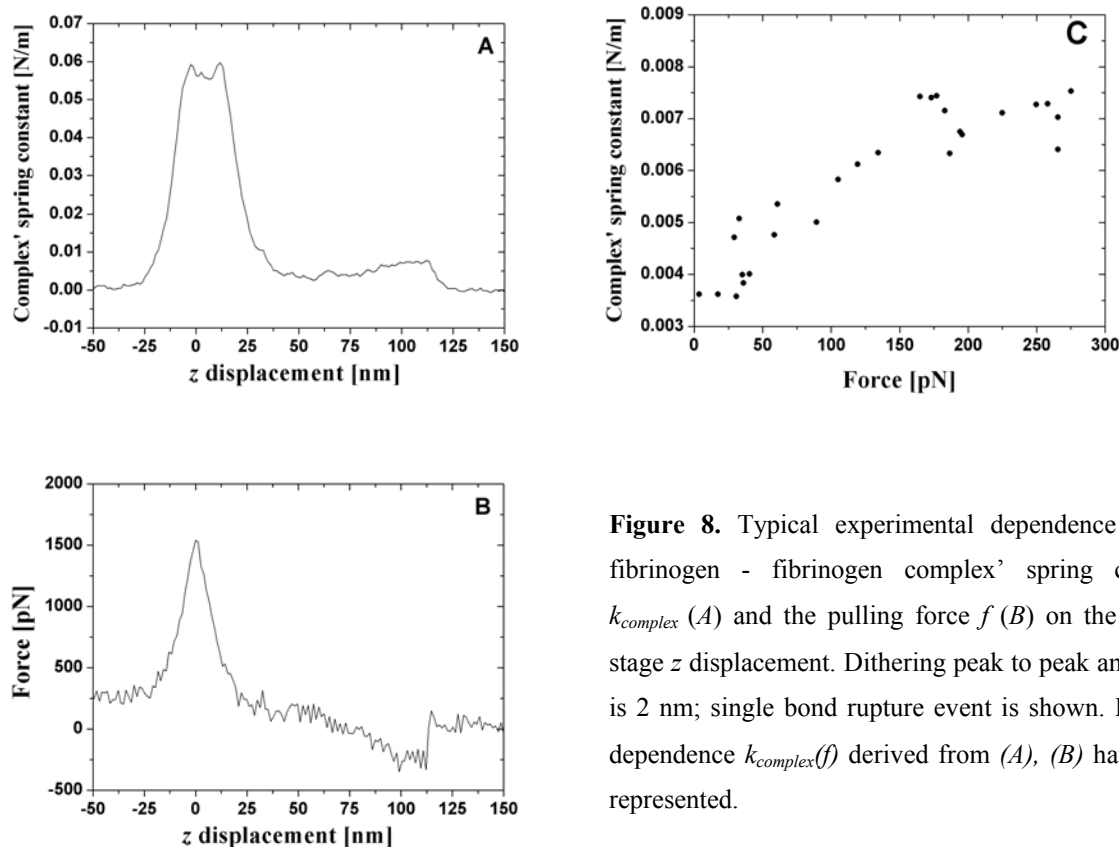


Figure 8. Typical experimental dependence of the fibrinogen - fibrinogen complex' spring constant $k_{complex}$ (A) and the pulling force f (B) on the sample stage z displacement. Dithering peak to peak amplitude is 2 nm; single bond rupture event is shown. In (C) a dependence $k_{complex}(f)$ derived from (A), (B) have been represented.

Accordingly, much broader distribution of the spring constant at the moment of the bond rupture has been also observed: such values vary from 0.003 N/m to 0.008 N/m for different events. Only single fibrinogen – fibrinogen bond rupture events are considered here and below; for the rupture events involving multiple bonds as large forces as 2 - 3 nN are usual and spring constants up to 0.055 N/m have been observed. At the same time, the distribution of z_{rupt} does not essentially depend on the number of bonds involved. Correlation between values of f_{rupt} and z_{rupt} measured for one concrete event is also rather poor, contrary to the BSA – Ab-BSA case.

Thus, the prominent difference between the experimental data concerning fibrinogen – fibrinogen and BSA – Ab-BSA complexes is evident. Especially, we would like to underline an enormous difference between attainable complex extensions. As large z_{rupt} values as 100 - 130 nm (simply unimaginable for the antigen – antibody experiments) have been often

observed for the fibrinogen – fibrinogen rupture events. These values are coherent with the known long and well stretchable molecular structure of the fibrinogen (as described in details in chapter IV). Given all the precautions used to eliminate any possible effects of linkers in the fibrinogen – fibrinogen case, similarly to that of the BSA – Ab-BSA, this circumstance should be considered as an additional prove of utility and reliability of the presented method for direct and continuous measurement of the spring constant applied to single molecules and molecular complexes.

5.3 Perspectives

The next important point is studying the possibility to use the measured signal (local values of spring constant, k) as a feedback signal for the AFM and hence, the possibility to obtain corresponding AFM images. Somewhat analogous approach, which is the far-off resonance excitation of the tip and using its amplitude change as feedback has been already reported in the literature [29]. In particular, it has been mentioned that the images obtained in this way are very easy to interpret (this is “a true differential of the force-displacement curve”). Often stated, disadvantage of such an approach is a relatively large value of the acting force (typically 100 pN or more). This essentially exceeds analogous values characteristic for standard contact or tapping AFM modes. If, however, we are interested in observing molecular recognition events during the scanning (cf. [5]), rather large value of the acting force is needed. To obtain clear results, the acting force should be comparable to the specific interaction force. Because the specific interaction forces range usually from 60 to 300 pN for different systems of biological importance [27, 30-37 and more others (see references in chapter II)], such far-off resonance scanning method, based on using the local k values as a feedback signal, should be really suitable for such task. Importance of the molecular recognition images in biophysics and medicine is evident.

Indeed, such modification of the AFM with the construction of k signal feedback loop has been already started in our laboratory for the experiments on the fibrinogen-fibrinogen complexes. We have prepared an independent electronic equipment to be inserted between the electronics of Veeco and the head of the microscope. Fig. 9 illustrates our experimental setup with constructed k -signal feedback loop. The experimental part concerning the k -measurements reminds the equivalent to one described above (fig. 1). However, the k signal is used as the input signal for the new feedback loop (fig. 9). The system of two converters, Analog-to-Digital Converter (ADC) and Digital-to-Analog Converter (DAC), is inserted between the Nanoscope and the z-piezo. The saw-tooth (or triangular) signal from Nanoscope passes through the ADC-DAC interface to the z-piezo.

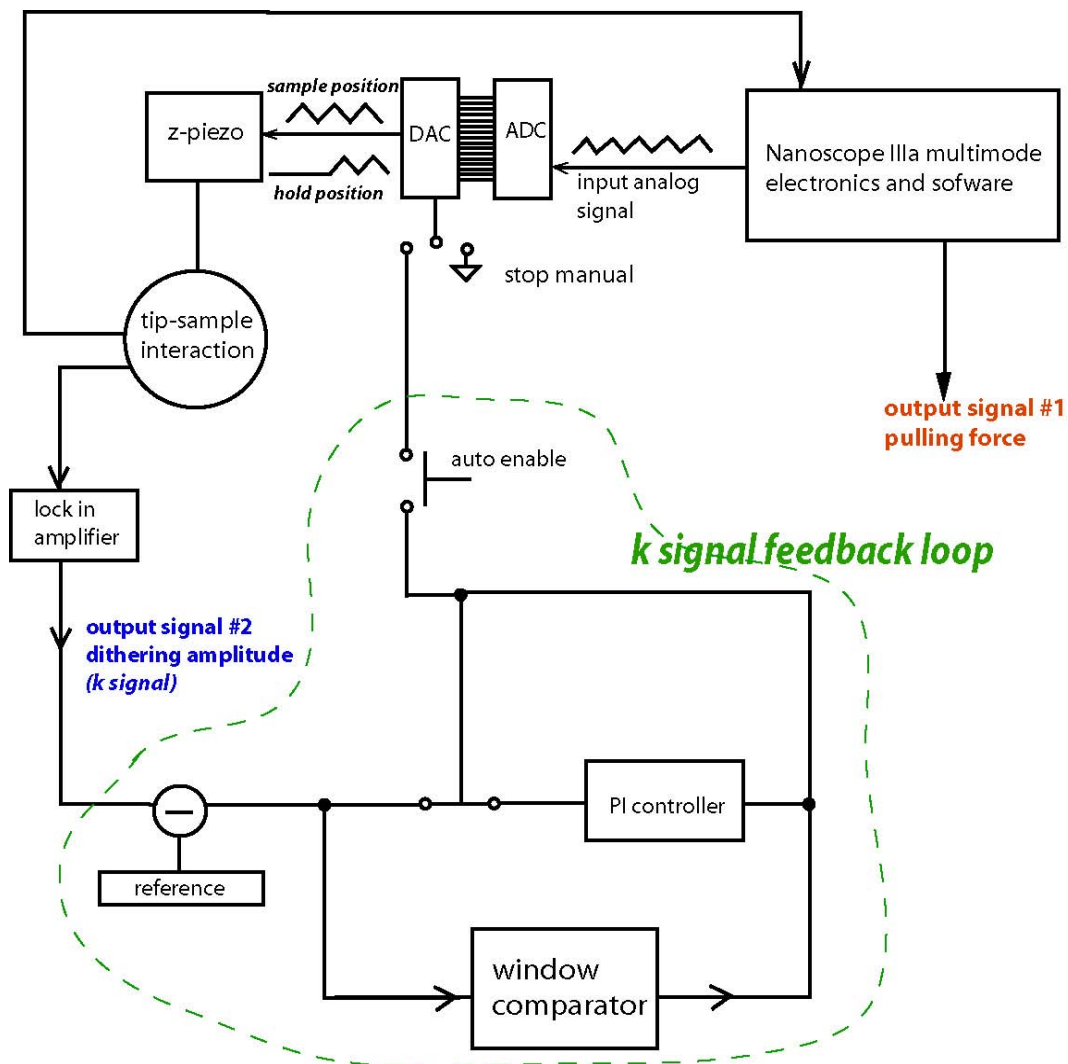


Figure 9. Schematic of the experimental setup with using of the local k -values as a feedback.

When the “stop manual” button is switched on, the output signal from Nanoscope is “frozen” and arrives to the z-piezo as a constant value. So, two output signals (the pulling force and the dithering amplitude (or k -signal)) become also constant.

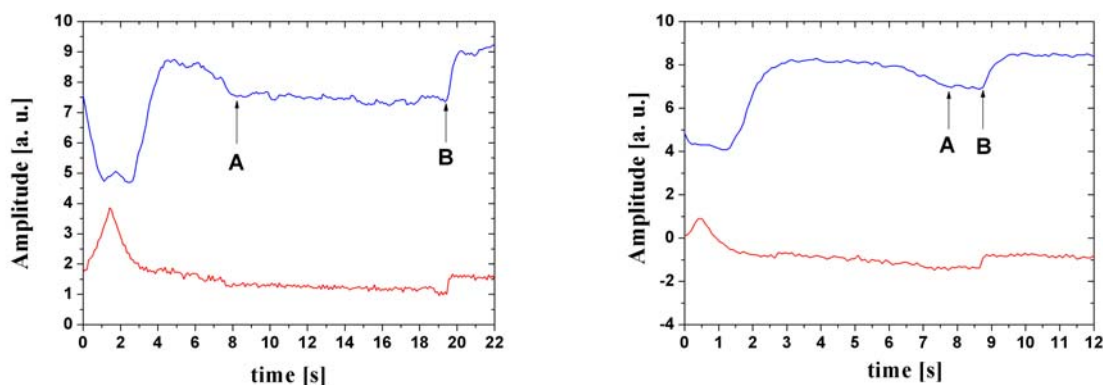


Figure 10. Examples of the time dependencies of pulling force (red curve) and dithering amplitude (blue curve) for fibrinogen – fibrinogen system.

It is clear that direct measurement of time of the bond rupture as a function of pulling force is now possible (fig. 10). As we know, a molecular bond stretching can be observed in our experiments by simultaneous recording the dithering amplitude and the tip deflection while pulling. Therefore, if the characteristic behavior of the dithering amplitude curve (decrease in the blue curve, fig.10) is observed, at certain moment (point A on the blue curves, fig. 10) the pulling process can be stopped by switching on the “stop manual” button. In this situation, molecular bond is not stretched any more (the position of the tip with respect to the sample is fixed), and then, due to the thermal motions the molecular bond can be ruptured (point B). The time between points A and B is the time needed for bond rupture (≈ 11 s (fig. 10-left image) and ≈ 1 s (fig.10-right image)). Of course, if we stop the pulling just at the beginning of the bond stretching, the bond rupture time will become much longer (fig. 11).

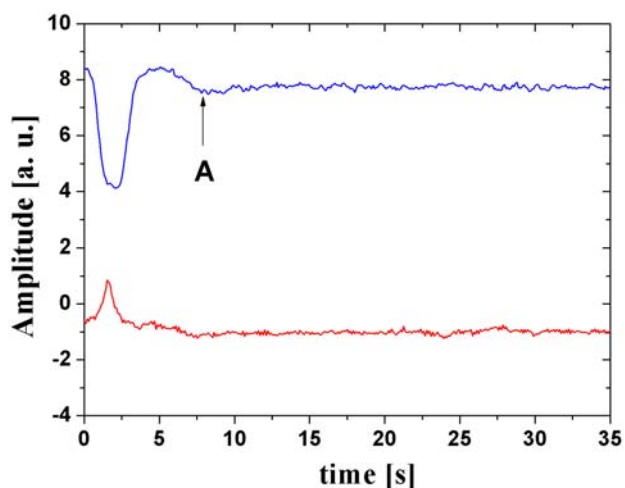


Figure 11. Example of “infinite” life time bond rupture measurement recorded for fibrinogen-fibrinogen complex.

To directly measure the time for bond rupture, it has been sufficient to use just the “stop manual” button without any k -signal feedback loop. Indeed,

the all feedback loop has been successfully tested but large instabilities on the z-piezo signal have been detected and further important improvement is still needed.

5.4 Conclusion

As far the scientific significance of this study is concerned, we would like to underline the high potential importance of our methodology for biomedical industry including the pharmaceutical one. Certainly, the development of the whole field of force spectroscopy applied to the molecular recognition events (immunoassay), is strongly motivated by the pharmaceutical research. Our original approach – the simultaneous measurement of the spring constant of the single molecules or molecular complexes and its application for sorting and recognition of antigens, etc. - definitely will be useful for these purposes. We are strongly believed that this method will finally become at rather short term an essential additional tool for all specific interaction force – based applications of the AFM.

References

1. Sarid D. Scanning force microscopy. Oxford University Press, New York, 1991.
2. Behrend, O. P., Oulevey, F., Gourdon, D., Dupas, E., Kulik, A. J., Gremaud, G., and Burnham, N. A. Intermittent contact: tapping or hammering? *Appl. Phys. A*. **66** (1998) S219-S221.
3. Sader, J. E. Frequency response of cantilever beams immersed in viscous fluids with applications to the AFM. *J. Appl. Phys.* **84** (1998) 64-76.
4. Liu, Y. Z., Leuba, S. H., and Lindsay, S. M. Relationship between stiffness and force in single molecule pulling experiments. *Langmuir*. **15** (1999) 8547-8548.
5. Raab, A., Han, W., Badt, D., Smith-Gill, S. J., Lindsay, S. M., Schindler, H., and Hinterdorfer, P. Antibody recognition imaging by force microscopy. *Nature Biotechnology*. **17** (1999) 902-905.
6. Schindler, H., Badt, D., Hinterdorfer, P., Kienberger, F., Raab, A., Wielert-Badt, S., and Pastushenko, V. Ph. Optimal sensitivity for molecular recognition MAC-mode AFM *Ultramicroscopy*. **82** (2000) 227-235.
7. Kienberger, F., Pastushenko, V. Ph., Kada, G., Gruber, H. J., Riener, C., Schindler, H., and Hinterdorfer, P. Static and dynamical properties of single poly(ethylene glycol) molecules investigated by force spectroscopy. *Single Mol.* **1** (2000) 123-128.
8. Kasas, S., Riederer, B., Catsicas, S., Cappella, B., and Dietler, G. Fuzzy logic algorithm to extract specific interaction forces from atomic force microscopy data. *Rev. Sci. Instrum.* **71** (2000) 2082-2086.
9. Doi, M., and Edwards, S. F. The theory of polymer dynamics. 1992. Clarendon, Oxford.
10. Grubmüller, H., Heymann, B., and Tavan, P. Ligand binding: molecular mechanics calculation of the streptavidin – biotin rupture force. *Science*. **271** (1996) 997-999.
11. Balsera, M., Stepananits, S., Izrailev, S., Oono, Y., and Schulten, K. Reconstructing potential energy functions from simulated force-induced unbinding process. *Biophys. J.* **73** (1997) 1281-1287.
12. Izrailev, S., Stepaniants, S., Balsera, M., Oono, Y., and Schulten, K. Molecular dynamics study of unbinding of the avidin – biotin complex. *Biophys. J.* **72** (1997) 1568-1581.
13. Strunz, T., Oroszlan, K., Schumakovitch, I., Güntherodt, H.-J., and Hegner, M. Model energy landscapes and the force-induced dissociation of ligand-receptor bonds. *Biophys. J.* **79** (2000) 1206-1212.

14. Heymann, B., and Grubmüller, H. AN02/DNP-hapten unbinding forces studied by molecular dynamics atomic force microscopy simulations. *Chem.Phys.Lett.* **303** (1999)1-9.
15. Heymann, B., and Grubmüller, H. Elastic properties of poly(ethylene)-glycol studied by molecular dynamics stretching simulations. *Chem. Phys. Lett.* **307** (1999) 425-432.
16. Heymann, B., and Grubmüller, H. Dynamic force spectroscopy of molecular adhesion bonds. *Phys. Rev. Lett.* **84** (2000) 6126-6129.
17. Heymann, B., and Grubmüller, H. Molecular dynamics force probe simulations of antibody/antigen unbinding: Entropic control and nonadditivity of unbinding forces. *Biophys. J.* **81** (2001) 1295-1313.
18. Marko, J. F., and Siggia, E. D. Stretching DNA. *Macromolecules.* **28** (1995) 8759-8770.
19. Carter, D. C., and Ho, J. X. Structure of serum albumin. *Adv. Protein Chem.* **45** (1994) 153-203.
20. Rief, M., Gautel, M., Oesterhelt, F., Fernandez, J. M., and Gaub, H. E. Reversible unfolding of individual titin immunoglobulin domains by AFM. *Science.* **276** (1997) 1109-1112.
21. Rief, M., Oesterhelt, F., Heymann, B., and Gaub, H. E. Single molecule force spectroscopy of polysaccharides by atomic force microscopy. *Science.* **276** (1997) 1295-1297.
22. Müller, H., Butt, H. J., and Bamberg, E. Force measurements on myelin basic protein adsorbed to mica and lipid bilayer surfaces done with the atomic force microscope. *Biophys. J.* **76** (1999) 1072-1079.
23. Minajeva, A., Kulke, M., Fernandez, J. M., and Linke, W. Unfolding of titin domains explains the viscoelastic behavior of skeletal myofibrils. *Biophys. J.* **80** (2001) 1442-1451.
24. Zhou, H. X. 2001. Loops in proteins can be modeled as worm-like chains. *J. Phys. Chem. B.* **105** (2001) 6763-6766.
25. Round, A. N., Berry, M., McMaster, T. J., Stoll, S., Gowers, D., Corfield, A. P., and Miles, M. J. Heterogeneity and persistence length in human ocular mucins. *Biophys. J.* **83** (2002) 1661-1670.
26. Liu, X. M., and Pollack, G. H. Mechanics of F-actin characterized with microfabricated cantilevers. *Biophys. J.* **83** (2002) 2705-2715.
27. Hinterdorfer, P., Baumgartner, W., Gruber, H. J., Schilcher, K., and Schindler, H. Detection and localization of individual antibody-antigen recognition events by atomic force microscopy. *Proc. Natl. Acad. Sci. U.S.A.* **93** (1996) 3477-3481.

28. Sakai, Y., Ikehara, T., Nishi, T., Nakajima, K., and Hara, M. Nanorheology measurement on a single polymer chain. *Appl. Phys. Lett.* **81** (2002) 724-726.
29. Jarvis, S. P., Lantz, M. A., Dürig, U., and Tokumoto, H. 1999. Off resonance ac mode force spectroscopy and imaging with an AFM. *Appl. Surf. Sci.* **140** (1999) 309-313.
30. Stuart, J. K., and Hlady, V. Effects of discrete protein-surface interactions in scanning force microscopy adhesion force measurements. *Langmuir.* **11** (1995) 1368-1374.
31. Dammer, U., Hegner, M., Anselmetti, D., Wagner, P., Dreier, M., Huber, W., and H.-J. Güntherodt, H.-J. Specific antigen/antibody interactions measured by force microscopy. *Biophys. J.* **70** (1996) 2437-2441.
32. Allen, S., Chen, X. Y., Davies, J., Davies, M. C., Dawkes, A. C., Edwards, J. C., Roberts, C. J., Sefton, J., Tendler, S. J. B., and P. M. Williams, P. M. Detection of antigen – antibody binding events with atomic force microscopy. *Biochemistry.* **36** (1997) 7457-7463.
33. Ros, R., Schwesinger, F., Anselmetti, D., Kubon, M., Schäfer, R., Plückettun, A., and L. Tiefenauer. Antigen binding forces of individually addressed single-chain Fv antibody molecules. *Proc. Natl. Acad. Sci. U.S.A.* **95** (1998) 7402-7405.
34. Willemsen, O. H., Snel, M. M. E., van der Werf, K. O., de Grooth, B. G., Greve, J., Hinterdorfer, P., Gruber, H. J., Schindler, H., van Kooyk, Y., and Figdor, C. G. Simultaneous height and adhesion imaging of antibody – antigen interactions by atomic force microscopy. *Biophys. J.* **75** (1998) 2220-2228.
35. Willemsen, O. H., Snel, M. M. E., Cambi, A., Greve, J., De Grooth, B. G., and Figdor, C. G. Biomolecular interactions measured by atomic force microscopy. *Biophys. J.* **79** (2000) 3267-3281.
36. Merkel, R., Nassoy, P. Leung, A., Ritchie, K., and Evans, E. 1999. Energy landscapes of receptor – ligand bonds explored with dynamic force microscopy. *Nature.* **397** (1999) 50-53.
37. Schwesinger, F., Ros, R., Strunz, T., Anselmetti, D., Güntherodt, H.-J., Honegger, A., Jermutus, L., Tiefenauer, L., and Plückettun, A. Unbinding forces of single antibody-antigen complexes correlate with their thermal dissociation rates. *Proc. Natl. Acad. Sci. U.S.A.* **97** (2000) 9972-9977.

General Conclusions

- It has been demonstrated that standard quasistatic force spectroscopy is useful tool for the characterization of antigen-antibody systems, especially to distinguish between different antibodies. Thus, force spectroscopy can be used as a complementary technique in immunoassay.
- The first steps of the process of fibrin polymerization have been studied in the frame of the quasistatic force spectroscopy. First measurements of the forces involved in this process have been performed.
- High resolution AFM images of fibrin strands reveal the molecular organization which is more consistent with the centrosymmetric structure of fibrinogen.
- A new method for direct measurement of elasticity of single molecules has been elaborated and successfully tested. A new physical parameter of the spring constant has been subsequently introduced for the characterization of molecular recognition processes.
- The direct measurement of lifetime of the molecular bond as a function of pulling force is now possible.
- The aim of this thesis work has been achieved.

CURRICULUM VITAE

Lilia Alexandrovna CHTCHEGLOVA

Place and date of birth: Moscow, 23 March, 1974

Nationality: Russian

Marital Status: single and one child (2.5 years old)

Address in Russia:

117588 Moscow

Novoyasenevskii prospect 3-16

Tel: 425-44-95

Education and Awards

- **Oct 1998 – June 1999** – University Louis Pasteur of Strasbourg (France), Diplôme d'Etudes Approfondies (DEA) « Physico-chimie des Matériaux Moléculaires et Macromoléculaires », mention « assez bien », (master degree)
- **Sept 1991 - Jan 1997** – Moscow M.V. Lomonosov State University, Physics Department, Chair of Polymer Physics and Crystallography, graduated with honors
- **June 1991** – Moscow Secondary School N91, graduated with gold medal.

Work Experiences

Oct 2003 – present time – assistante-doctorante, Ecole Polytechnique Fédérale de Lausanne, Faculté de Sciences de Bases, Institut de Physique de la Matière Complexe, Laboratoire de Physique de la Matière Vivante.

Nov 1999 – Sept 2003 – assistante-doctorante, Institut de Physique de la Matière Condensée, University of Lausanne, Switzerland.

March – July 2001 – maternity.

May – Sept 1998 – tour manager, ANKOR tourist agency, Moscow.

Oct 1997 – May 1998 – engineer, A.N. Nesmeyanov Institute of Elemento-Organic Compounds (INEOS) of Russian Academy of Science.

Research interest: biophysics, polymer physics, AFM and its applications.

Language Proficiency: Russian (mother tongue), English and French (fluent), German (speaking, reading and writing).

Publications related to the present thesis work:

1. Lilia A. Chtcheglova, George T. Shubeita, Sergey K. Sekatskii, and Giovanni Dietler. "Force Spectroscopy with a Small Dithering of AFM Tip: a Method of Direct and Continuous Measurement of the Spring Constant of Single Molecules and Molecular Complexes". *Biophysical J.* **86** (2004) 1176-1184.
2. L. A. Chtcheglova, G. T. Shubeita, S. Sekatskii, G. Dietler. "An application of AFM to measure the spring constant of single antigen-antibody complex". *Phys. Low-Dim. Struct.*, **3/4** (2003) 39-44.
3. Lilia Chtcheglova and Giovanni Dietler. "Force Spectroscopy of Polyclonal and Monoclonal Anti-Bovine Serum Albumin antibodies – BSA Complexes". *Acta Physica Polonica A.* **104** (3-4) (2003) 321-327.
4. Lilia A. Chtcheglova and Giovanni Dietler. "Force spectroscopy study of fibrin gel formation". (in preparation).
5. Lilia A. Chtcheglova and Giovanni Dietler. "Visualization of fibrin strands: AFM study". (in preparation).
6. Lilia A. Chtcheglova, Sergey K. Sekatskii, Dmitri Lapshin, and Giovanni Dietler. "Possibility of direct measurements of single molecular bond lifetimes with AFM". (in preparation).
7. Lilia Chtcheglova, Jackeline Romero, Giampietro Corradin, and Giovanni Dietler, "Atomic Force Microscopy for Imaging and Force Mapping of Plasmodium *Berghei* Sporozoite", *Phys. Low-Dim. Struct.* **5/6** (2002) p.189-192.

Participation at conferences:

1. Lilia A. Chtcheglova and Giovanni Dietler. "Antigen-antibody unbinding forces and spring constant of single antigen-antibody complex : AFM study". International SPS'03 Symposium, Poznan, Poland, July 16-19, 2003. (oral presentation).
2. L.A. Chtcheglova, J. A. DeRose , S. Kasas, G. Dietler. "Recognition and comparison between polyclonal and monoclonal antibodies: AFM study". International STM'03 Conference, Eindhoven, Holland, July 21-25, 2003, Proceedings Mo-Pos-1 (poster).
3. L. A. Chtcheglova, G. T. Shubeita, S. Sekatskii, G. Dietler. "An application of AFM to measure the spring constant of single antigen-antibody complex". Scanning Probe Microscopy-2003, International Workshop, Nizhny Novgorod, Russia, March 2-5. 2003. (oral presentation).
4. Chtcheglova L.A., Kasas S., Dietler G. « A method to characterize specific antibody-antigen interactions and distinguish between them » Jahrestagung in Lausanne, Swiss Physical Society, Lausanne 28.02.02-01.03.02 (oral presentation)
5. Chtcheglova L., Romero J., Corradin G., Dietler G., « Atomic force microscopy for imaging and force mapping of Plasmodium berghei sporozoite » Scanning Probe Microscopy-2002, Nizhny Novgorod, Russia, March 3-6.2002, Proceedings p.175 (poster)
6. Lilia Chtcheglova, James DeRose, Gerit Jänchen, Sandor Kasas and Giovanni Dietler: « Force Spectroscopy: A potential Method to Characterize Antibody Assays with High Sensitivity » Structure and Stability of Biomacromolecules, SSB'01, Košice, Slovak Republic, September 11-15, 2001 (poster).